NASA CONTRACTOR REPORT

UACRL E-920243-27
NASA CR- 72076

INVESTIGATION OF COLLISION PROBABILITY OF ELECTRONS AND IONS WITH ALKALI METAL ATOMS

PREPARED BY R. H. BULLIS AND W. L. NIGHAN

FINAL REPORT
AUGUST 1966

PREPARED UNDER CONTRACT NO. NAS 3-4171

BY

United Aircraft Research Laboratories
UNITED AIRCRAFT CORPORATION
EAST HARTFORD, CONNECTICUT

FOR

NATIONAL AERONAUTICS & SPACE ADMINISTRATION
LEWIS RESEARCH CENTER
CLEVELAND, OHIO

NOTICE

#92

UNITED AIRCRAFT CORPORATION
RESEARCH LABORATORIES
East Hartford, Connecticut

NASA Report No.: CR- 72076
United Aircraft Corporation Research Laboratories Report No.: E-920243-27
Final Report
Date of Reporting Period: April 22, 1964, to July 21, 1966
Title of Contract: Investigation of Collision Probability of Electrons and Ions with Alkali Metal Atoms
Contract Number: NAS3-4171
Contractor: United Aircraft Corporation Research Laboratories
East Hartford, Connecticut
203-565-7046
Principal Investigator: R. H. Bullis

National Aeronautics and Space Administration
Lewis Research Center
Space Power Systems Division
Project Manager: Mr. H. E. Nastelin, MS 500-309

Reported By: R. H. Bullis
R. H. Bullis

W. L. Nighan
W. L. Nighan

Approved By: H. D. Taylor
Harlan D. Taylor
Manager, Physics Department

Date: October 12, 1966

Report E-920243-27

Final Report Under Contract NAS3-4171
for the Period April 22, 1964, through July 21, 1966

Investigation of Collision Probability of Electrons and Ions with Alkali Metal Atoms

TABLE OF CONTENTS

Report E-920243-27

Investigation of Collision Probability of Electrons and Ions with Alkali Metal Atoms

Final Progress Report - April 22, 1964, through July 21, 1966

Contract NAS3-4171

Summary

This report is a summary of the experimental and analytical research investigations conducted at the United Aircraft Research Laboratories to determine the collision cross sections for electrons and cesium ions interacting with cesium atoms over the energy range of importance to ignited-mode thermionic converter operation. This work, which was conducted during the period from April 22, 1964, through July 21, 1966, represents a logical extension of collisional studies conducted under NASA Contract NASr-112.

In the first year of the contract, the momentum transfer collision probability for electrons interacting with cesium atoms was determined over an energy range from 0.2 to 0.6 eV by measuring the transport properties of the plasma existing in the positive column of a cesium arc discharge. The total cesium ion-cesium atom collision probability data previously obtained by beam techniques in a modified Ramsauer cross-section experiment under Contract NASr-112 were analyzed to determine low-energy cesium ion mobilities, and further investigations of the low-energy cesium ion-cesium atom collision cross sections were made in an effort to extend the energy range of these measurements. In the course of these investigations, ion beams with energies as low as 0.058 eV were detected successfully. The results of the ion mobility analysis were reported at the IEEE Thermionic Conversion Specialist Conference held in Cleveland, Ohio, on October 26 through 28, 1964, and the over-all results of both the electron-cesium atom and the cesium ion-cesium atom collision probability measurements were reported in two papers presented at the Fourth International Conference on the Physics of Electronic and Atomic Collisions held in Quebec, Canada, on August 2 through 6, 1965.

In the second year of the contract, a modified Brode-type experiment was designed and constructed in order to measure low-energy electron-cesium atom total collision cross sections. With this system electron beams with energies as low as 0.095 eV have been successfully detected.

A knowledge of both the collision probability of electrons and cesium ions with cesium atoms is essential in order to meaningfully analyze the neutralization plasma existing in the ignited-mode thermionic converter and other devices employing cesium vapor in an ionized state.

ELECTRON-CESIUM ATOM COLLISION PROBABILITY MEASUREMENTS (MOMENTUM TRANSFER)

1. Introduction

Electron momentum transfer collisions play a dominant role in the determination of plasma transport properties, such as electrical and thermal conductivity, diffusion coefficients, and thermoelectric coefficients. These transport properties can usually be expressed in terms of an effective electron momentum transfer collision frequency representing the velocity average of electron-heavy particle collisions. Therefore, quantitative knowledge of the effective collision frequency for electrons in cesium plasmas bears directly on the physical properties of plasmas existing in many devices of current interest. In most practical cesium devices electron mean energies are between 0.1 and 1.0 eV. Unfortunately, in this range there is approximately an order of magnitude variation in the reported values of effective collision frequency as determined from measurements of various plasma transport properties.

With a knowledge of the velocity dependence of the electron-cesium atom momentum transfer cross section, the effective collision frequency can be determined. Monoenergetic electron beam techniques are particularly well suited for determining this velocity dependence, particularly for electron energies in excess of a few electron volts. However, many beam experiments result in a "total" elastic scattering cross section which may be quantitatively compared with the "momentum transfer" cross section of significance in the analysis of plasma transport effects, only if the scattering is isotropic. As an alternative the so-called electron "swarm" experiments provide a means whereby momentum transfer collisional interactions can be investigated. Application of this technique, requiring the measurement and analysis of electron transport properties, is the subject of this section of the report.

An arc discharge in cesium was chosen as the laboratory plasma for this investigation because the variations in electron temperature and degree of ionization in the positive column of the discharge were in the range of interest. Measurement of plasma properties under conditions of known discharge current and axial electric field produced sufficient information to determine the dc electrical conductivity which can be expressed in terms of an effective collision frequency. Once the effective collision frequency was obtained experimentally as a function of electron temperature and degree of ionization, a numerical analysis of the velocity integral describing the effective collision frequency was undertaken in order to determine the velocity structure of the electron-cesium atom momentum transfer cross section in the appropriate electron velocity range. A trial-and-error procedure was followed until the cross section resulting in the best fit between the calculated and measured effective collision frequency was obtained. The electron-atom momentum transfer cross section determined in this manner was then used to calculate the effective collision frequency over an

extended range of electron temperature and degree of ionization so that comparison could be made with the data available in the literature. The results of this comparison, based on an effective collision frequency formulation including the effect of electron-ion as well as electron-atom collisions, are described in detail in subsequent paragraphs. A comparison is also made between the electron-atom cross section determined from this analysis and that predicted theoretically.

2. Theory and the Plasma Model

In this section the relationship between current flow and axial electric field in the cesium arc column will be derived in terms of the measurable plasma properties, and the effective momentum transfer collision frequency will be defined. The equation describing the electron current flow through a plasma under the influence of a dc electric field is derived on the basis of the well-known Lorentz model. On this basis the following equation may be obtained for the electron current density, J:[1,2,3]

$$J = -\frac{4\pi}{3}\frac{n_e e^2}{m}\int_0^\infty \frac{v^3(\partial f_o/\partial v)}{\nu_{ea}(v)+\nu_{ei}(v)}\,dv\,E \quad , \qquad (1)$$

where

- m is the electron mass;
- e is the electron charge;
- v is the electron velocity;
- n_e is the electron number density;
- E is the electric field intensity;
- f_o is the isotropic part of the electron velocity distribution function normalized to unity;
- $\nu_{ea}(v)$ is the elastic electron-atom collision frequency for momentum transfer;
- $\nu_{ei}(v)$ is the elastic electron-ion collision frequency for momentum transfer.

The coefficient of the electric field intensity, E, on the right-hand side of Eq. 1 is the plasma electrical conductivity. In the derivation of Eq. 1 it has been assumed that the plasma is homogeneous, that the collisional friction force exerted on electrons is due to elastic momentum transfer encounters with heavy particles which are assumed infinitely massive in comparison with electrons, and that electron-electron encounters have no direct influence on the momentum of the electron gas. The velocity-dependent electron-atom and electron-ion momentum transfer collision frequencies appearing in Eq. 1 are related to their respective momentum transfer cross sections by the usual relations

$$\nu_{ea}(v) = n_a Q_{ea}(v)v \qquad \nu_{ei}(v) = n_i Q_{ei}(v)v \quad , \qquad (2)$$

where

n_a is the atom number density;
$Q_{ea}(v)$ is the elastic electron-atom momentum transfer cross section;
n_i is the ion number density (assumed equal to the electron number density);
$Q_{ei}(v)$ is the effective elastic electron-ion momentum transfer cross section.

The effective electron-ion cross section is given by the following expression:[1,4]

$$Q_{ei}(v) = \frac{e^4}{4\pi\epsilon_0^2 m^2 v^4} \cdot \log_e \left[\frac{12\pi(\epsilon_0 k T_e/e^2)^{3/2}}{n_e^{1/2}} \right] \quad , \qquad (3)$$

where

ϵ_0 is the permittivity of free space;
k is Boltzmann's constant;
T_e is the electron temperature.

For the cesium arc discharge plasma, the relatively high degree of ionization results in extremely short electron thermalization times. Therefore, as has been verified experimentally, electron-electron collisions are instrumental in establishing a Maxwellian distribution of electron velocities at least for the body of slow electrons responsible for the transport properties in the plasma. Using the Maxwellian form for the electron velocity distribution and Eq. 2 relating collision frequency to cross section results in the following expression for the current density:

$$J = \frac{8}{3\sqrt{\pi}} \frac{\alpha e^2}{m} \left(\frac{m}{2kT_e} \right)^{\frac{5}{2}} \int_0^\infty \frac{v^3 e^{-\frac{mv^2}{2kT_e}}}{Q_{ea}(v) + \alpha Q_{ei}(v)} \, dvE \quad , \qquad (4)$$

where α, the degree of ionization, is defined as the ratio of electron density to atom density.

In the analytical development leading up to Eq. 4, it was assumed that the plasma was homogeneous. In the case of the cylindrical arc discharge used in this experiment, measurements have shown that axial and circumferential uniformity exist, and the only gradient in the radial direction is the electron density variation resulting from particle diffusion to the walls of the discharge tube. Because there are no significant plasma gradients in the direction of discharge current flow, the plasma behaves as though it were nearly homogeneous, and a simple averaging process can be used to account for the radial variation in discharge current density caused by the diffusion gradient in electron density. Therefore, the

current flow through a cross-sectional area of the discharge tube is given by:

$$I = 2\pi \int_0^R J(r)\, r\, dr \,, \tag{5}$$

where I is the discharge current and R the tube radius. It has been determined experimentally that the radial variation in degree of ionization can be reasonably represented by a parabola of the form $\alpha(r) = \alpha_o(1 - r^2/R^2)$, where α_o is the degree of ionization on the tube axis ($\alpha_o \equiv n_{e_o}/n_a$). Using this form for the degree of ionization in conjunction with Eqs. 4 and 5 results in the following expression for the discharge current:

$$I = \frac{16\sqrt{\pi}}{3} \frac{\alpha_o e^2}{m} \left(\frac{m}{2kT_e}\right)^{\frac{5}{2}} \int_0^R \int_0^\infty \frac{(1 - r^2/R^2) v^3 e^{-\frac{mv^2}{2kT_e}}}{Q_{ea}(v) + \alpha_o (1 - r^2/R^2) Q_{ei}(v)} r\, dv\, dr\, E. \tag{6}$$

Since r and v are independent, the radial integration can be performed, and Eq. 6 reduces to

$$I = \frac{16}{3\sqrt{\pi}} \cdot \frac{\alpha_o e^2}{m} \left(\frac{m}{2kT_e}\right)^{\frac{5}{2}} \int_0^\infty \frac{v^3 e^{-\frac{mv^2}{2kT_e}}}{\alpha_o Q_{ei}(v)} \left[1 + \frac{Q_{ea}(v)}{\alpha_o Q_{ei}(v)} \log_e \left(\frac{Q_{ea}(v)}{Q_{ea}(v) + \alpha_o Q_{ei}(v)}\right)\right] dv \frac{\pi R^2}{2} E. \tag{7}$$

At this point it is convenient to define an effective collision frequency from the relationship between discharge current flow and electric field intensity, i.e.,

$$I \equiv \frac{\bar{n}_e e^2}{m \nu_{eff}} \cdot AE \,, \tag{8}$$

where $\bar{n}_e$ is an average electron density ($n_{e_o}/2$), and A is the cross-sectional area of the discharge tube. The expression $\bar{n}_e e^2/m\nu_{eff}$ in Eq. 8 can be thought of as the effective electrical conductivity of the arc column. Solving for the effective collision frequency defined by Eqs. 7 and 8 and normalizing with respect to atom density yields

$$\nu_{eff}^{*-1} = \frac{16}{3\sqrt{\pi}} \left(\frac{m}{2kT_e}\right)^{\frac{5}{2}} \int_0^\infty \frac{v^3 e^{-\frac{mv^2}{2kT_e}}}{\alpha_o Q_{ei}(v)} \left[1 + \frac{Q_{ea}(v)}{\alpha_o Q_{ei}(v)} \log_e \left(\frac{Q_{ea}(v)}{Q_{ea}(v) + \alpha_o Q_{ei}(v)}\right)\right] dv = g(T_e, \alpha_o) \,. \tag{9}$$

Equation 9, defining the normalized effective collision frequency, represents an average of the total normalized electron-heavy particle momentum transfer collision frequency and is a function of electron temperature and degree of ionization alone. This normalized effective collision frequency is not the simple average of collision frequency over the electron velocity distribution but rather is an average of the reciprocal sum of momentum transfer collision frequencies representing the over-all resistive effect of momentum transfer collisions on dc current flow. Spatial

averaging has been performed to account for the radial dependence of the electron-ion contribution to the over-all resistance to discharge current flow.

The normalized effective collision frequency of Eq. 9 can be related to the measurable parameters of the cesium arc discharge plasma from Eq. 8. Using the perfect gas relationship $n_a = p/kT_g$, where p and T_g are the cesium vapor pressure and temperature, respectively, the following expression for the normalized effective collision frequency is obtained:

$$\nu^*_{eff} = \frac{e^2 k}{m} \frac{\bar{n}_e AE}{(P/T_g)I} \quad . \qquad (10)$$

Equation 10 was used to determine experimentally the normalized effective collision frequency from measurements of electron density, electric field intensity, gas pressure and temperature, and discharge current.

3. Description of the Experiment and Diagnostic Techniques

A schematic of a typical discharge tube is shown in Fig. 1. Cathode-to-anode separation was 50 cm, and the inside diameter was nominally 3.8 cm. During operation the tube was located within a two-component oven, the main portion of which controlled the gas temperature and prevented cesium from condensing on the tube walls. The liquid cesium well shown in the figure extended down to the lower portion of the oven, which was temperature-stabilized and always held at a lower temperature than the main oven in order to control the cesium vapor pressure. The cesium pressure was determined from the vapor pressure expression of Ref. 5.

The electron temperature, electron density, and plasma potential variations in the discharge were measured using electrostatic probe techniques. From an analysis of the current-voltage characteristics of the electrostatic probes, the electron temperature and density were determined, and the assumption that the electron velocity distribution in the plasma was Maxwellian was checked. In addition, the electric field was determined from potential measurements made with probes positioned axially along the positive column at 8-cm intervals. The electrostatic probe assemblies were constructed in such a way that the probes, which protruded through a small hole in the wall of the discharge tube, could be moved radially into the plasma by means of a magnet. The probes were constructed of 0.010-in. diameter tungsten rod covered with a glass sheath which served as an electrical insulator. The entire assembly averaging 0.018 in. in diameter was ground flat, so that the 0.010-in. tungsten tip was exposed to the plasma. The probe tips were periodically examined with a microscope at operating temperature in the discharge tube so that any flaw could be detected. A pulsing system was used to apply a cleaning pulse, sweep voltage or data acquisition pulse, and rest voltage to the probe. The time duration of each portion of the probe pulse could be varied independently with the time scale of the total pulse variable from

approximately 100 microseconds to 100 milliseconds. With such versatility the effect of changing probe surface conditions, errors due to circuit and plasma response limitations, and the effect of plasma drift or instability could be detected. The importance of being able to vary sweep speed and applied voltage in this manner is detailed in Refs. 6 and 7.

A schematic of the pulse waveform is shown in Fig. 2 along with a typical photograph of a probe current-voltage characteristic. When data was being taken, the waveform was adjusted so that the probe was drawing current only about 5 per cent of the time; i.e., the time of the cleaning and rest levels was approximately twenty times as long as the data acquisition pulse. The linear behavior of the semilog plots of the electrostatic probe current-voltage characteristics, an example of which is shown in Fig. 3, was experimental verification of the existence of a Maxwellian distribution of velocities at least for the slow-moving electrons in the body of the distribution. Deviations from linearity at the low probe currents (approximately 10 microamps) were random in nature and due to the limits of sensitivity of the system. A plot of the radial electron density profile is shown in Fig. 4 for various arc currents, where a comparison is made with both the zero-order Bessel function, typical of cylindrical diffusion-dominated discharges, and the assumed parabolic form. It is apparent from this figure that the radial dependence for the electron density, and consequently the degree of ionization was adequately approximated by the assumed parabolic form. The electron temperature determined from the radial and axial measurements showed no significant dependence on position.

Of the plasma parameters required to determine the normalized effective collision frequency, the electron density is the most difficult to measure quantitatively. Under certain conditions the physical presence of a probe may perturb the plasma resulting in errors in the determination of electron density. Therefore, in order to check the values measured by the probe, microwave phase-shift measurements of electron density were also made. A 50-Gc microwave interferometer was used for these measurements. Focused microwave radiation was directed through the plasma between electrostatic probe locations as shown schematically in Fig. 1. The microwave beam diameter as well as the free-space wavelength (6 mm) was quite small with respect to the plasma size, and therefore, a plane slab one-dimensional plasma model was applicable.[9] Positioning the microwave horns at approximately a 30° angle with respect to the tube resulted in removal from the beam pattern of any radiation scattered from the air-glass or glass-plasma interfaces. Scattered radiation was absorbed by microwave-absorbent material positioned around the tube to form a tunnel for the microwave beam. As a check on the validity of the plasma slab model, analog experiments were performed in which precision dielectric materials of known dielectric constant were substituted for the plasma. Measurements made under exactly the same conditions as encountered by the plasma indicated that the dielectric constant of the material could be determined to within a few per cent of its certified value.

For comparison with the electron density determined by electrostatic probes positioned on the tube centerline, it was necessary to relate the phase shift of the microwave to the centerline or peak value of electron density rather than to some average value. In the case considered here, $\nu_{eff}^2 << \omega_p^2 << \omega^2$ (ν_{eff}, ω_p, and ω are the collision frequency, plasma frequency, and microwave frequency, respectively), and therefore, a simple adiabatic approximation was applicable.[9] For these conditions the phase shift was a simple average over the microwave path length of the plasma phase constant which depends on the predetermined parabolic variation of electron density. Consequently, the value of electron density on the tube axis could be determined from the microwave phase shift for direct comparison with that determined by the probes.

As a check on the potential measurements made with electrostatic probes and on discharge current measurements, rf conductivity probes were used to measure the plasma conductivity. With this technique a small probing rf coil was inserted in the plasma through the end of a discharge tube specially constructed for this purpose. The magnetically induced rf (10 mc) electric field of the coil penetrated into the plasma which behaved as a lossy medium for the rf power, loading the coil to an extent determined by the plasma conductivity. Therefore, a measurement of the power dissipated was related to the plasma conductivity. These measurements provided an independent check on the experimentally determined ratio of current density to electric field intensity, the effective plasma conductivity. A description of the rf probe and its associated instrumentaion is presented in Ref. 10.

4. Measurements and Results

Typical measurements of plasma properties were conducted with cesium pressure and discharge current as independent experimental variables. A typical set of experimental data is presented in Table I (Fig. 4a). For moderate cesium pressures (10^{-2} to 10^{-1} torr) and arc currents (0.2 to 2.0 amps), the electron temperature determined from the slope of the probe semilog current-voltage characteristics varied from approximately 2500 to 4500°K which is typical of cesium discharges of this type. From measurements of potential obtained with probes positioned along the tube axis and from a knowledge of the probe spacing, the electric field intensity was determined and found to be uniform along the tube axis, varying with discharge current and pressure from about 0.2 to 0.6 x 10^2 volts/m. The effective plasma conductivity which was determined using rf probing techniques was found to vary from approximately 10 to 100 mho/m over the experimental range of pressure and arc current. The conductivity determined in this manner was found to be in good agreement with the experimentally determined ratio of discharge current to electric field intensity. Measurements of electron density were made for varying discharge conditions using both electrostatic probe and microwave techniques. For the lower cesium pressures ($\sim$ 2 x 10^{-2} torr), the values of peak electron density as determined by the probes and by the microwaves agreed to within

approximately 10 per cent over the entire current range. However, as the cesium pressure was increased, the values of the probe-measured electron density fell below those measured by the microwaves. This apparent perturbation in electron density gradually increased with arc current (increasing degree of ionization) as well as with cesium pressure, the discrepancy between the two techniques reaching a maximum of 40 per cent for the high-pressure, high-current condition. Further investigation revealed that the magnitude and qualitative behavior of the depression was consistent with predictions,[8] and therefore, the microwave-measured electron densities were assumed to be correct and a correction was applied to the values obtained with probes.

Using the relationship of Eq. 10, the normalized effective electron-cesium heavy particle collision frequency was determined over the range of plasma variables from the experimental data of many test runs, such as those of Table I. Shown in Fig. 5 is the effective collision frequency as a function of electron temperature and degree of ionization, α_o, on the tube axis. The experimental data was processed in such a way that ν^*_{eff} could be determined for values of α_o which were successively doubled in the range from 3×10^{-4} to 4.8×10^{-3}. The effective collision frequency data of this figure were obtained from two different discharge tubes and several electrostatic probes positioned at different points along the tube axis. It is felt that the relative variation of ν^*_{eff} with respect to T_e is correct to within about $\pm$ 10 per cent while the absolute value of ν^*_{eff} is to within approximately $\pm$ 20 per cent. Also shown in Fig. 5 are numerical data (solid lines) obtained from computer integration of Eq. 9; the techniques used in arriving at these curves are presented in the next section.

Of considerable significance is the fact that the effective momentum transfer collision frequency data of Fig. 5 shows a pronounced dependence on degree of ionization in the 10^{-4} to 10^{-2} range where electron-ion collisional effects in cesium plasmas are often neglected.[11] Also evident in Fig. 5 is the bunching of the data for the lower degrees of ionization. An increase in α_o from 3 to 6×10^{-4} results in an increase in ν^*_{eff} of only about 10 per cent, and an increase of over a full decade from 3×10^{-4} to 4.8×10^{-3} results in about a factor of two increase in ν^*_{eff}. Therefore, the trend with degree of ionization exhibited by the data of Fig. 5 indicates that in the 2000 to 5000°K range of electron temperature, electron-ion collisions first become noticeable for degrees of ionization of approximately 10^{-4}, begin to contribute significantly to collisional effects at about 10^{-3}, and dominate collision processes for degrees of ionization in the 10^{-2} range and above. Consequently, the necessity of including the effect of electron-ion collisions in the analysis of cesium plasma transport properties in the ranges of electron temperature and degree of ionization of current interest becomes apparent. Also noticeable from the data of Fig. 5 is that the effective collision frequency is increasing rather significantly with electron temperature in the temperature range under consideration. This suggests that the electron-cesium atom collision cross section is strongly velocity-dependent.

5. Electron-Cesium Atom Momentum Transfer Cross Section

The experimental measurement of plasma properties leads to a normalized effective collision frequency which is an average over all electron velocities involving the electron-cesium atom momentum transfer cross section. Numerical integration techniques were undertaken in order to extract from ν^*_{eff}(Eq. 9) the velocity structure of $Q_{ea}(v)$. Various trial forms for $Q_{ea}(v)$ were initially selected on the basis of best estimates as to the magnitude of the cross section and on trends observed in the available experimental and theoretical data. No attempt was made to restrict $Q_{ea}(v)$ to a particular mathematical form, such as a power law dependence. Rather, $Q_{ea}(v)$ trial functions were introduced on a point-by-point basis. Using this technique, hundreds of trial functions were numerically integrated yielding a variety of hypothetical ν^*_{eff} curves with T_e and α_o as parameters. This procedure permitted convenient appraisal of the sensitivity of the integral to any given variation in $Q_{ea}(v)$, as agreement with experiment was sought.

The electron-atom cross section determined from a trial function analysis as described above cannot be unique in the general sense, as rapid fluctuations in the cross section over an energy spread narrow compared to the range over which the electrons are distributed have little or no effect on the plasma transport properties. Neglecting the possibility of such rapid variations and assuming for the moment that the ν^*_{eff} data is available for all values of T_e and α_o, it is apparent that $Q_{ea}(v)$ could be determined in an effectively unique manner for all values of v. In any practical situation, however, ν^*_{eff} is known only in a narrow range of electron temperature and degree of ionization. In fact, in the slightly ionized limit ($\alpha << 10^{-4}$), ν^*_{eff} depends only on T_e for the range of temperature covered in this experiment. Therefore, the relevant questions are: What is the electron velocity range within which $Q_{ea}(v)$ can be determined approximately from the ν^*_{eff} data available and what are the limits of uncertainty associated with this approximation? Numerical experimentation, as described in the previous paragraph, has shown that the range of velocity most closely coupled to the given electron temperature range is approximately 3 to 6 x 10^5 m/sec (~ 0.5 to $1.0\sqrt{eV}$). The velocity range and strength of this coupling is of course dependent on the velocity structure of Q_{ea} itself. As would be expected, the fact that the experimental ν^*_{eff} data depends on two variables (T_e and α_o), rather than on T_e alone, results in a significant improvement in the resolution of the trial function technique. Experimentation with various trial functions has clearly illustrated the fact that the coupling between the experimental electron temperature range and the velocity range of sensitivity is substantially strengthened by the ν^*_{eff} dependence on α_o. This is a consequence of the fact that $Q_{ei}(v)$ has a known velocity dependence ($\sim v^{-4}$), placing specific requirements on the exact $Q_{ea}(v)$ velocity structure required to satisfy the experimental effective collision frequency data variation with T_e and α_o. The $Q_{ea}(v)$ resulting in the best agreement between the numerical and experimental ν^*_{eff} data of Fig. 5 has been found to be a strong function of electron velocity having a Ramsauer-like structure in the velocity range of

sensitivity. Shown in Fig. 6 is this cross section as a function of electron velocity. The solid portion of the curve is that required to satisfy the experimental data of Fig. 5. The extrapolated portions of $Q_{ea}(v)$ were chosen to yield the best over-all agreement with the ν^*_{eff} data available at lower and higher electron energies. This comparison with available data will be the subject of a subsequent section. The dashed lines in Fig. 6 indicate the limits of uncertainty in the velocity structure of $Q_{ea}(v)$ and were determined by numerical experimentation with various trial functions as described previously. This uncertainty is a result of the limited range of T_e and α_o over which the ν^*_{eff} data is available, the known limits of accuracy associated with this data, and the uncertainties associated with the theoretical plasma model used to describe the arc discharge plasma. It should be pointed out, however, that the limits of uncertainty established in Fig. 6 are not analogous to experimental error bars, and therefore, not all cross-section curves falling within these limits will, when averaged, satisfy the experimental data. Rather, the limit of uncertainty outlines the range within which $Q_{ea}(v)$ curves could be found which would result in reasonable agreement with the data available.

6. Comparison of Results

Experiment

The necessity of including electron-ion effects in the analysis of cesium plasmas for degrees of ionization as low as 10^{-4} and the importance of consistent averaging of collisional effects when the electron-atom cross section has a strong velocity dependence have prompted a re-evaluation of the available cesium collision cross-section data.[12-22] For the most part earlier workers inferred an average or effective electron-atom collision cross section from a collisional term defined to represent the over-all effect of collisions on the particular transport property under investigation. A cross section determined in this manner is subject to uncertainties associated with differences in the averaging of the cross section over electron velocity, since collisions do not affect all transport properties in the same manner. In addition, since the velocity integrals for the transport properties under study were not analyzed, the average or most probable velocity determined from the measured electron temperature was associated with the effective cross section. Interpretation of the available data is further complicated in some cases by the influence of electron-ion collisions. An improvement in the understanding of the average cesium cross-section data results if the data is converted to a normalized effective collision frequency form. An approximate ν^*_{eff} form is recovered by multiplying each average cross-section point by the most probable electron velocity corresponding to the experimental electron temperature. This procedure was followed for the data of Refs. 12 through 22 with the exception of those of Chen and Raether[12] from which the correct $\nu^*_{eff(dc)}$ was directly recoverable, the data of Boeckner and Mohler,[21] and the data of Terlouw.[22] A detailed explanation of the analysis applied to both the Boeckner and Mohler, and Terlouw

data is presented in Appendix I. Although uncertainties in the data cannot be completely eliminated, this conversion process results in a presentation of the experimental data in a form more closely associated with the manner in which the measurements were actually made and provides a base for a reasonable comparison with the results of the present investigation.

Shown in Fig. 7 is the available experimental data in effective collision frequency form as a function of electron temperature and degree of ionization. Table II (Fig. 7A) contains a legend explaining the symbols used for each investigator's work for various degrees of ionization. Also shown in the figure is the family of ν^*_{eff} curves which has been found to yield the best compromise fit to the available data in the 500 to 5000°K range of electron temperatures and the 10^{-4} to 10^{-1} range of degree of ionization. All the data for degrees of ionization significantly higher than 10^{-4} were obtained from diffusion-dominated cesium discharge plasmas[21,22] under conditions similar to those encountered in this investigation. Therefore, the curves in Fig. 7 were obtained using Eq. 9 in which the parabolic radial dependence of degree of ionization was retained. The ν^*_{eff} integral was calculated for values of α_o chosen to be consistent with the conditions under which the data were obtained. The electron-cesium atom velocity-dependent cross section resulting in the generation of the ν^*_{eff} curves of Fig. 7 is the one previously described in Section 5 and shown in Fig. 6. In spite of the lack of comprehensive experimental ν^*_{eff} data and the difficulties associated with the interpretation of the data that is available, a trend consistent with the interpretation of this investigation is apparent in Fig. 7. Although the data is widely scattered in the 1000 to 2000°K range, there is definite experimental indication of a minimum in ν^*_{eff} in this range of electron temperature, lending support to the $Q_{ea}(v)$ curve used in the calculation. The minimum value of ν^*_{eff} in this range of electron temperatures is determined by the magnitude and location of the minimum in the velocity structure of $Q_{ea}(v)$. Also of significance is the fact that the extrapolation of the $Q_{ea}(v)$ curve required to generate the experimental ν^*_{eff} data of this paper results in quantitative agreement with data obtained at much lower electron temperatures[12,13] and much higher degrees of ionization.[21] Numerical experimentation has shown that the relative spacing between the ν^*_{eff} curves in the 10^{-2} to 10^{-1} range of α_o is still quite sensitive to the velocity structure of Q_{ea}, even though electron-ion collisions dominate in this range. On the basis of these results, it is felt that the consistent trend displayed by the calculated and experimental data of Fig. 7 is evidence that the numerically determined family of ν^*_{eff} curves represents a qualitative and quantitative picture of dc electron-cesium heavy particle momentum transfer collisional effects in the 500 to 5000°K range of electron temperature and the 10^{-4} to 10^{-1} degree of ionization range.

Theory

Although even approximate theoretical calculations leading to the electron-atom cross section are quite complicated, it is of interest to analyze some of the more recent theoretical results in light of the conclusions drawn from

the experimental and analytical results of this work. The electron-cesium atom elastic scattering and momentum transfer cross sections were calculated theoretically by Stone and Reitz[23] and more recently by Crown and Russek.[24] The results of this work are shown in Fig. 8. As is apparent from the figure, a pronounced Ramsauer-like velocity structure in the cross section is predicted which is the result of atomic polarization effects. Numerical experimentation in Refs. 23 and 24 indicated considerable sensitivity to the exact choice of the polarizability used in the calculations, and therefore, the curves of Fig. 8 are thought to represent only the general qualitative and semiquantitative behavior of the electron-atom cross section in the electron velocity range covered. With this consideration the theoretical predictions of a polarization minimum in the range of a few tenths of an electron volt are consistent with the interpretation of this paper. Also shown in Fig. 8 is the total elastic scattering cross section as determined by Brode[25] using an electron beam technique. Brode's results indicate structure in the cross section near the first excitation level which has been attributed to coupling between the ground state and the first excited states.[26] The location of this resonance at the first excitation level may be fortuitous, however, due to the difficulties associated with exact determination of beam energies in the low energy regime, particularly in cesium systems. In addition, the calculations of Refs. 23 and 24 suggest the possibility of significant quantitative differences between the total and momentum transfer cross sections as a result of nonisotropic scattering. If this is the case, the use of the total elastic scattering cross section to calculate plasma transport effects could lead to serious errors. Nevertheless, the comparison of available experimental and theoretical results as described above reveals considerable evidence in support of the existence of structure in the velocity dependence of the electron-cesium atom elastic scattering cross section in the electron energy range from 0.1 to 1.0 eV.

7. Conclusions

The effective momentum transfer collision frequency for electrons in cesium plasmas has been found from these measurements to depend significantly on the degree of ionization existing in the plasma for degrees of ionization greater than about 3×10^{-4}. An analysis of the experimental results indicates that electron-ion collisions first become noticeable for degrees of ionization of approximately 10^{-4}, contribute significantly to collisional effects at about 10^{-3}, and dominate momentum transfer collision processes for degrees of ionization in the 10^{-2} range and above. In contrast, for degrees of ionization in the 10^{-3} to 10^{-1} range and electron temperatures in the 2000 to 3000°K range, the temperature dependence of the effective collision frequency has been found to be less significant than the variation due to changes in the degree of ionization. For a fixed degree of ionization in the 10^{-3} to 10^{-1} range, the change in the effective collision frequency due to an electron temperature variation of several hundred degrees in the 2000 to 3000°K range is less than 25 per cent. Therefore, in converter plasmas in which the degree of ionization is typically in the range

from 10^{-3} to 10^{-1}, the most important effect to consider in the analysis of electron transport through the plasma is the contribution of electron-ion collisional interactions to the effective momentum transfer collision frequency.

Appendix I. Effective Collision Frequency for High Degrees of Ionization

In one of an excellent series of papers appearing in the early thirties, Boeckner and Mohler[21] inferred an effective electron-cesium atom cross section from measurements of electron mobility in a highly ionized cesium arc discharge plasma. Their technique relied upon the successful extrapolation of experimental data obtained at high degrees of ionization ($\alpha > 10^{-3}$) to regions of low degrees of ionization ($\alpha < 10^{-4}$) so that the electron-atom collisional effects could be extracted from the data independent of any electron-ion contribution. However, an error in the electron density measured with electrostatic probes was discovered.[27] Nolan and Phelps[28] have applied a pressure-dependent correction to account for this error and, in addition, have included a vapor pressure correction to the original data of Ref. 21. Having applied this correction, they have reprocessed Boeckner and Mohler's extrapolated data and have reported a corrected value in ν^*_{eff} form of approximately 1×10^{-12} $sec^{-1}m^3$. This value is assumed to be representative of electron-atom collisions in the 2000 to 3000°K range of electron temperatures. The microwave and electrostatic probe measurements carried out in conjunction with this investigation under conditions similar to those of Ref. 21 support the magnitude of the correction applied by Nolan and Phelps. However, it has been found that the proper correction is dependent on discharge current as well as pressure because of the strong dependence of effective collision frequency on degree of ionization. Such behavior is consistent with the prediction of Waymouth's probe perturbation theory.[8] In addition, since electron-ion collisions begin to influence the effective collision frequency for degrees of ionization as low as 10^{-4}, it is felt that an accurate extrapolation over one to two decades in degree of ionization in order to determine ν^*_{eff} for essentially the zero degree of ionization case is not possible. Using the original data of Boeckner and Mohler (Fig. 1, Ref. 21), correction factors based on the microwave and probe data obtained in conjunction with this investigation and the vapor pressure correction of Nolan and Phelps, a revised set of data has been obtained. Boeckner and Mohler's corrected $\bar{A}/N_o$ (an effective cross section) data are shown in Fig. 9 and are plotted as a function of electron density as in the original reference. The family of curves drawn through the data was chosen to blend smoothly into the $\bar{A}/N_o$ values corresponding to the ν^*_{eff} data of this paper (Fig. 7) for a degree of ionization of 10^{-4} which is essentially the range where electron-ion effects are no longer important. The dotted lines in the figure represent constant degree of ionization lines in the 10^{-4} to 10^{-1} range. While a few of Boeckner and Mohler's data points were obtained for a degree of ionization as low as 10^{-3}, for the most part their measurements were made in the 10^{-2} to 10^{-1} range. Consequently, an accurate extrapolation, based on Boeckner and Mohler's data alone, to degrees of ionization of 10^{-4} and below would be extremely difficult. As an alternative, the absolute magnitude of the Boeckner and Mohler data was used to determine ν^*_{eff} in the 10^{-3} to 10^{-1} range of α_o for comparison with the work of other investigators. Examination of Figs. 7 and 9 reveals that the corrected Boeckner and Mohler data are consistent with those of other workers.

Terlouw has made measurements of plasma resistivity on a cesium arc discharge similar to the discharge used in Ref. 21. Microwave and electrostatic probe techniques were used to determine the plasma properties in the discharge. From the measurements of resistivity, the average electron density, and the atom density, it is possible to determine ν^*_{eff}. These results are presented in Fig. 10 as a function of degree of ionization. Once again the significant influence on ν^*_{eff} of Coulomb collisions is apparent. From the data of Fig. 10, ν^*_{eff} was determined for degrees of ionization corresponding to those of this work and the Boeckner and Mohler data. These results appear in Fig. 7 for comparison with the data of other workers.

CESIUM ION ATOM TOTAL COLLISION PROBABILITY MEASUREMENTS

1. Introduction

In order to obtain an insight into the mechanism responsible for the production of the volume ionization which exists in the neutralization plasma of arc-mode thermionic converters, the loss rate of ions from the plasma must be accurately shown. In diffusion-dominated plasmas the loss rate of ions is determined by their mobility. Preliminary measurements of the total collision cross section of cesium ions interacting with cesium atoms have been made over the energy range of 0.12 to 9.7 eV using a modified Ramsauer experiment under Contract NASr-112. The present investigations are extensions of this work. Knowledge of the cesium ion mobility provides an insight not only into the loss rate of ions from the plasma but also of the possible energy transfer mechanisms from the plasma to the emitter surface which can cause a significant change in the emitter surface work function.

Extrapolations of high-energy charge exchange information reported in the literature to the energy range of interest in the converter have been made by Sheldon.[29] These extrapolations, which have included approximations to account for polarization effects at energies below 1.0 eV, vary by as much as an order of magnitude. The lowest energy at which charge exchange cross sections have been measured using beam techniques is 6.0 eV (Ref. 30). Due to the nature of the experimental apparatus employed in these charge exchange measurements, no correction for contact potential effects could be made in these investigations. Therefore, the reported charge exchange cross-section information at an energy of 6.0 eV can be in serious error due to a large uncertainty in the determination of the energy of the ion beam. Other attempts have been made to determine cesium ion mobilities by observing the decay rate of the afterglow of a cesium plasma.[12,31] In these measurements no attempt was made to determine the nature of the ion energy distribution, and in some cases, the dominant ionic species existing in the plasma was not identified. In the present experiment, which uses a modified Ramsauer beam technique, contact potential effects have been eliminated from the measurement by employing an electroformed collision chamber. The energy, as well as the species of the ion beam interacting with the cesium atoms in the collision chamber, has been positively identified in these investigations. The one limitation of this measurement has been that the cross section determined by these techniques is a quasi total collision cross section which is dependent on the resolution of the system. However, completely classical techniques have been successfully used to analyze the total collision cross-section information to determine the magnitude of the charge exchange contribution.

2. Description of Experiment and Measurement Techniques

Beam techniques have been employed by many investigators to determine ion-atom collision probabilities. The most noteworthy of these measurements are the investigations conducted by Ramsauer,[32] the results of which are quoted in the English literature incorrectly. The use of beam techniques at energies less than several electron volts is seriously limited by uncertainties in the determination of the ion beam energy due to contact potential effects which are particularly severe in cesium environments. In this investigation, as in the earlier Ramsauer beam experiments, the total collision cross section is determined by measuring the attenuation of an ion beam of known energy produced by an increase in collision chamber neutral particle density. In the present cesium ion-atom total collision cross-section measurements, contact potential problems were eliminated by employing an electroformed collision chamber in which no metal interfaces exist that can give rise to possible contact potential effects. Shown in Fig. 11 is a schematic drawing of the system employed in these measurements. Cesium ions are produced by diffusing cesium atoms through a porous tungsten cap which is maintained at a temperature of approximately 1200°C. Standard accelerating-decelerating ion optics are employed to extract ions from the porous cap. Two sets of deflection plates, one located immediately adjacent to the ion gun and the other located directly in front of the collision chamber entrance slit, are employed to align the ion beam with the collision chamber. A magnetic field applied perpendicular to the plane of the schematic is employed to energy-select ions produced on the porous tungsten cap. The collision chamber is designed so that the entrance and exit slits and the necked-down portion in the center of the collision chamber serve as three degrees of restraint which define the radius of a circle. The energy of the ion beam passing through the collision chamber is uniquely determined from a knowledge of chamber geometry and the magnitude of the applied magnetic field. Re-entrant type entrance and exit slits are employed on the collision chamber to prevent external electric fields from penetrating into the chamber, which can seriously perturb ion trajectories. In these measurements the energy of the ion beam is uniquely determined only while the beam is within the collision chamber. Prior to entering the chamber the beam energy can be significantly altered by the accelerating-decelerating optics system. Similarly once the beam exits the collision chamber, an accelerating plate is used to deflect the ion beam off its initial trajectory in the magnetic field and into an electron multiplier. Only a knowledge of the energy of the ion beam while it is in the collision chamber is essential in the measurement. The measured total collision cross section is composed of elastic scattering events that produce deflections of the ion beam greater than 0.0074 radians and essentially all charge exchange interactions. All charge exchange collisions are measured in this system because the newly formed ions produced by the interaction have incorrect trajectories in the magnetic field to exit the chamber. The attenuation of the ion beam can be predicted by

$$I = I_o e^{-p_o P_t x} \qquad (11)$$

where

I is the ion beam current exiting the collision chamber for a finite pressure in the chamber;
I_o is the ion beam current exiting the collision chamber for zero pressure in the chamber;
p_o is the pressure in the collision chamber reduced to 273^{o} K;
P_t is the number of collisions per cm of path per mm of pressure; and
x is the path length of the ion beam through the chamber.

The total collision cross section is determined by gradually increasing the cesium pressure in the collision chamber and measuring the number of particles missing from the ion beam produced by the increase in chamber pressure. Also shown in the schematic drawing of Fig. 11 is a surface ionization gauge which is designed so that it can be moved to a position directly in front of the exit slit of the electroformed collision chamber. The surface ionization gauge was used to obtain a cross calibration between the cesium reservoir temperature and the density of neutral atoms within the collision chamber. The length of the collision chamber was chosen so that the operating cesium pressure in the chamber ranged from 10^{-7} to 10^{-5} mm Hg. Therefore, at this pressure level the exit and entrance slits on the collision chamber were always operating in the free molecular flow regime. The operating pressure range of the vacuum system in the multiplier was always several orders of magnitude lower than the cesium pressure in the chamber so that additional collision events produced by interactions of the ion beam with the background gas in the system could not produce spurious results. As Eq. 11 indicates, the cross section can be determined by making a relative measurement of the attenuation of the ion beam intensity and an absolute measurement of the cesium pressure existing in the collision chamber.

Method of Determining Ion Beam Energy

As outlined in the previous section, the ion beam energy is determined uniquely in these measurements from the radius of curvature determined by the geometry of the electroformed collision chamber and the magnitude of the applied magnetic field. Since the collision chamber slits have a finite width, the ion beam focused through the collision chamber has a finite energy width. For the collision chamber used in these investigations, the geometrical energy resolution of the chamber is essentially the center energy $E \pm \Delta E$, where ΔE is approximately $\pm$ 8 per cent of the center energy E. Shown in Figs. 12 through 18 are typical ion beam distributions obtained with this system. Shown in Fig. 19 is a comparison between theoretically calculated and experimentally measured ion beam energies at half-width. As can be seen from this figure, the agreement between theory and experiment is extremely good. The determination of the absolute magnitude of the ion beam energy is dependent upon the absolute magnitude of the applied magnetic field and the geometry of the collision chamber.

The collision chamber geometry is determined by making careful measurements prior to plating of the dimensions of the aluminum mandrel over which the copper collision chamber is electroformed. These measurements include shadowgraphing the shape of the mandrel so that the thickness of the copper plate can be determined absolutely upon completion of the electroforming of the chamber. After the aluminum mandrel is removed with caustic solutions from the electroformed chamber, X rays are taken to determine the actual build-up of copper in various portions of the chamber and also to inspect the chamber for possible traces of aluminum from the mandrel which have not been entirely removed by the caustic solutions. Shown in Fig. 20 is a typical X ray obtained of an electroformed collision chamber. As can be seen in this figure, the width of the collision chamber slits is clearly defined as is the width of the necked-down portion in the center of the chamber. Excellent agreement has been obtained between the width of the necked-down portion determined by measuring the thickness of the aluminum mandrel prior to plating and the thickness of this portion determined by X-ray measurements.

Hall probes were used to align the Helmholtz coils employed to generate the magnetic field in these measurements. To insure that proper alignment was achieved between the coils and the collision chamber, a jig which represented the trajectory of the ion beam within the collision chamber was mounted in the vacuum tank. Hall probes were positioned along the jig to determine the magnetic field intensity at various locations along the ion beam trajectory. The spatial resolution of probes employed in these measurements was one eighth of an inch. This is large in comparison to the finite slit width of the chamber which runs from 0.020 to 0.030 of an inch depending upon the particular chamber employed in the measurements. However, Hall probes were used to determine the average field and for alignment purposes since it was not anticipated that a widely diverging magnetic field would be produced by the Helmholtz coil configuration and since magnetic materials were eliminated from critical regions of the experiment. In earlier measurements the absolute magnitude to which the Hall probes could be calibrated over the energy range from approximately 50 to 700 gauss was $\pm$ 3 per cent. To increase the accuracy in these measurements, a rotating-field gauss meter was employed. The absolute accuracy of this system was $\pm$ 0.1 per cent or 2 gauss. The accuracy of the rotating field gauss meter at low magnetic fields was improved by employing a null balance technique with a galvanometer to determine the magnitude of the field. The rotating-field gauss meter was calibrated against a 100-gauss laboratory standard which had an accuracy of $\pm$ 1 gauss at 100 gauss. The rotating-field gauss meter coil employed in these measurements encompasses a volume with a total diameter of 0.125 in. As has been previously indicated, only the magnetic field along the trajectory of the ion beam within the collision chamber is essential in the determination of ion beam energies. The accuracy of the determination of the center-line energy from these calibrations is $\pm$ 2 per cent at 0.21 eV. In subsequent measurements improved accuracy in the magnetic field calibration was obtained by using a three-axis Hall probe and a laboratory standard calibration coil which was certified by the National

Bureau of Standards. In the latest cross-section measurements the absolute accuracy of the magnetic field determination was ± 1 per cent.

The most important aspect of the determination of the ion beam energy in this system which makes it unique in comparison to other techniques is the use of an electroformed collision chamber to eliminate uncertainties in the energy determination produced by contact potential effects. Contact potential effects produced by preferential adsorption of cesium on electrode surfaces can significantly change the work functions of these surfaces, thereby producing large uncertainties in ion beam energy if retarding potential techniques are used.

Shown in Fig. 21 is a comparison of ion beam energies determined by using electroformed collision chamber techniques with energies determined using essentially retarding potential techniques. In this figure the results for two different experimental conditions are presented. For one set of measurements, which are represented by circular data points, the variation in the energy of the ion beam determined from the potential applied to the ionizer cap to the energy of the beam determined from the magnetic field energy analysis is approximately 0.25 eV across the entire energy range. By maintaining all conditions constant in the experiment and changing the cesium feed rate to the ionizer cap surface, thereby reducing the work function, the difference in the energy determined by the two techniques is once again constant but in this case is displaced by approximately 2.5 eV. This data is represented by the triangular points in Fig. 21. The effect of contact potentials which is so vividly illustrated by these results can be responsible for the wide discrepancy in cross-section information obtained by beam techniques at energies below 10.0 eV.

Cross-Section Determinations

The method employed to determine total collision cross sections in these investigations is to increase the cesium pressure in the collision chamber by increasing the temperature of the cesium well. Accurate control and correct determination of the cesium well temperature is one of the most difficult aspects of the experiment. From cross-section measurements with target gases, such as argon and nitrogen, it was found that the response time of the ion beam attenuation to changes in collision chamber pressure was essentially instantaneous. In the cesium measurements the pressure of cesium in the upper collision chamber was determined by measuring the temperature of the coldest spot in the cesium reservoir. The cesium reservoir system is shown schematically in Fig. 22. In earlier cross-section measurements difficulty was encountered in determining the true cesium pressure from temperature measurements of the cold spot in the cesium reservoir. This same problem was encountered by Sheldon and Manista[33] and Nolan and Phelps.[34] In addition, both groups of investigators reported that times on the order of a half hour were required to establish pressure equilibrium within the system once a temperature change occured in the cesium reservoir. These results were contrary to the observations made in the initial cesium ion-cesium atom cross-section

measurements in which it was found that a temperature change in the cesium reservoir reflected itself almost instantaneously as a change in the magnitude of the attenuated ion beam current. In addition, once this initial change occurred, no subsequent decrease in the ion beam current level was observed over long periods of time. Since the measurement conducted with an attenuated ion beam is essentially an indirect measurement and since the absolute accuracy of the cross-section determination is directly related to the accuracy of the pressure measurement, further experimental measurements were conducted to determine directly the neutral density existing in the collision chamber for various operating conditions. Shown schematically in Fig. 23 is a neutral efflux source patterned after the geometry of the electroformed collision chamber. Several tests were conducted with this source to determine times required for equilibration of the neutral density. The neutral efflux source was composed of two chambers, one which was operated at low temperatures and served as a cesium reservoir for the system. The second chamber, which was operated at a higher temperature and had a small diameter hole in the upper surface, acted as the superheated chamber in the ion-atom cross-section measurements. In these investigations the neutral cesium efflux emanating from a small diameter hole in the chamber was measured with a surface ionization gauge. Shown in Fig. 24 is the variation with time of the neutral efflux of cesium atoms effusing from the small hole in the high-temperature chamber. On the basis of these measurements in which only relatively coarse temperature control could be maintained over the cesium reservoir and the high-temperature chamber, it was found that cesium pressure changes occurred over a shorter time scale than that reported by other investigators. However, it was found in the course of these measurements that if all the cesium which effused from the small hole in the collision chamber was not directly trapped, the background pressure of neutral cesium in the vacuum system increased with operating time and collision chamber pressure. This increase in the neutral cesium pressure in the vacuum system appeared as an increase in the background ion current level measured by the surface ionization gauge detector. For conditions of low cesium pressure in the collision chamber, the increase in neutral cesium background due to the presence of untrapped cesium in the system gave the appearance of a strong hysteresis effect when the cesium reservoir was temperature-cycled. In addition, since the untrapped neutral cesium was gradually pumped from the system, the surface ionization gauge data at low collision chamber pressures also exhibited what appeared to be a long-time constant for the system to reach equilibrium. In reality this long-time constant was not associated with the time required to change the neutral cesium density in the collision chamber, but rather it was the time constant associated with reducing the neutral cesium background pressure level in the vacuum system. With the addition of the proper amount of cryopumping to the system so that all the cesium which effused from the small hole in the collision chamber was directly trapped, it was found that the cesium efflux measurements were completely reproducible in this mock-up system and that there was no hysteresis as a result of temperature cycling of the cesium reservoir. Results of these measurements are shown in Fig. 25. Calculation of the neutral cesium efflux from this mock-up system based on the hole size in the collision

chamber and the vapor pressure data of Kubaschewski and Evans[35] was in excellent agreement with the experimental results. These results are shown in Fig. 26. A series of several measurements were taken with this system operating at various temperature levels of the superheat chamber of the system. The over-all variation in the results as shown in Fig. 26 is on the order of ± 15 per cent. In the course of these measurements it was found that it was extremely difficult to obtain accurate readings from the thermocouples positioned at various points. One of the major problems in using thermocouples for precise temperature information is that small contact emf's are generated at the connecting junctions of the thermocouples. Based on information from the National Bureau of Standards the resolution and absolute accuracy to which platinum resistors can be calibrated is approximately three orders of magnitude greater for the temperature range of these measurements than for thermocouples. The criticality of accurate temperature determination of the cesium reservoir is more vividly illustrated by the error analysis presented in Fig. 27. An error of ± 0.1°C across the pressure range of these measurements results in a 3 per cent error in the determination of the pressure. For inaccuracies larger than ± 0.1°C the inaccuracy of the pressure determination rises drastically. Therefore, on this basis platinum resistors were substituted for thermocouples as temperature sensors in the cesium reservoir. The design of the cesium reservoir system was modified so that a solid copper block constituted the region in which the puddle of liquid cesium was placed. In order to accurately control the temperature of this copper block, a variable temperature controller with the capability of maintaining temperatures to within 0.1°C was constructed. A photograph of the temperature controller and ion cross-section apparatus is shown in Fig. 28. The dynamic capability of the controller allowed temperature variations on the order of 5°C to be achieved in about one minute. After two to three minutes the system was stable to within ± 0.1°C. The platinum resistors located in the cesium reservoir were calibrated against a quartz vibrating fiber temperature-sensing element. The quartz fiber system which has resolution far in excess of the platinum resistors is calibrated by the manufacturer at seven triple points throughout the range of interest and was subsequently calibrated at the Laboratories against two triple points to insure accuracy in the temperature determination. With this system and a surface ionization gauge which was located in a pump port adjacent to the ion multiplier, as shown schematically in Fig. 11, measurements of the cesium efflux from the collision chamber were made in the actual system. Shown in Fig. 29 is a typical spatial distribution obtained from the surface ionization gauge. Measurements of the cesium efflux from the chamber as a function of reservoir temperature are shown in Fig. 30. The displacement of the measured efflux from the theoretical value shown in Fig. 30 amounts to approximately 30 per cent at the higher operating pressures. These measurements also show that there is no inherent hysteresis in the establishment of the neutral pressure in the collision chamber. Shown in Fig. 31 is the variation of cesium pressure with reservoir temperature and time. The results of this measurement indicate that the cesium pressure in the collision chamber responds on the order of a few seconds to temperature changes in the reservoir. In addition, the time required to establish equilibrium is on the order of several minutes rather than a half hour.

One additional problem that has been experienced in the pressure determination measurements is accurate control of the location of the cold spot in the reservoir. In earlier cross-section measurements it was found that cold spots existed in the feed line that was used to introduce cesium into the collision chamber. In these latest measurements the cesium is introduced into the chamber through a small hole in the reservoir sidewall with a stainless steel hypodermic tube. Once an initial charge of cesium is placed in the chamber, the stainless steel hypodermic tube is withdrawn from the reservoir, and a trap door closes over the hole. By this technique, it has been found that it is possible to eliminate problems associated with additional cold spots in various portions of the reservoir cesium feed system.

3. Analysis of Cross-Section Data

Since ion-atom cross sections at thermal energies are being measured, the experimental results can no longer be interpreted in terms of a monoenergetic beam of ions interacting with a gas of fixed target atoms.

A computer program has been written which extracts the total ion-atom cross section from the average cross section as measured in the modified Ramsauer experiment. The experimentally measured cross section is really the true cross section as a function of relative velocity of the interacting particles, $Q(V_r)$, averaged over the velocity distributions of the beam particles $f_b(V_b)$, of the gas atoms $f_g(V_g)$, and over the ratio of the relative velocity of the encounter to the beam particle velocity, V_r/V_b. The last term, V_r/V_b, converts the number of collisions per second to the number of collisions per unit path length of the ion beam. Therefore, the averaged cross section is given by

$$\overline{Q\left(\frac{V_r}{V_b}\right)} = \frac{\int f_b(V_b)\, f_g(V_g) \frac{V_r}{V_b} Q(V_r)\, d^3 V_g\, d^3 V_b}{\int f_b(V_b)\, f_g(V_g)\, d^3 V_g\, d^3 V_b} \qquad (12)$$

which is similar to a form derived by Berkling, et al.[36] By assuming a true cross section of the form $Q(V_r) = \alpha/V_r^{\beta}$ and knowing $f_b(V_b)$ and $f_g(V_g)$, a double numerical integration may be performed for a particular β giving $\overline{Q}$ in terms of α. The α may then be adjusted to give the least squares fit of $\overline{Q}$ to the experimental data. Computing $\overline{Q}$ for a series of β's, a best least squares fit may be obtained. This gives the best over-all values for α and β or equivalently the best cross section $Q(V_r) = \alpha/V_r^{\beta}$.

Since the slits on the collision chamber have a finite width, a range of ion velocities pass through the chamber for any applied magnetic field. A calculation based on the geometry of the collision chamber shows that the window for ion velocities is from $0.96\ V_c$ to $1.04\ V_c$, where V_c is the velocity of the particle which moves through the centers of the three slits, that is, on a radius of

7.63 cm. Therefore, the size of the window is directly proportional to the center energy of the beam. The limits of the window are used as the limits of integration for the component of the velocity in the direction of the beam current.

The ion beam is formed in an accelerating-decelerating-focusing system which is space-charge limited. Depending on whether the ions in the beam have enough time to thermalize, the velocity distribution function of the beam may range from an accelerated half-Maxwellian[37] to a Maxwell-Boltzmann distribution moving with a drift velocity. Based on the estimated ion number density in the beam of 10^6 to $10^8/m^3$, and an ion temperature of 0.1 eV, a thermalization time of about 10^{-1} to 10^{-3} sec may be calculated from Spitzer's formula.[38] The ions in the beam spend from 10^{-2} to 10^{-3} sec in transit through the 10-cm path length of the collision chamber. For these conditions at least some thermalization should be expected. The beam distribution may also be affected by space-charge effects and by high thermal velocities parallel to the magnetic field removing some ions from the beam. Ion beam current distributions were calculated on the basis of an accelerated half-Maxwellian and also on the basis of a Maxwellian moving with a drift velocity. By varying the limits of integration, plots of beam current as a function of energy were obtained for various center energies. Comparing the energy widths at half-height of the ion current distribution with the experimentally measured half-widths, it was observed that the accelerated half-Maxwellian gave a much closer fit to the experimental data than did the drifting Maxwellian which gave half-widths much too wide. The results which indicate that the accelerated half-Maxwellian should be used as the beam distribution function in this case are presented in Fig. 19.

$\overline{Q}$ was calculated for a series of β's. In all these calculations, $f_g(V_g)$ was assumed to be a Maxwellian distribution at the temperature of the collision chamber, and the beam distribution was assumed to be an accelerated half-Maxwellian. The value of β which gave the best least squares fit to the experimental data was 0.76; the α at this point was 7.16×10^5. Therefore, the cross section which best describes the experimental data on the basis of this analysis is

$$Q(V_r) = \frac{7.16 \times 10^5}{V_r^{0.76}} \text{ Å}^2 \qquad (13)$$

The results of this analysis are presented in Fig. 32.

4. Analysis of Total Scattering Cross-Section Data

In the anlaysis of the total collision cross-section information, as has been previously outlined,[39] the diffusion cross section used in the mobility calculations was determined by calculating classically the elastic contribution

to the measured total collision cross section. By subtracting this elastic contribution from the measured total collision cross section, the charge exchange contribution can be determined. In this analysis an inverse fourth power interaction potential was assumed to hold for the lower energy scattering interactions under investigation in the ion-atom measurements. The validity of this assumption as a result of the recent measurements reported by Menendez and Datz[40] is subject to considerable question. In the measurements of Menendez and Datz, it was found that a significant rainbowing effect occurred at relatively large scattering angles for cesium ions interacting with argon, krypton, and nitrogen. The presence of this rainbow in the experimental differential scattering cross section implies that the use of an inverse fourth power potential to describe the elastic scattering interaction at these low energies is undoubtedly incorrect. It has been suggested by Mason and Vanderslice[41] that a 4-6-12 type potential should be considered even for extremely low energy interactions, especially when dealing with relatively large particles, such as the cesium system. The general form of the potential used to calculate differential scattering cross sections is given by

$$Q(r) = \frac{\epsilon}{2}\left[(1+\gamma)\left(\frac{r_m}{\gamma}\right)^{12} - 4\gamma\left(\frac{r_m}{\gamma}\right)^{6} - 3(1-\gamma)\left(\frac{r_m}{\gamma}\right)^{4}\right] \qquad (14)$$

where

ϵ is the potential well depth;
γ is a strength parameter of the r^{-6} portion of the potential; and
r_m is equilibrium internuclear distance.

In Eq. 14 the r^{-4} term includes the charge-dipole and the charge-induced dipole interactions, and the r^{-6} term includes charge-quadrupole, charge-induced quadrupole, and induced dipole-induced dipole interactions. The last term in this expression which is the r^{-12} portion of the potential is the short-range repulsion term. When there is an interaction between two particles having the potential function of the type described in Eq. 14, in which there are both attractive and repulsive portions, there is a relative energy region in which rainbow phenomena will be observed in the angular scattering distribution. This effect will also significantly alter the magnitude of the differential scattering cross section. Calculations have been carried out to determine the differential elastic scattering cross section as a function of energy for the cesium system to see if any significant alteration in the magnitude of the predicted elastic scattering cross section would result from the inclusion of these additional terms in the interaction potential. In these calculations a value of 4.4 Å was used for the equilibrium internuclear distance. This value was obtained from the work of DeBoer[42] on the spectra of the cesium molecular system. A value of $\gamma = 0.5$ and a value of the polarizability of cesium equal to 52.3 Å^3 as determined from the measurements of Salop, et al.[43] were used to determine the value of the well depth, ϵ,

from the following expression:

$$3/2\,(1-\gamma)\,\epsilon r_m^4 = \frac{e^2\alpha}{2} \qquad (15)$$

Shown in Fig. 33 is the differential scattering cross section calculated for a relative interaction energy of 3.38 eV. As can be seen in this figure, there is a significant rainbowing effect observed in the differential scattering cross section at an angle of approximately 1.7 radians in the center-of-mass system. Shown in Fig. 34 is the calculated differential scattering cross section for a relative energy of 0.543 eV. In this case the rainbowing effect is not as readily apparent. However, as in the case of the higher energy calculation, the differential scattering cross section determined from the 4-6-12 interaction potential as a function of angle is significantly larger than that predicted with only an inverse fourth power interaction potential. The over-all contribution of this effect to the predicted elastic scattering cross section results in approximately a 15 per cent increase in the predicted elastic scattering cross-section values in the energy range of the cesium ion-cesium atom cross-section measurements. The magnitude of the cross section predicted using the 4-6-12 type interaction potential is sensitive to the values of r_m, ϵ, and γ used in the calculation. In the results presented, every attempt was made to use the most reliable estimates of these values. However, even on the basis of these results, it is seen that even though significant additional information can be obtained on the interaction potential in the cesium system, the use of a 4-6-12 interaction potential over the use of only a direct polarization interaction potential does not grossly change the magnitude of the value of the elastic scattering cross section.

5. Measurements and Results

Further measurements of low-energy total cesium ion-atom collision cross sections have been attempted with the newly designed cesium reservoir system which does not have an integrally connected cesium feed line. These measurements are being made in order to resolve the problems previously experienced with determining the actual operating cesium pressure in the collision chamber. The results of the initial studies under NASr-112 are shown in Fig. 35 as triangular points. The measurements which were completed at the end of last year under Contract NAS3-4171 are shown in this figure as circular points. In the initial measurements the attenuation curves did not exhibit exponential behavior at low pressures. Lack of complete exponential attenuation was attributed in these measurements to localized cold spots that existed only at low reservoir temperatures in various portions of the system. The second set of measurements which are in fairly good agreement with the initial results as shown in Fig. 35 were felt to be inaccurate due to problems encountered in the cold spots in the cesium feed line despite the fact that directly exponential attenuations were obtained in the measurements. Exhaustive studies with a surface ionization gauge detector in the past year of

the contract indicate that an accurate determination of the cesium pressure can be achieved in the present system. Despite this result in the latest measurements in all attenuation curves that were taken at energies below 1 eV, the ion beam failed to return to the unattenuated ion beam current level for zero pressure conditions in the collision chamber. Detailed surface ionization gauge measurements indicate that the pressure in the collision chamber was returning as would be predicted on the basis of the temperature behavior of the reservoir. The exact explanation for the failure to obtain reproducibility of the ion beam characteristics at this time is not completely understood because the system is essentially similar in design to the systems used in earlier measurements. It was noted, however, that even though the ionizer gun design was similar to those used in previous investigations, the focusing characteristics of the ion beam were slightly different. One possible explanation for this lack of reproducibility in the reverse pressure direction can be that a small undetected plasma was present in the gun optics between various electrodes in the system. If a plasma were present, this would be sufficient to cause unreproducibility in the characteristics of the ion gun that would be strongly pressure dependent and would be drastically affected by small changes in the ambient cesium background pressure. Further investigation of this effect is definitely warranted in view of the fact that it has been possible with previous gun assemblies to successfully produce ion beams with energies as low as .058 eV.

ELECTRON-CESIUM ATOM TOTAL COLLISION CROSS-SECTION MEASUREMENTS

1. Introduction

The measurements described in the first section of this report indicate that the electron-cesium atom momentum transfer cross section has a very strong velocity dependence in the energy range from 0.2 to 0.6 eV. Although it has become commonplace to draw a direct comparison between momentum transfer and total cross-section data, such comparison is strictly correct only when the angular dependence of the differential scattering cross section is very weak. Since swarm techniques are particularly insensitive to rapid variations in the cross section, in order to further investigate the velocity structure of the electron-cesium atom cross section in detail, monoenergetic beam techniques must be used. Momentum transfer cross-section information can be determined from beam-type measurements by first determining the total scattering cross section and then determining the differential scattering cross section. The advantage of conducting two measurements, one to determine the total cross section and the second to determine the differential scattering cross section, is that only a relative measure of the charge particle beam intensity is needed in order to determine the cross section.

In the past the problems which have limited the use of low-energy beam techniques in electron-atom measurements have been three-fold: 1) Extremely low magnetic energy-selection fields are required in order to maintain reasonable dimensions in the experimental apparatus. The usual operating magnetic energy-analyzing field intensity in these systems is on the order of or below the earth's magnetic field. 2) Due to the low beam energies, the beam current level is very low in intensity. Therefore, sophisticated detectors must be employed in these measurements. 3) In cesium measurements, contact potential effects, which are normally difficult to overcome in conventional systems, are even more severe due to the fact that cesium readily adsorbs on surfaces producing drastic work function changes and can also result in significant thermionic emission from surfaces at relatively low temperatures.

2. Description of Experiment and Measurement Techniques

A beam measurement of electron total cross sections in cesium was reported by Brode over thirty years ago.[25] In this work the effects of contact potentials could not be completely eliminated from the measurements. Therefore, it would not be surprising to find in the low energy range (below 1.0 eV) that the electron total cross section could vary significantly from that reported by Brode due to inaccuracies in the technique used to determine the energy of the electron beam. In addition to contact potential problems which can produce uncertainties in the beam energy determination, there can also be a large uncertainty

introduced into the measurements by the techniques used to determine the absolute intensity of the magnetic energy-analyzing field. In the total cross-section measurements conducted in this investigation, metal interfaces, which can give rise to contact potential effects, were eliminated by employing an electroformed collision chamber. Shown in Fig. 36 is a schematic drawing of the system employed in these measurements. A standard indirectly heated cathode, which is maintained at a temperature of less than 1000°C is used to produce electrons which are focused into the collision chamber with a series of accelerating-decelerating electron optics and two sets of deflection plates. The deflection plates are used to align the beam extracted from the cathode cap with the electroformed collision chamber. A magnetic field applied perpendicular to the plane of the schematic is employed to energy-select electrons. The collision chamber is designed so that the entrance and exit slits and the necked-down portion in the center of the chamber serve as three degrees of restraint which define the radius of a circle. The energy of the electron beam passing through the collision chamber is uniquely determined from a knowledge of chamber geometry and the magnitude of the applied magnetic field. Re-entrant type entrance and exit slits are employed to prevent external electric fields, which can seriously perturb electron trajectories, from penetrating into the chamber. In these measurements the energy of the electron beam is uniquely determined only while the beam is within the collision chamber. Prior to entering the chamber, the beam energy can be significantly altered by the electron gun optics of the system. Similarly, once the beam exits the collision chamber, the inverted Pierce gun optics used to deflect the electron beam from its initial trajectory in the magnetic field into a channel-type electron multiplier also alter the beam energy. Only a knowledge of the energy of the electron beam while it is in the collision chamber is crucial in the measurement. Since all scattering events producing a deflection of the electron beam of greater than 0.5 degrees are counted in these measurements as a collisional event, inelastic interactions are also measured. The attenuation of the electron beam is given by

$$I = I_o e^{-p_o P_t x} \tag{16}$$

where

- I is the electron beam current exiting the collision chamber for a finite pressure in the chamber;
- I_o is the electron beam current exiting the collision chamber for zero pressure in the chamber;
- p is the pressure in the collision chamber reduced to 273°K;
- P_t^o is the number of collisions per cm of path per mm of pressure, or total collision probability; and
- x is the path length in cm of the electron beam through the chamber.

The total collision cross section, related to P_t by a constant factor, is determined by gradually increasing the pressure in the collision chamber and

measuring the number of electrons missing from the electron beam as a result of the increase in chamber pressure. The length of the collision chamber was chosen so that the operating pressure regime was such that the entrance and exit slits are always operating in the free molecular flow regime. As indicated in Eq. 16, the total collision cross section can be determined by making a relative measurement of the attenuation of the electron beam intensity and an absolute measurement of the cesium pressure in the collision chamber.

Method of Determining Electron Beam Energy

As outlined previously, the electron beam energy is defined uniquely in these measurements by the radius of curvature determined by the geometry of the electroformed collision chamber and the magnitude of the applied magnetic field. As in the ion cross-section measurements, the collision chamber slits have a finite width, and therefore, the electron beam focused through the collision chamber has a finite energy width. For the collision chamber used in these investigations, the geometrical energy resolution of the chamber is the center energy $E \pm \Delta E$, where ΔE is $\pm$ 7 per cent of the center energy. In these measurements the actual generation and measurement of the magnetic-analyzing field is considerably more difficult than in the ion cross-section experiment. This is primarily due to the fact that the required magnitude of the energy-analyzing field is below the ambient level of the earth's magnetic field. As a further complication sharp spatial gradients in the earth's magnetic field intensity exist due to the structural steel and equipment in any laboratory building. In these measurements a zero magnetic field region along the trajectory of the electron beam was generated by the use of a combination of 8-foot diameter three-axis Helmholtz coils and a magnetic shield. As shown in the schematic in Fig. 36, the magnetic shield is located outside the vacuum tank of the experiment. Shown in Fig. 37 is a photograph of the physical layout inside the magnetic shield of the experiment depicted schematically in Fig. 36. Located directly outside the vacuum tank but within the shield is a set of Helmholtz coils which was used to produce the energy-analyzing field. The diameter and operating flux intensity of the analyzing-field Helmholtz coils, as well as the diameter and thickness of the shield, were chosen so that the field produced by the analyzing coils does not saturate the magnetic shield. The 8-foot diameter three-axis Helmholtz coils shown in Fig. 38 are used to reduce the level of the ambient magnetic field; the magnetic shield is used to reduce the effects of spatial gradients in the ambient field intensity; and the internal Helmholtz coils are used to generate the energy-selection field once zero ambient magnetic field conditions are established along the electron beam trajectory. To achieve one per cent accuracy in the energy determination, the ambient field intensity had to be maintained at a level below 1×10^{-3} gauss in the experiment. To detect and calibrate the magnetic field intensity in this system, single axis, highly directional magnetometers were employed. The method of calibrating the magnetometer was to achieve zero field conditions inside the magnetic shield with no experimental apparatus present. Zero magnetic field conditions were generated inside the shield by driving the three-axis Helmholtz coil system until

a condition was reached in which it was possible to rotate the directional magnetometer in any direction about a point inside the shield and detect no change greater than 10^{-4} gauss. With this technique, which is a relative measurement, it was possible to insure near zero ambient field conditions without obtaining a prior absolute calibration of the magnetometer system. Once zero field conditions were achieved, a standard solenoid of known area-turns was placed within the shield. The directional magnetometer was then calibrated by measuring the current to the solenoid, which had been calibrated and certified by the National Bureau of Standards to be accurate to within $\pm$ 0.5 per cent. Once four magnetometers were completely calibrated by this procedure, it was then possible to calibrate the energy-analyzing field. In anticipation of possible variations with time of the background magnetic field and possible changes in the shield characteristics, continuous sensing of the magnetic field existing within the shield as close to the electron trajectory as possible was deemed necessary. Therefore, a calibration was obtained between the magnetic field intensity existing on the electron beam trajectory in three mutually perpendicular directions and the intensity existing in three directions with similar orientation at another point within the system. By this technique it was possible to continuously adjust the system for various changes in both the environmental magnetic field as well as for changes produced in the shield characteristics. The absolute accuracy in the energy determination based on measurement of the magnetic field intensity is deemed to be within one per cent across the entire energy-operating regime. It was found in the course of fabricating the vacuum system and associated parts that only special materials that have been heat-treated could be safely employed in the system without producing gross perturbations in the magnetic field.

As presented in detail in the ion cross-section measurement section, the geometry of the collision chamber was carefully checked through the use of several experimental techniques which included shadowgraphing the collision chamber mandrel prior to electroplating, X-raying the electroformed collision chamber after plating, and obtaining high-resolution photographs of the collision chamber entrance and exit slits. Through the use of these techniques, it is felt that the dimensional tolerances can be held to well within one per cent.

Cross-Section Determinations

The method employed to determine the total collision cross section in these investigations is to increase the cesium pressure in the collision chamber and to measure the magnitude of the current exiting the chamber. With increases in chamber pressure, the electron current exiting the collision chamber decreases in a manner predicted by Eq. 16. From previous experience in the ion cross-section investigations, it has been found that control of cesium pressure through control of the cesium reservoir temperature is extremely difficult and can lead to large inaccuracies in the cross-section determination. The main origin of these inaccuracies is the exact determination of the location of the pool of liquid cesium within the reservoir and the accuracy to which the temperature of the reservoir

can be measured. Shown in Fig. 39 is a schematic of the electroformed collision chamber and cesium reservoir system. The cesium reservoir in this schematic is shown in a sectional view. A more detailed view of the actual physical chamber and reservoir system can be seen in Fig. 37. A large copper block with cooling coils embedded in the lower side, as shown in the schematic in Fig. 39, was used as the base of the cesium reservoir. This copper base was sealed to the stainless steel sidewalls of the reservoir with a knife-edge seal. By this technique all small pockets or enclosures were eliminated from the inner surface of the reservoir. Two platinum resistors, which were used for temperature sensing, were located approximately one-eighth inch from the top of the copper surface. Platinum resistors rather than thermocouples were used because of the higher resolution and accuracy that can be achieved in the operating temperature range of the measurements with platinum resistors. The platinum resistors were calibrated in the block in an isothermal condition against a calibration temperature transfer standard which was a quartz vibrating crystal that had been previously calibrated over the operating range of interest against seven triple points by the supplier and two triple points at the Laboratories. It was felt that this calibration procedure was warranted, since small errors in the temperature determination on the order of $0.1^{o}C$ can result in major errors in the determination of the true cesium pressure existing in the collision chamber. A better appreciation of the errors in the pressure determination based on the temperature of the reservoir can be obtained from the error analysis presented in Fig. 27. To eliminate previously experienced problems with control of the temperature of the cesium feed tube, which was used to introduce cesium into the reservoir, an entirely different approach was taken. Cesium was introduced through a small hole in the sidewall of the cesium reservoir with a hypodermic tube. After introduction of the cesium into the reservoir, the hypodermic tube was removed entirely from the reservoir system and maintained at an extremely low temperature. The small hole in the sidewall of the reservoir was closed through the use of a spring-actuated trap door.

3. Measurements and Results

With the system outlined in the previous sections, it has been possible to focus electron beams with energies as low as 0.09 eV through the electroformed collision chamber. Shown in Figs. 40 through 46 are typical electron energy distributions obtained with this system over the energy range from thermal to 2.5 eV. These distributions were obtained prior to introduction of cesium into the collision chamber reservoir of the system. After introduction of cesium into the system, it was found that the focusing characteristics of both the electron gun optics, as well as the electron multiplier optics, were drastically changed. This result was not entirely unexpected, since it was anticipated that various electrode surfaces would change work function upon adsorption of cesium, even though the operating pressure levels in the external parts of the vacuum system were in the 10^{-8} mm regime. Current levels in the electron system were found to be several orders of magnitude higher than ion beam current levels at comparable energies.

This can partially be attributed to space-charge limitation effects. However, it is also felt that the improvement in optics of the electron system, as well as the extremely uniform energy-analyzing fields used in this system, has also contributed to this increased current level.

In attempts to measure the total collision cross section, it was found that the electron current measured at the detector did not decrease in an exponential manner with pressure increases in the chamber as would be predicted by Eq. 16. In a detailed investigation of this problem, it was found that even though the collision chamber was operated in the range of 100 to 200°C above the cesium reservoir temperature, significant adsorption of cesium was occurring on the face of the collision chamber and isothermal heating block. This adsorption of cesium reduced the work function of the isothermal block and collision chamber and resulted in a small but finite amount of thermionic emission. This emission, which was found to be a strong function of cesium pressure, was sufficient to mask to a great extent the effects of scattering interactions occurring between the electron beam and the neutral cesium within the collision chamber. Even though the magnitude of the thermionic emission from the collision chamber block was found to be completely reproducible, it was not deemed advisable to attempt to obtain a calibration of this emission current and then simply subtract this from the total magnitude of the electron current detected at the multiplier. At present to overcome this problem, phase-sensitive-detection techniques are being employed to detect the electron beam current, which is modulated by applying an ac potential to the cathode surface, in the presence of a high or comparable background electron current being emitted from the collision chamber. The discovery of this effect which certainly should be present in any experiment of this nature raises further questions about the validity of earlier measurements.

REFERENCES

1. H. Dreicer, Phys. Rev. 117, 343 (1960).

2. D. H. Sampson and J. Enoch, Phys. of Fluids 6, 28 (1963).

3. H. Margenau, Phys. Rev. 69, 508 (1946).

4. D. J. Rose and M. Clark, Jr., "Plasmas and Controlled Fusion" published jointly by the M.I.T. Press and J. Wiley and Sons (1961), Chapter 8.

5. J. B. Taylor and I. Langmuir, Phys. Rev. 51, 753 (1937).

6. J. F. Waymouth, J. Appl. Phys. 30, 1404 (1959).

7. R. H. Bullis and W. J. Wiegand, Proceedings of the Twenty-third Annual Conference on Physical Electronics (M.I.T., Cambridge, Massachusetts, 1963).

8. J. F. Waymouth, Phys. of Fluids 7, 1843 (1964).

9. M. A. Heald and C. B. Wharton, "Plasma Diagnostics with Microwaves," J. Wiley and Sons (1965), Chapter 4.

10. E. C. Lary and R. A. Olson, AIAA Journal 1, 2513 (1963).

11. W. L. Nighan, Proceedings of the 1965 IEEE Thermionic Conversion Specialist Conference (San Diego, California).

12. C. L. Chen and M. Raether, Phys. Rev. 128, 2679 (1962).

13. R. K. Flavin and R. G. Meyerand, Jr., Proceedings of the 1963 IEEE Thermionic Conversion Specialist Conference (Gatlinburg, Tennessee).

14. L. P. Harris, J. Appl. Phys. 34, 2958 (1963).

15. C. Warner and L. K. Hansen, Proceedings of the Twenty-third Annual Conference on Physical Electronics (M.I.T., Cambridge, Massachusetts, 1963).

16. J. Bohdansky and R. Langpape, Proceedings of the Sixth International Conference on Ionization Phenomena in Gases, Paris, Vol. IV, 543 (1963).

17. D. N. Mirlin, G. E. Pikus, and V. G. Yur'ev, Sov. Phys.-Tech. Phys. 7, 559 (1962).

18. F. Rufeh, S. Kitrilakis, and D. Lieb, Proceedings of the 1965 IEEE Thermionic Conversion Specialist Conference (San Diego, California).

19. D. Wilkins and E. Gyftopoulos, Proceedings of the Twenty-sixth Annual Conference on Physical Electronics (M.I.T., Cambridge, Massachusetts, 1966).

20. D. Roehling, Adv. Energy Conv. 3, 69 (1963).

21. C. Boeckner and F. L. Mohler, BSJR 10, 357 (1933).

22. J. C. Terlouw, "Rijnhuizen Report 64-15," FOM Instituut voor Plasma Fysica, Rijnhuizen, Jutphaas, The Netherlands.

23. P. M. Stone and J. R. Reitz, Phys. Rev. 131, 2101 (1963).

24. J. C. Crown and A. Russek, Phys. Rev. 138, A669 (1965).

25. R. B. Brode, Phys. Rev. 34, 673 (1929).

26. A. Salmona and M. J. Seaton, Proc. Phys. Soc. (London) 77, 617 (1961).

27. F. L. Mohler, BSJR 17, 849 (1936).

28. J. F. Nolan and A. V. Phelps, Phys. Rev. 140, A792 (1965).

29. J. W. Sheldon, "Mobility of Positive Ions in Their Own Gas: Determination of Average Momentum-Transfer Cross Sections," NASA Technical Note D-2408, August, 1964.

30. R. M. Kushnir, B. M. Palyukh, and L. A. Sena, Bulletin of the Academy of Sciences, U. S. S. R. (Physics Series) 23, 995 (1959).

31. L. M. Chanin and R. D. Steen, Phys. Rev. 132, 2554-2557 (1963).

32. C. Ramsauer and O. Beeck, Ann. Physik 87, 1 (1928).

33. E. J. Manista and J. W. Sheldon, "Influence of Opposing Slits on Molecular Flow from an Isothermal Enclosure at Low Densities," NASA Technical Note D-2986, September, 1965.

34. J. F. Nolan and A. V. Phelps, Bull. Amer. Phys. Soc. 8, 445 (June, 1963).

35. O. Kubaschewski and E. L. Evans, "Metallurgical Thermochemistry," Pergamon Press, Third Edition, New York, 1958.

36. K. Berkling, R. Helbing, K. Kramer, H. Pauly, Ch. Schlier, and P. Toschek, Zeit. fur Physik 166, 406 (1962).

37. P. A. Lindsay, "Velocity Distribution in Electron Streams," ADVANCES IN ELECTRONICS AND ELECTRON PHYSICS XIII, (Edited by L. Marton, Academic Press, New York, 1960).

38. L. Spitzer, Jr., PHYSICS OF FULLY IONIZED GASES (Interscience Publishers, New York, 1962), Chapter 5.

39. R. H. Bullis, "The Measurement of Low-Energy Cesium Ion-Atom Cross Sections by Beam Techniques," presented at the Fourth International Conference on the Physics of Electronic and Atomic Collisions held in Quebec, Canada, on August 2 through 6, 1965.

40. M. G. Menendez and S. Datz, "Measurement of the Angular Distribution of Elastically Scattered Cs^+ Ions from Ar, Kr, and N_2," presented at the Fourth International Conference on the Physics of Electronic and Atomic Collisions held in Quebec, Canada, on August 2 through 6, 1965.

41. E. A. Mason and J. T. Vanderslice, J. Chem. Phys. 31, 594 (1959).

42. J. H. DeBoer, ELECTRON EMISSION AND ABSORPTION PHENOMENA, Cambridge Press, 1935, page 171, reprint University Microfilms, Ann Arbor, Michigan, 1962.

43. A. Salop, E. Pollack, and B. Bederson, Phys. Rev. 128, 2243 (1962).

LIST OF FIGURES

E-920243-27

FIG. 1

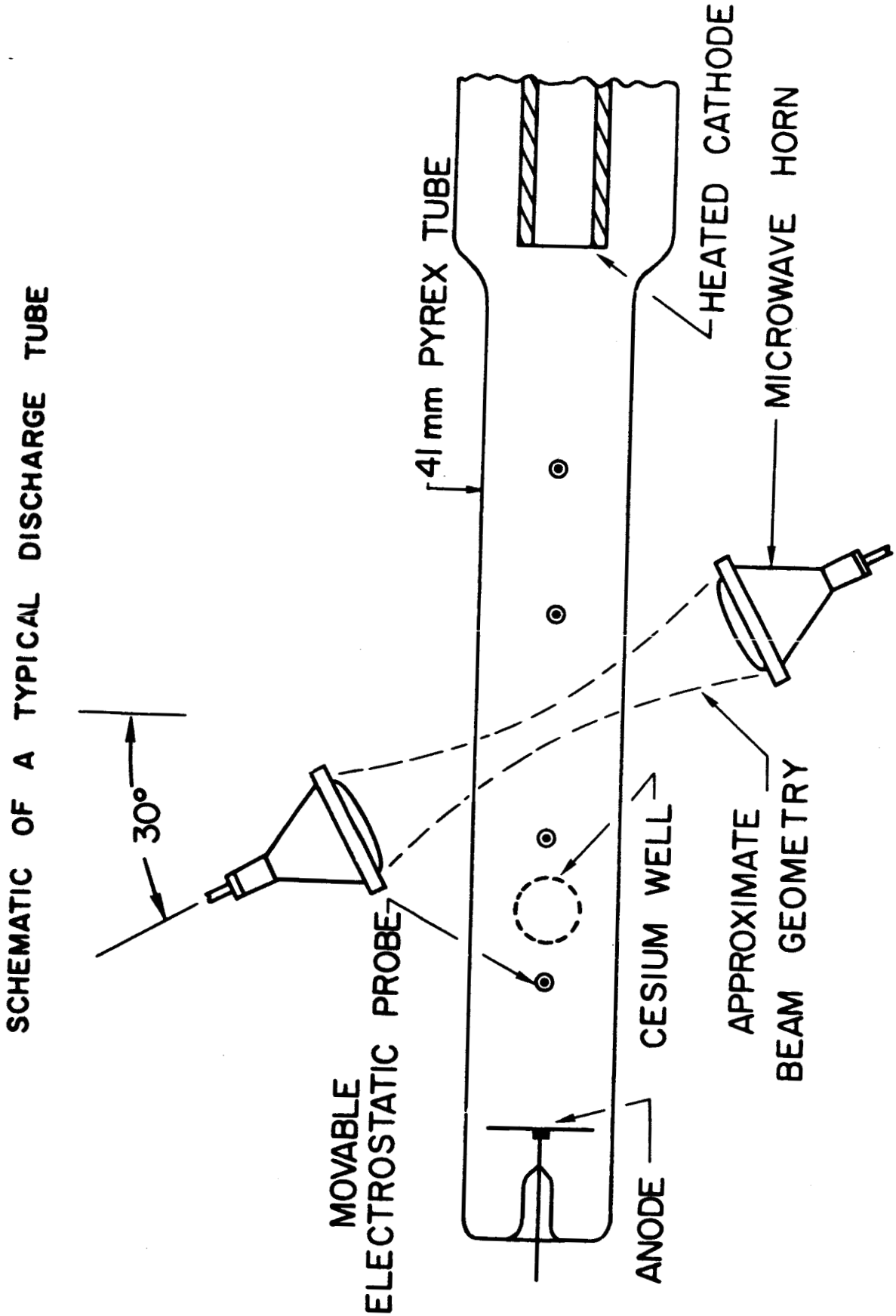

FIG. 2

PROBE CURRENT - VOLTAGE CHARACTERISTIC

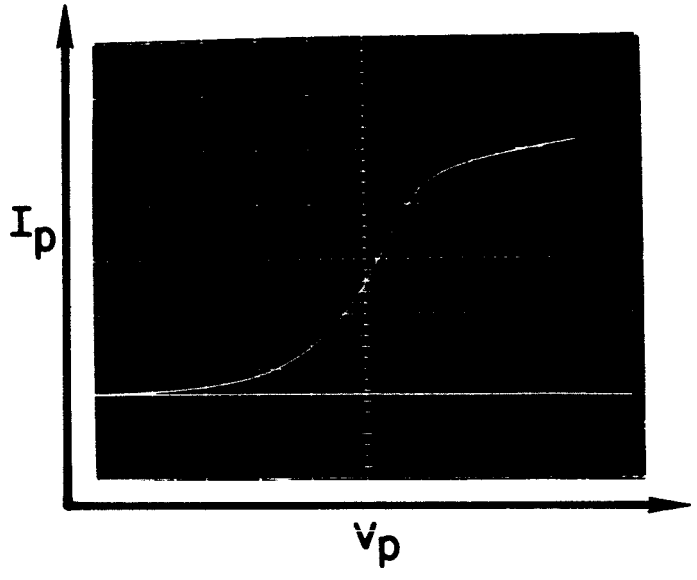

SCHEMATIC OF PULSE WAVEFORM

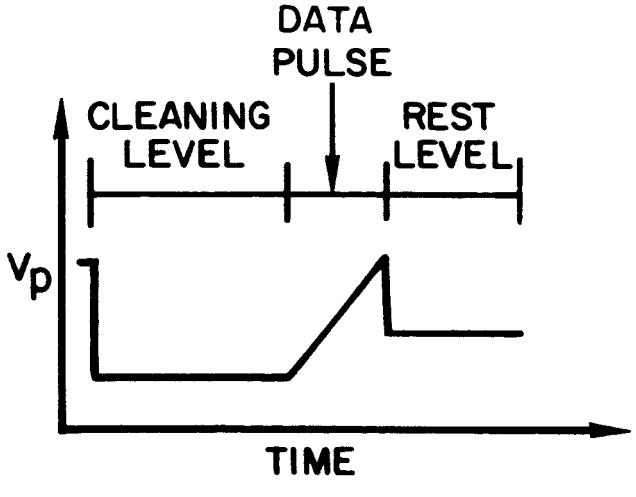

FIG. 3

SEMI-LOG PLOT OF PROBE CURRENT - VOLTAGE CHARACTERISTIC

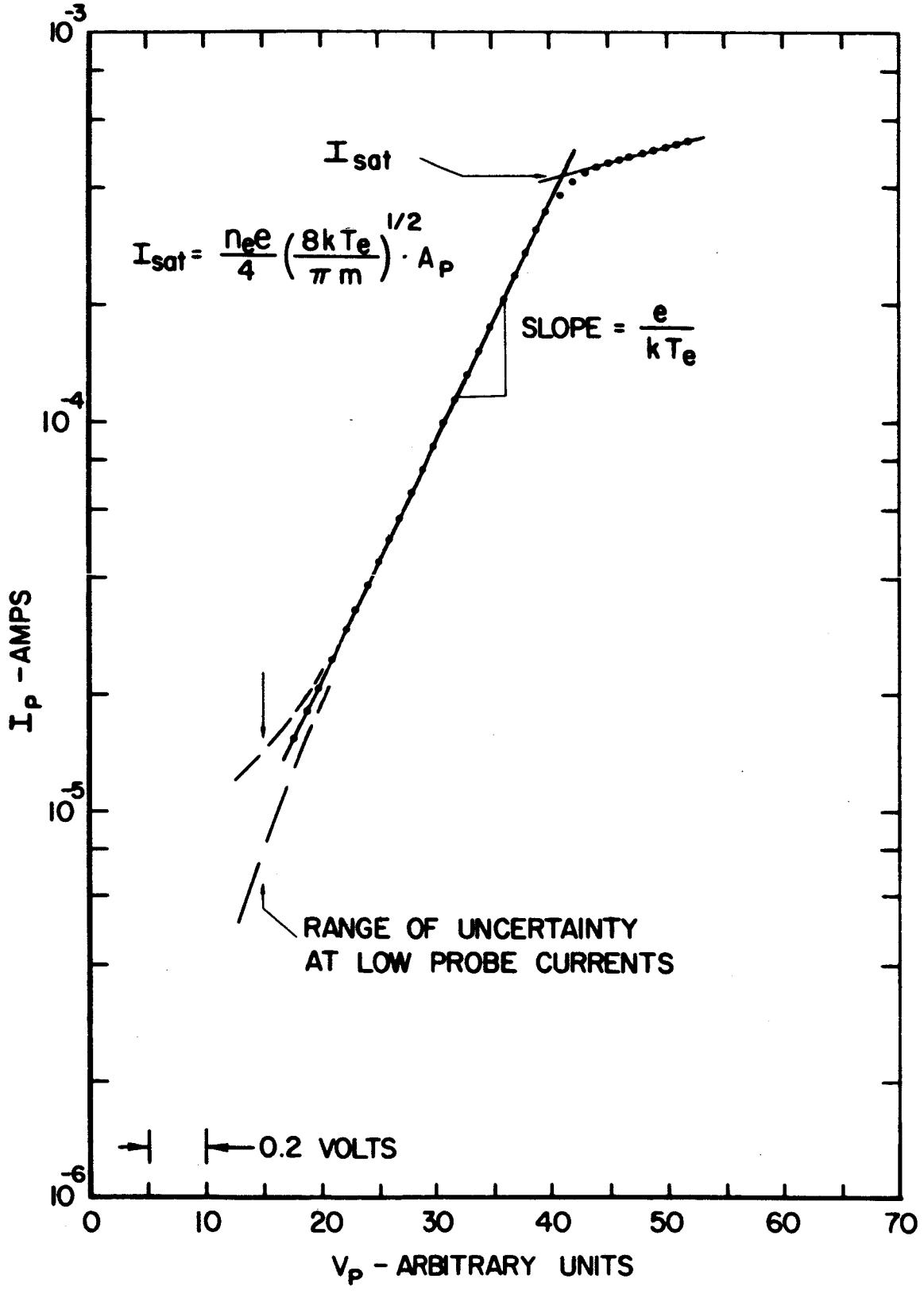

FIG. 4

RADIAL ELECTRON DENSITY PROFILE

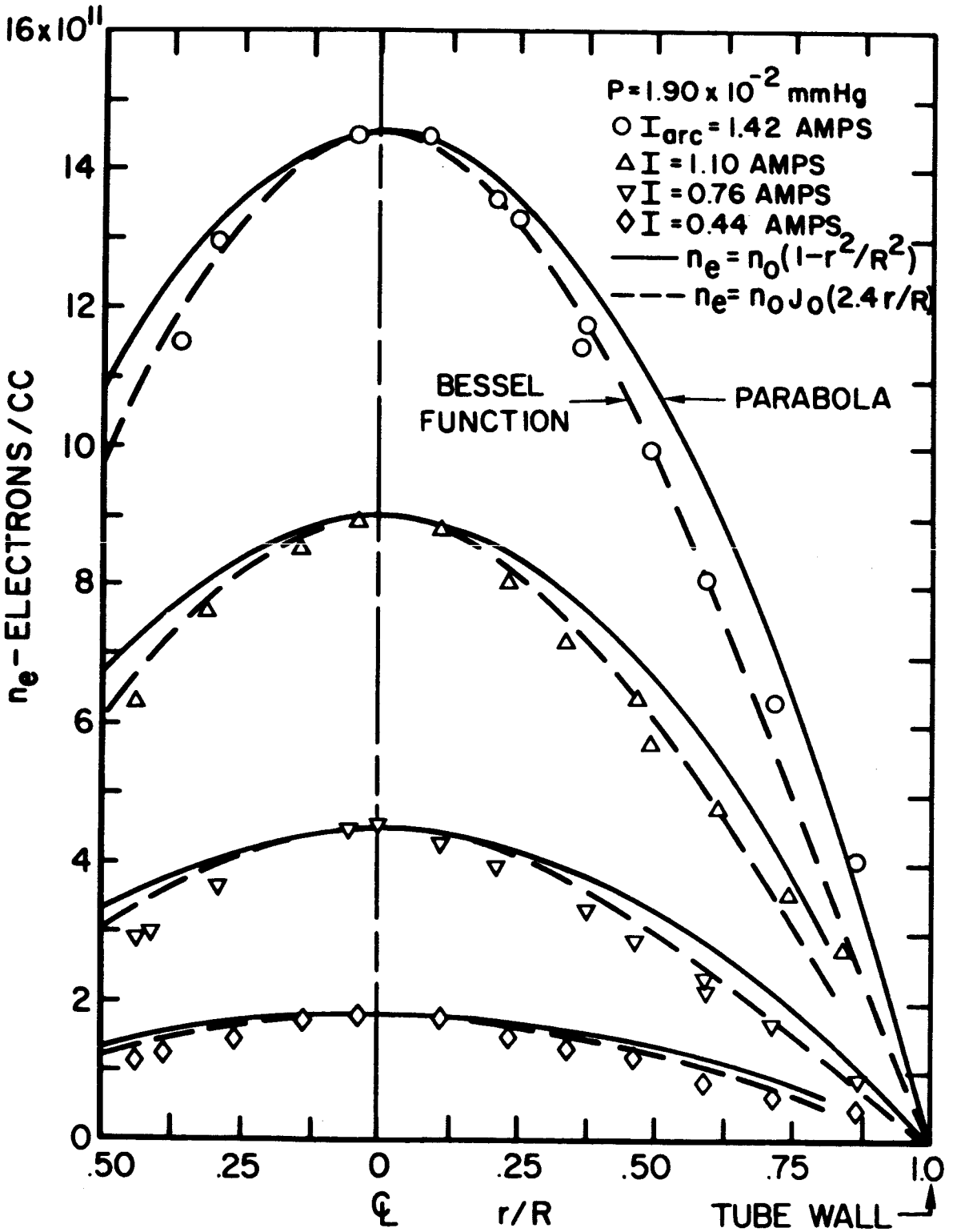

E-920243-27

TABLE I

TYPICAL EXPERIMENTAL DATA

$a_o \times 10^4$	$n_{e_o} \times 10^{-17}$ per m^3	T_e °K	$E \times 10^{-2}$ v/m	I amps	$\nu^*_{eff} \times 10^{12}$ m^3/sec
3	3.25	3400	0.435	0.410	0.513
3	2.42	3900	0.486	0.370	0.590
6	6.24	3375	0.370	0.600	0.570
6	3.15	3525	0.360	0.540	0.633
12	9.65	3150	0.294	0.845	0.650
12	3.68	3550	0.294	0.770	0.714
24	27.90	2575	0.243	1.135	0.746
24	18.70	3325	0.240	1.035	0.830
48	39.00	2550	0.197	1.500	0.965
48	26.70	2875	0.195	1.440	0.992

FIG. 4a

EXPERIMENTALLY DETERMINED AND NUMERICALLY CALCULATED EFFECTIVE COLLISION FREQUENCY VARIATION WITH ELECTRON TEMPERATURE AND DEGREE OF IONIZATION

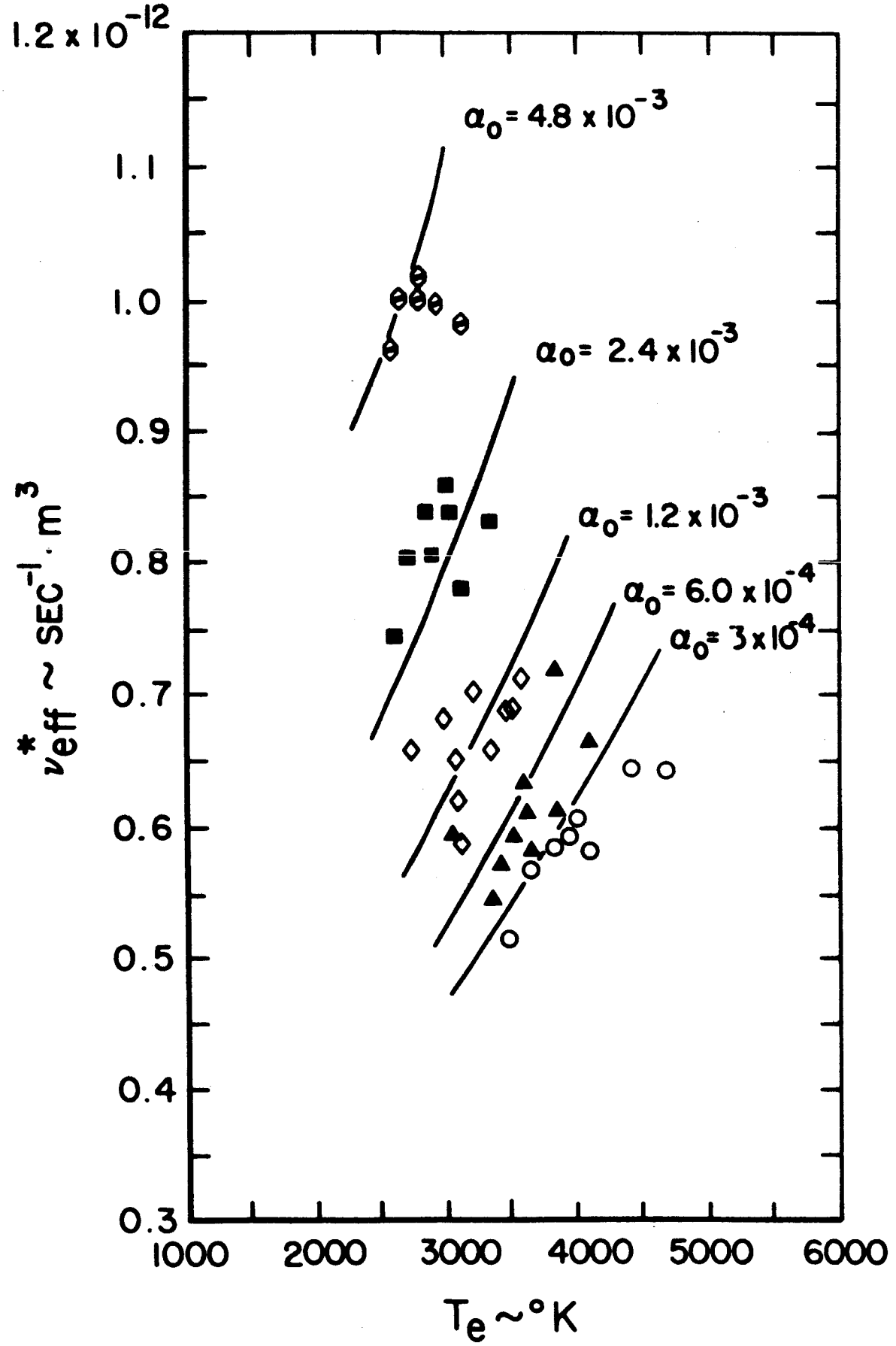

FIG. 6

VARIATION OF ELECTRON-CESIUM ATOM MOMENTUM TRANSFER CROSS SECTION WITH ELECTRON VELOCITY

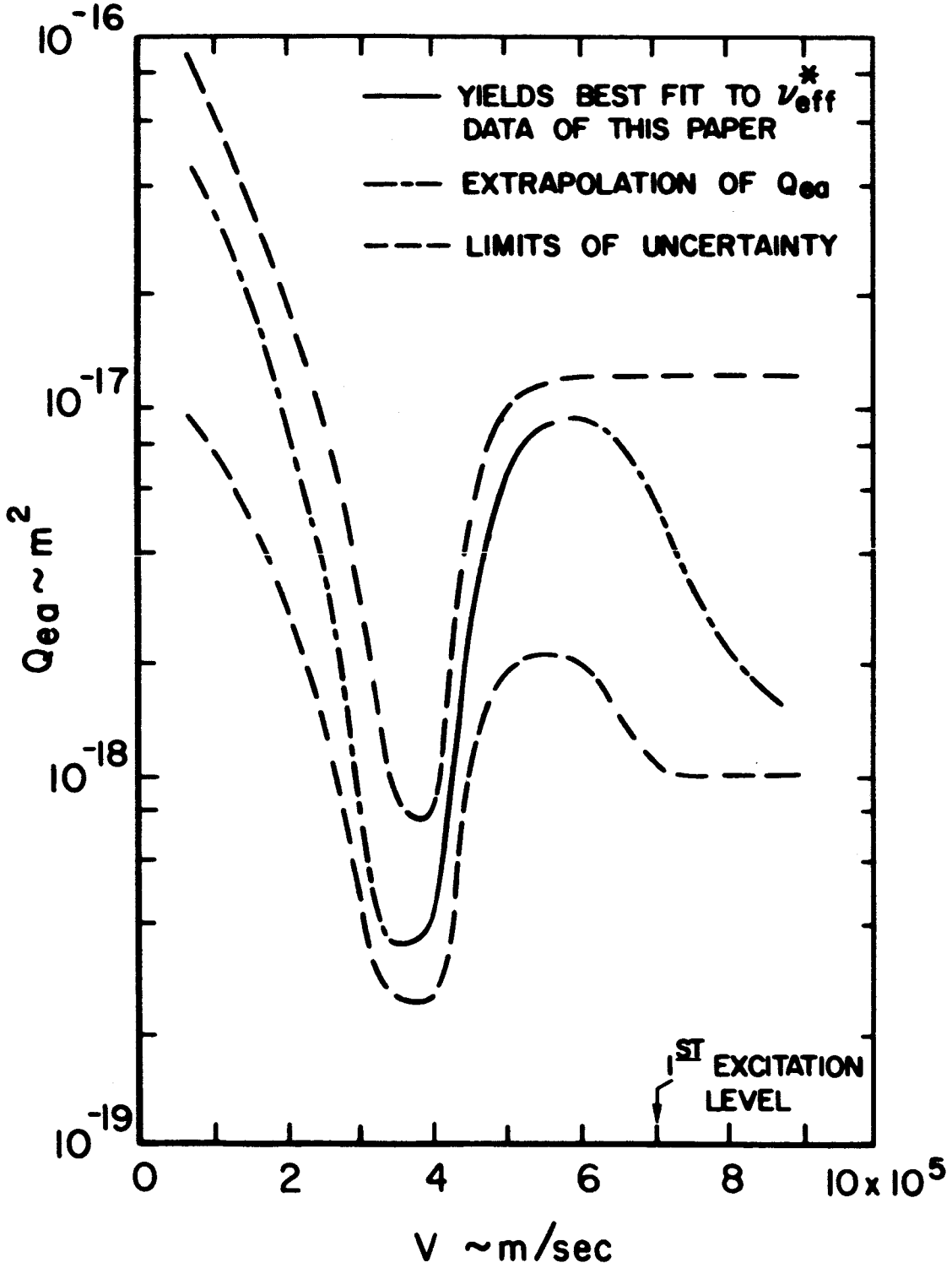

FIG. 7

COMPARISON OF AVAILABLE EXPERIMENTAL DATA IN EFFECTIVE COLLISION FREQUENCY FORM

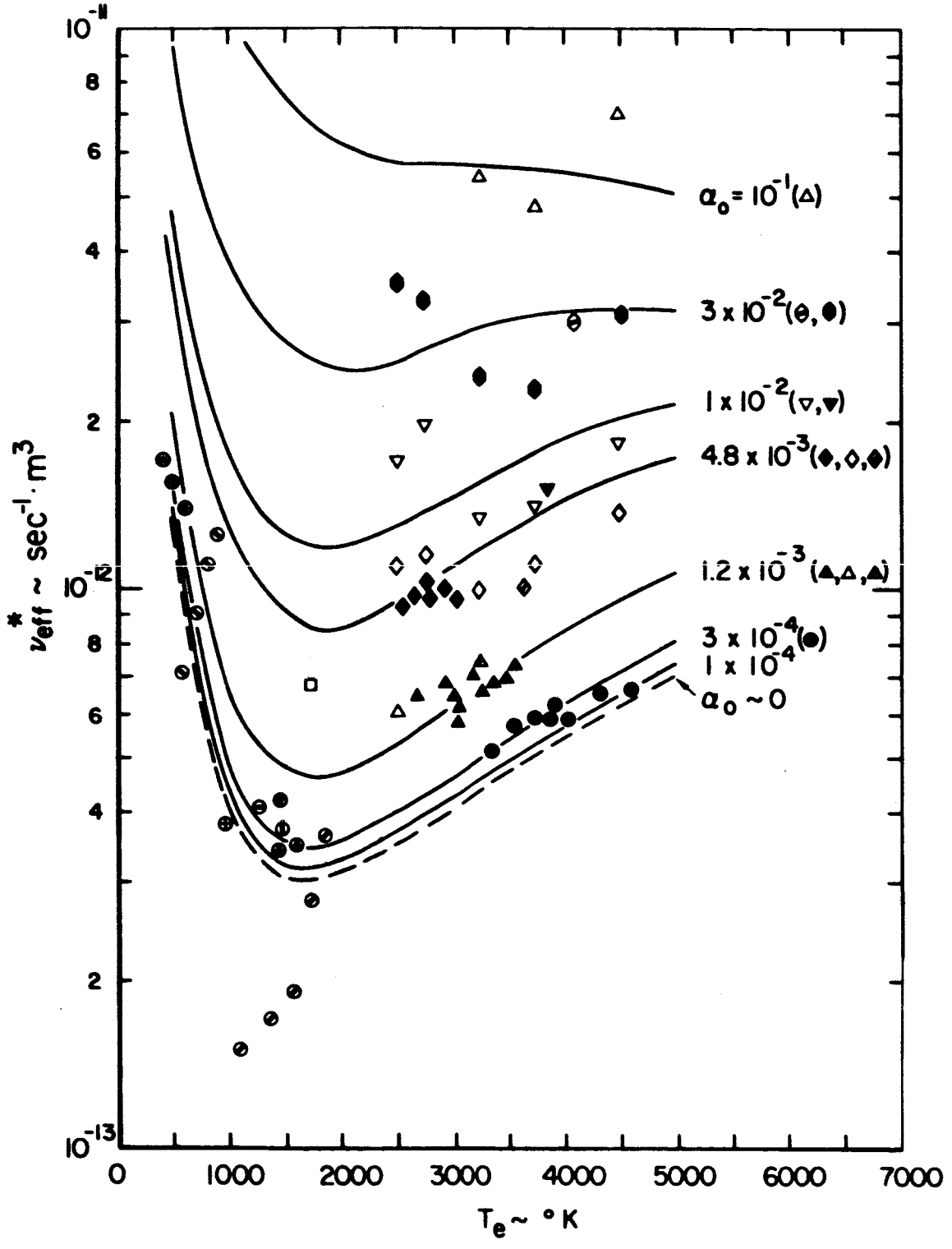

TABLE II

EXPLANATION OF SYMBOLS USED IN FIG. 7

Degree of Ionization	Investigators and Symbols Used in Fig. 7
10^{-6} to 10^{-4}	Chen and Raether (◉), Flavin and Meyerand (⊘), Harris (□), Warner and Hansen (◒), Bohdansky and Langpape (◔), Mirlin, et al. (◧), Rufeh, et al. (⊕), Wilkins and Gyftopoulos (⊖), Roehling (⊘).
3×10^{-4}	This Paper (●).
1.2×10^{-3}	This Paper (▲), Boeckner and Mohler (△), Terlouw (▲).
4.8×10^{-3}	This Paper (◆), Boeckner and Mohler (◇), Terlouw (◈).
1×10^{-2}	Boeckner and Mohler (▽), Terlouw (▼).
3×10^{-2}	Boeckner and Mohler (⬮), Terlouw (⊖).
1×10^{-1}	Boeckner and Mohler (△).

FIG. 8

THEORETICALLY CALCULATED ELECTRON-CESIUM ATOM CROSS-SECTION VARIATION WITH ELECTRON VELOCITY

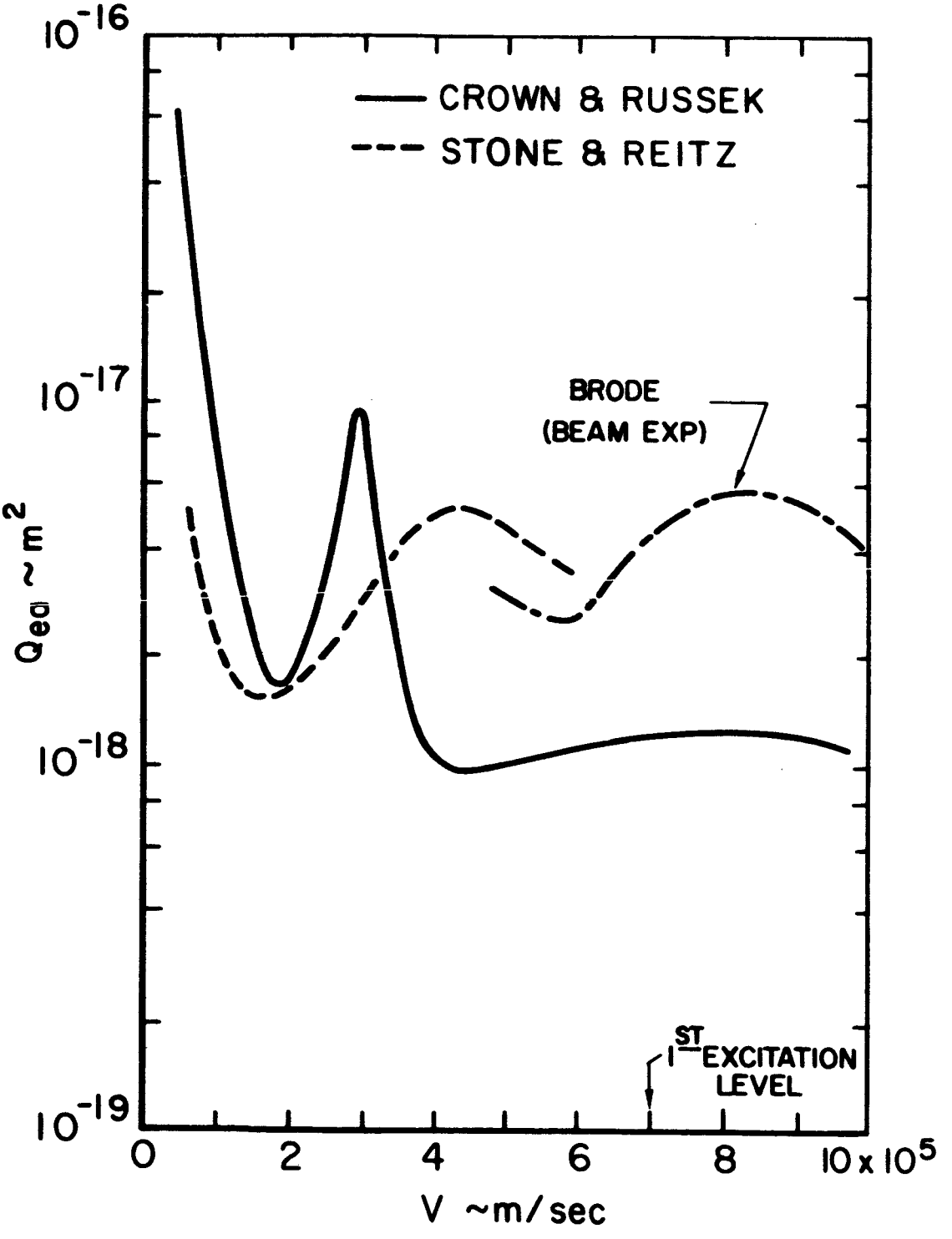

FIG 9

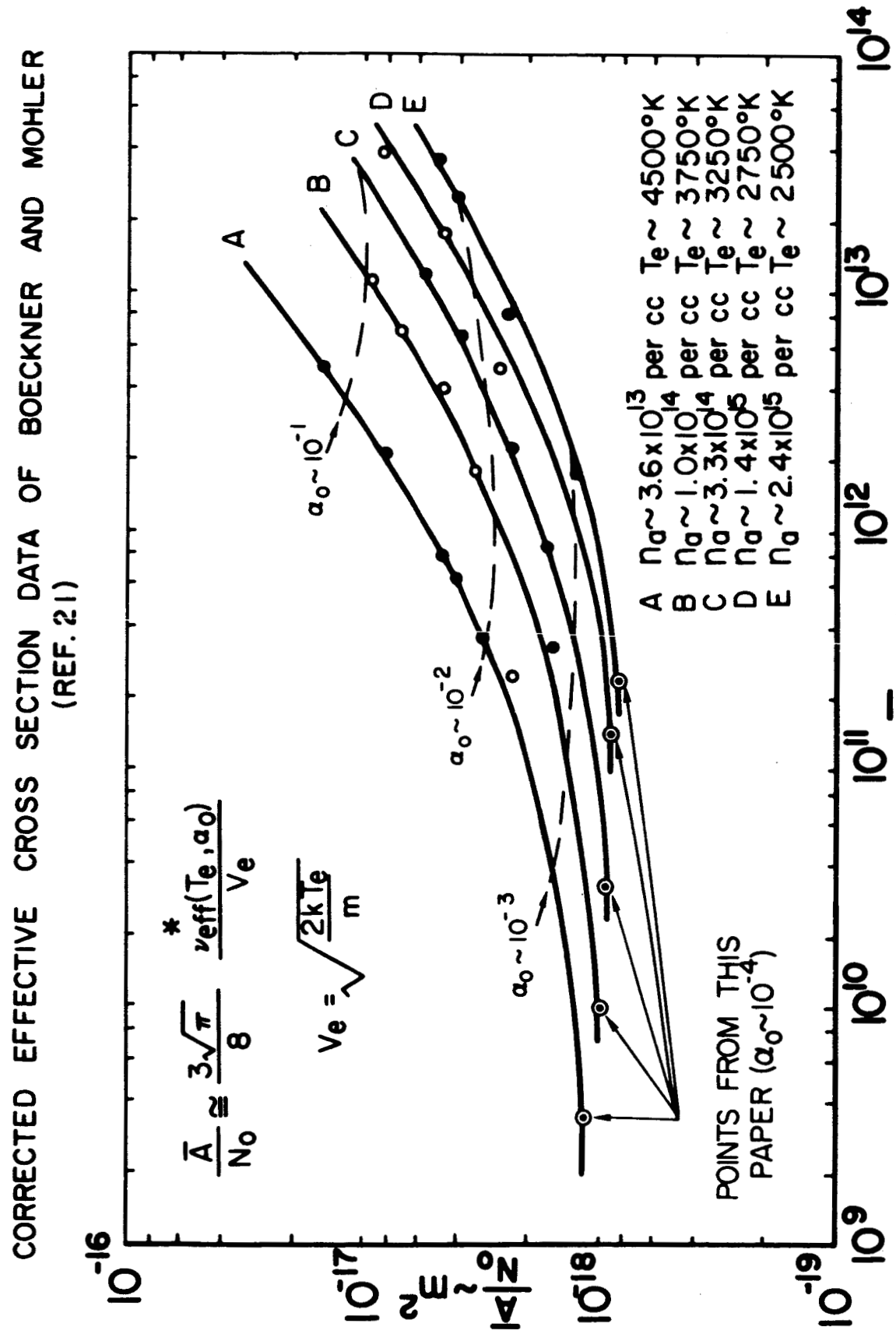
CORRECTED EFFECTIVE CROSS SECTION DATA OF BOECKNER AND MOHLER
(REF. 21)
$\frac{\bar{A}}{N_0} \cong \frac{3\sqrt{\pi}}{8} \frac{\nu^*_{eff}(T_e, a_0)}{V_e}$
$V_e = \sqrt{\frac{2kT_e}{m}}$
$a_0 \sim 10^{-1}$
$a_0 \sim 10^{-2}$
$a_0 \sim 10^{-3}$
A $n_a \sim 3.6 \times 10^{13}$ per cc $T_e \sim 4500°K$
B $n_a \sim 1.0 \times 10^{14}$ per cc $T_e \sim 3750°K$
C $n_a \sim 3.3 \times 10^{14}$ per cc $T_e \sim 3250°K$
D $n_a \sim 1.4 \times 10^{15}$ per cc $T_e \sim 2750°K$
E $n_a \sim 2.4 \times 10^{15}$ per cc $T_e \sim 2500°K$
POINTS FROM THIS PAPER ($a_0 \sim 10^{-4}$)
$\bar{n}_e$ per cc
$\frac{\bar{A}}{N_0} \tilde{\nu}^2$

FIG. 10

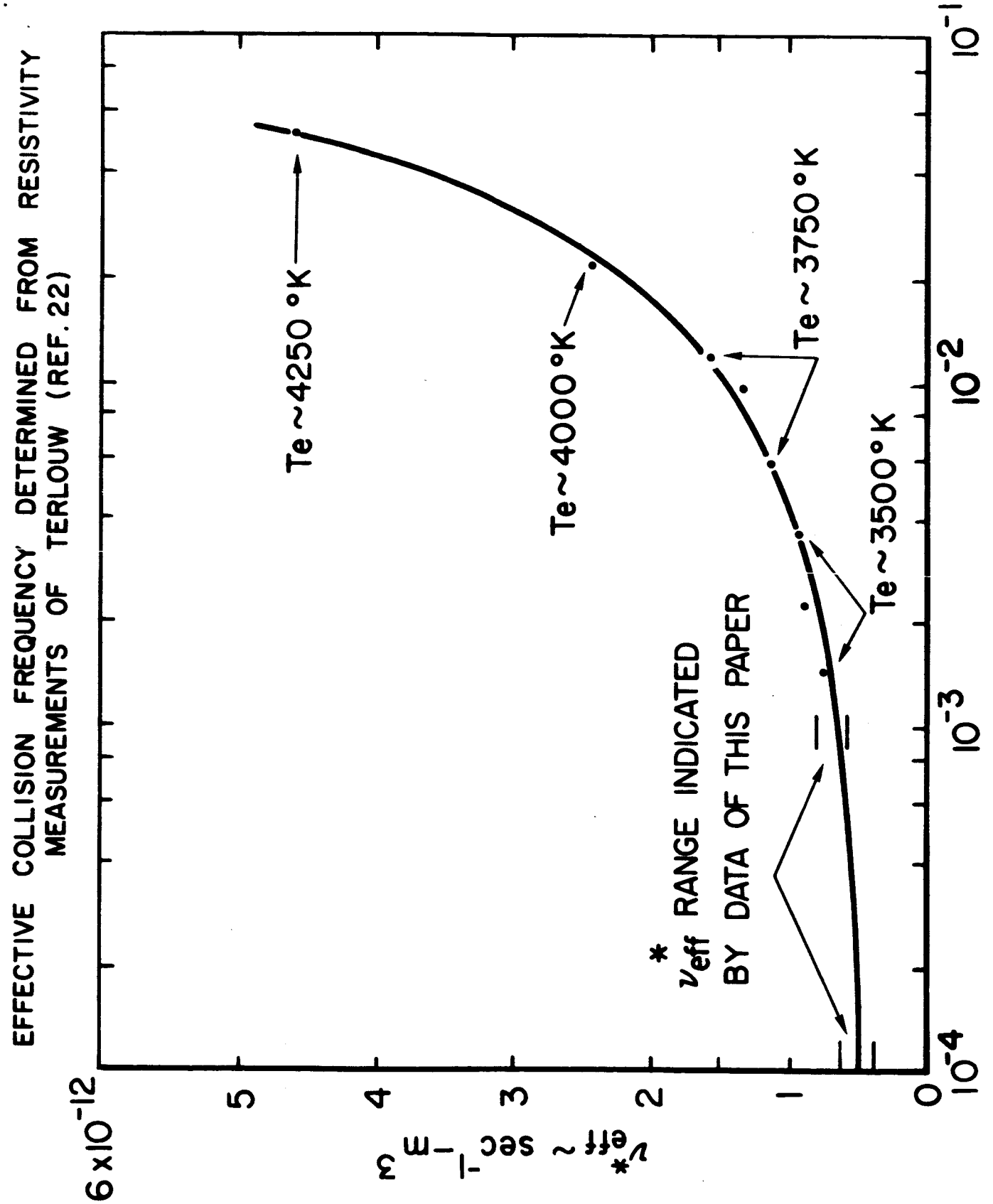
EFFECTIVE COLLISION FREQUENCY DETERMINED FROM RESISTIVITY MEASUREMENTS OF TERLOUW (REF. 22)
Te ~ 4250 °K
Te ~ 4000 °K
Te ~ 3750 °K
Te ~ 3500 °K
* ν_eff RANGE INDICATED BY DATA OF THIS PAPER
ν*_eff ~ sec⁻¹ – m³
6 x 10⁻¹²
5
4
3
2
1
0
10⁻¹
10⁻²
10⁻³
10⁻⁴
α₀ ≡ η_eα/η_α

SCHEMATIC DIAGRAM OF ION COLLISION CROSS-SECTION APPARATUS

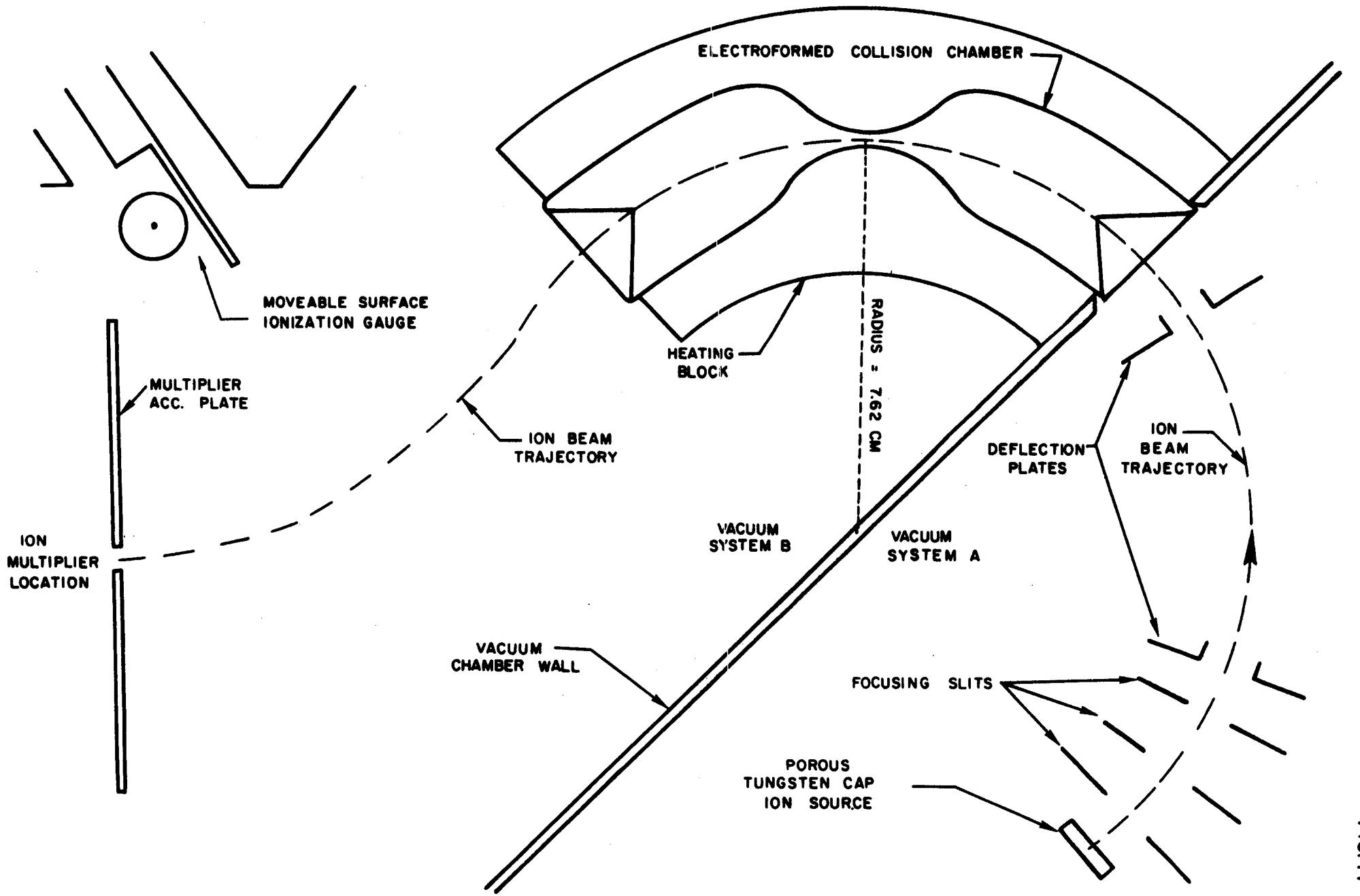

E-920243-27

FIG. 11

FIG. 12

NORMALIZED ION BEAM ENERGY DISTRIBUTION

PEAK ENERGY = .107 eV

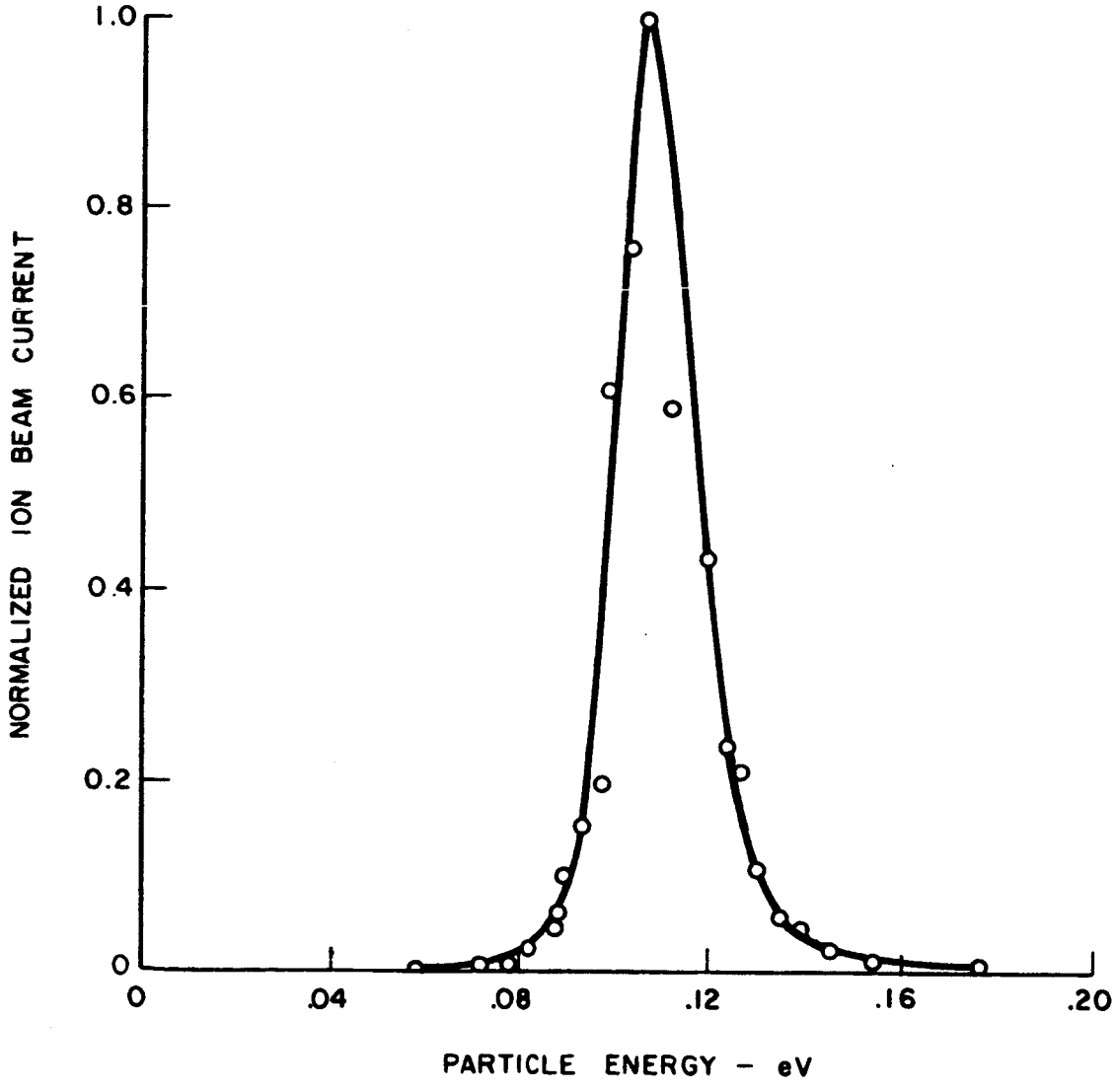

FIG. 13

NORMALIZED ION BEAM ENERGY DISTRIBUTION

PEAK ENERGY = 0.88 eV

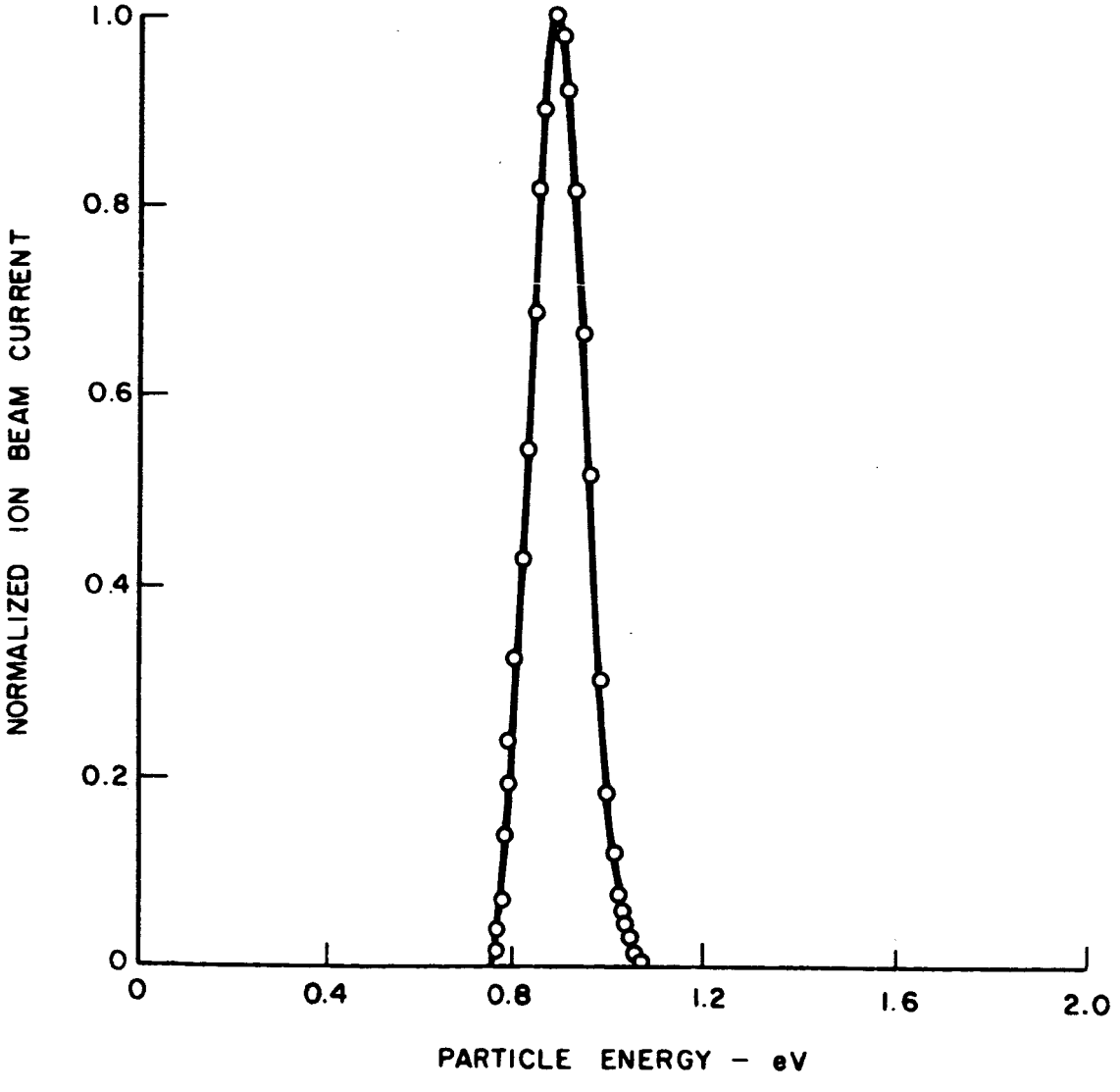

FIG. 14

NORMALIZED ION BEAM ENERGY DISTRIBUTION

PEAK ENERGY = 0.97 eV

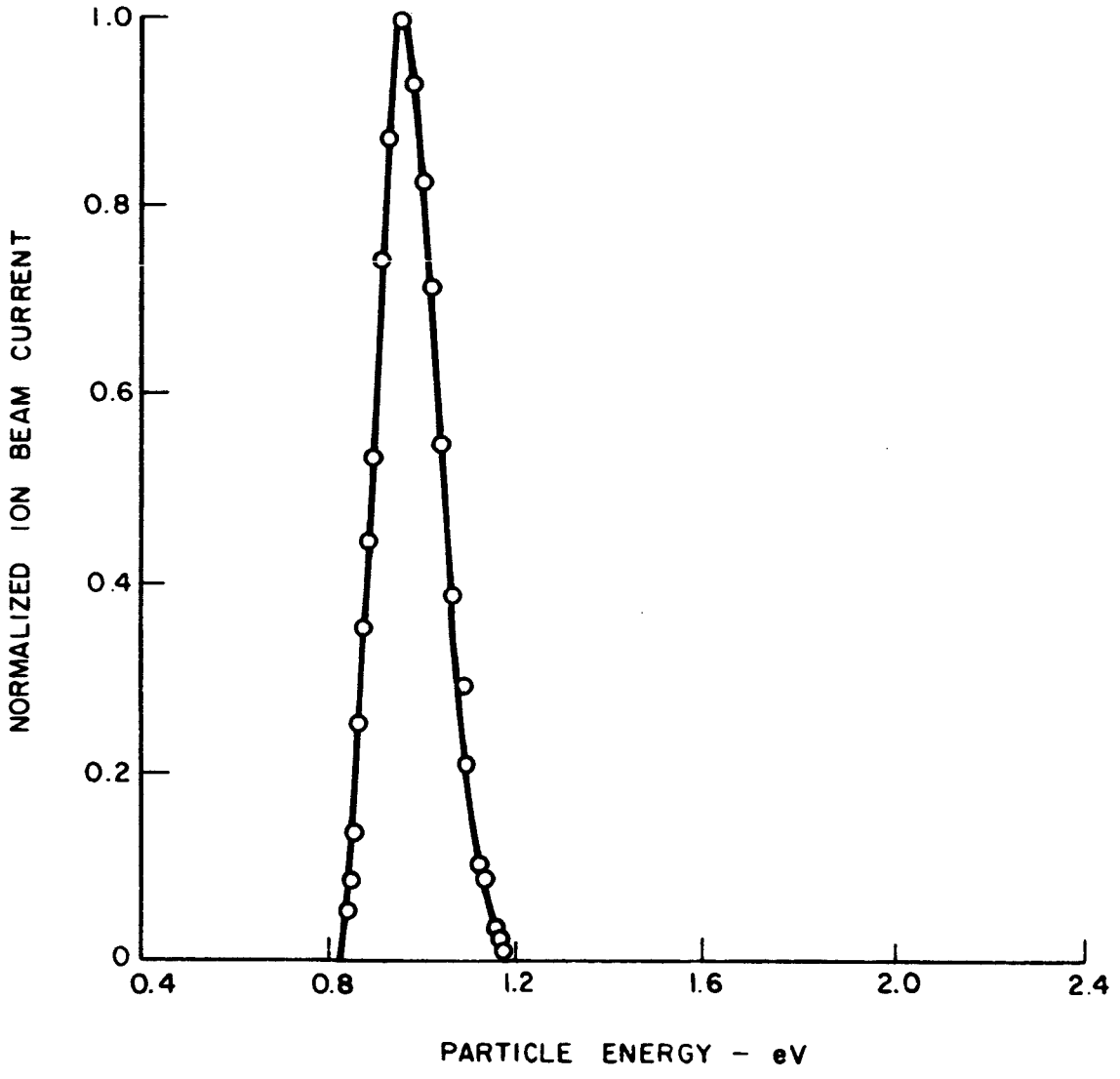

FIG. 15

NORMALIZED ION BEAM ENERGY DISTRIBUTION

PEAK ENERGY = 1.14 eV

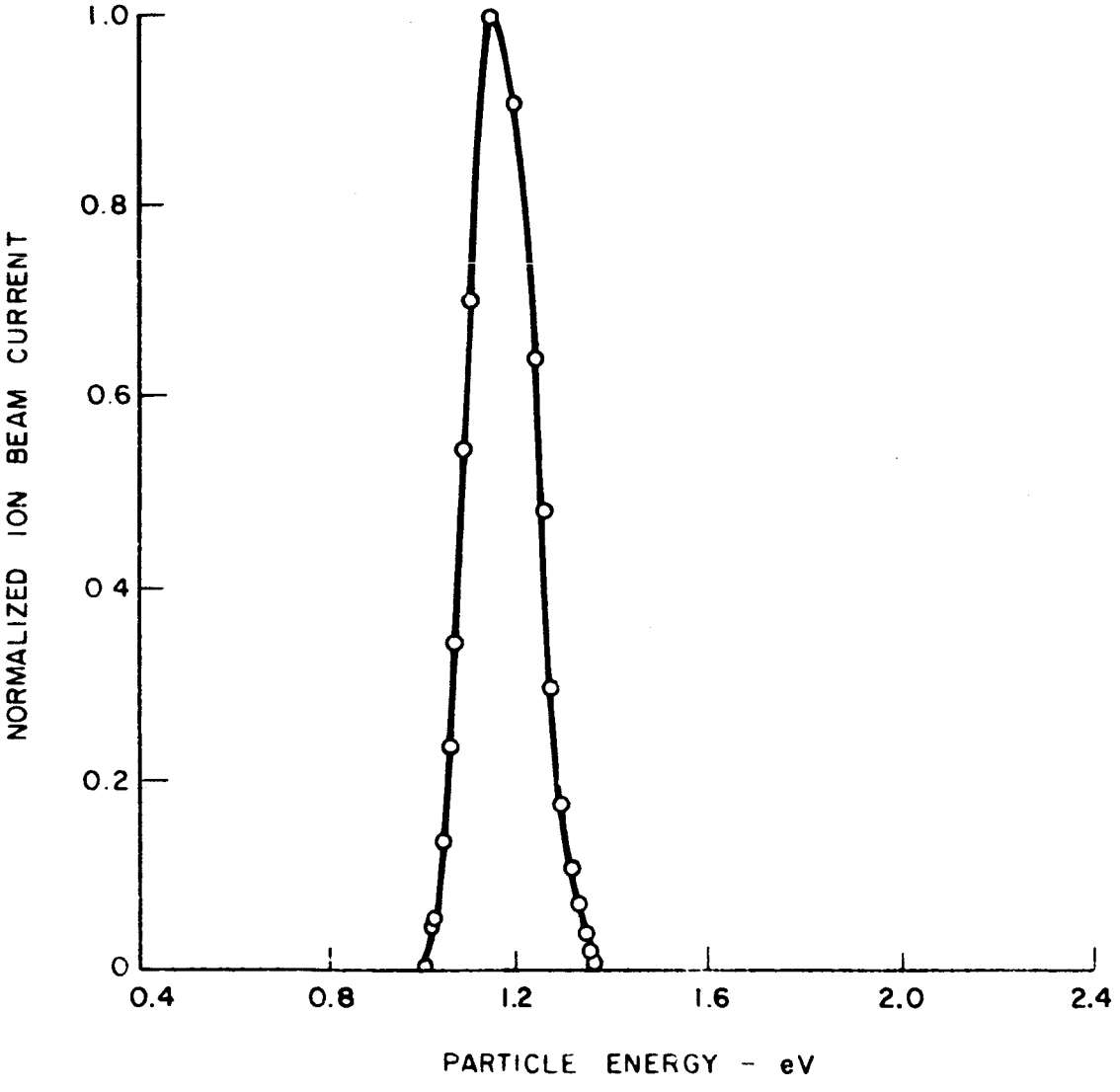

FIG. 16

NORMALIZED ION BEAM ENERGY DISTRIBUTION

PEAK ENERGY = 1.40 eV

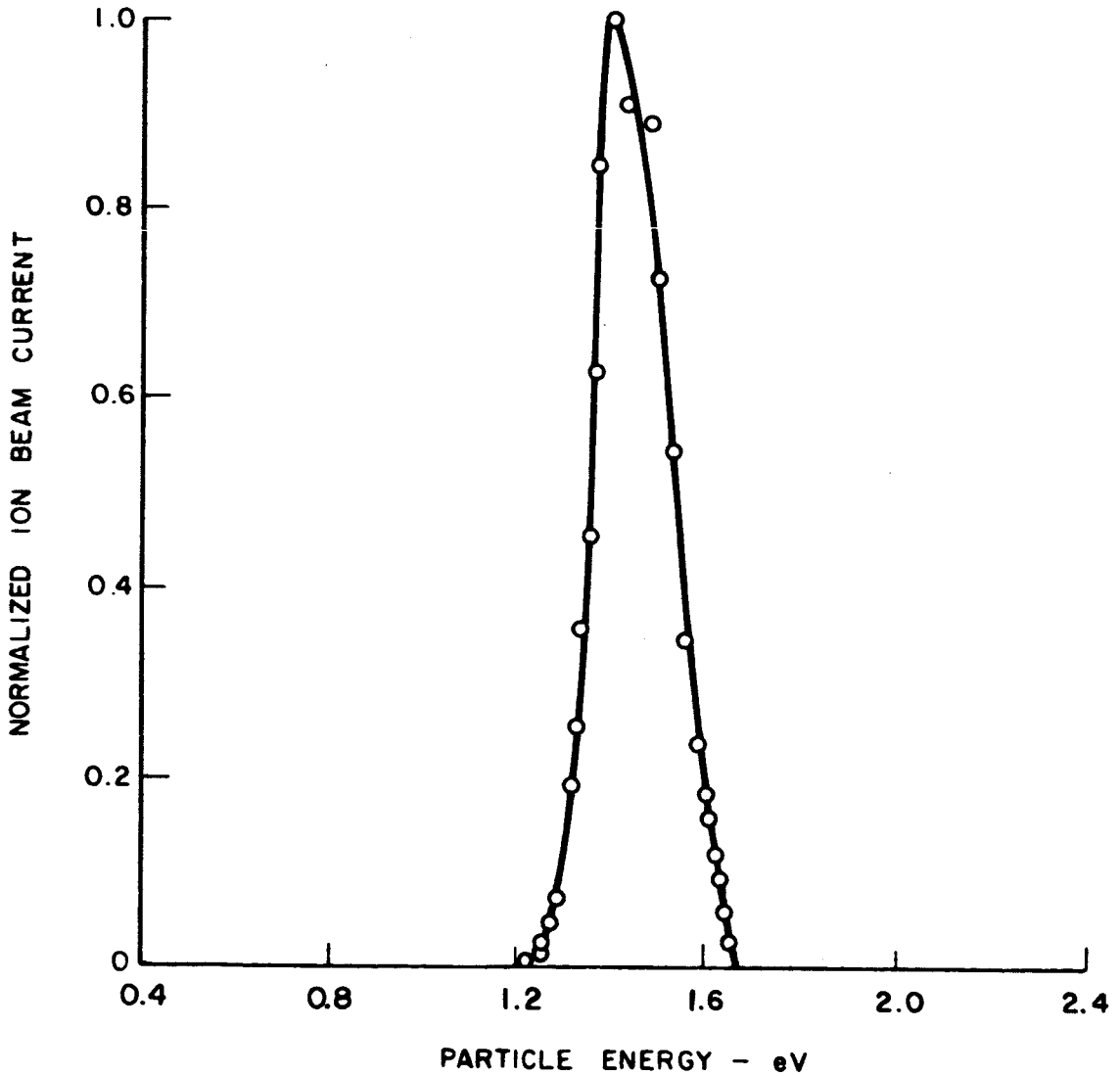

FIG. 17

NORMALIZED ION BEAM ENERGY DISTRIBUTION

PEAK ENERGY = 2.36 eV

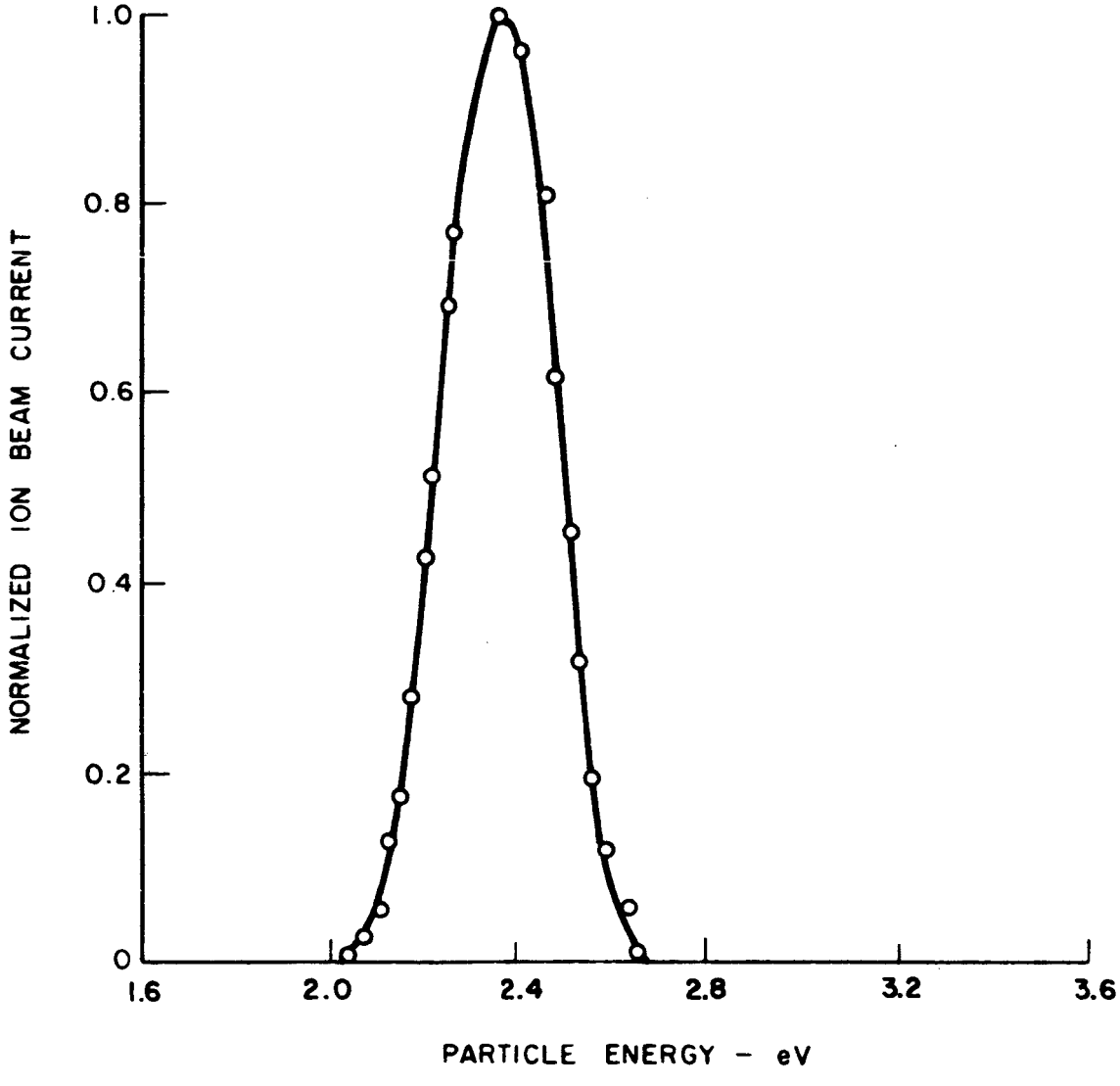

FIG. 18

NORMALIZED ION BEAM ENERGY DISTRIBUTION

PEAK ENERGY = 2.59 eV

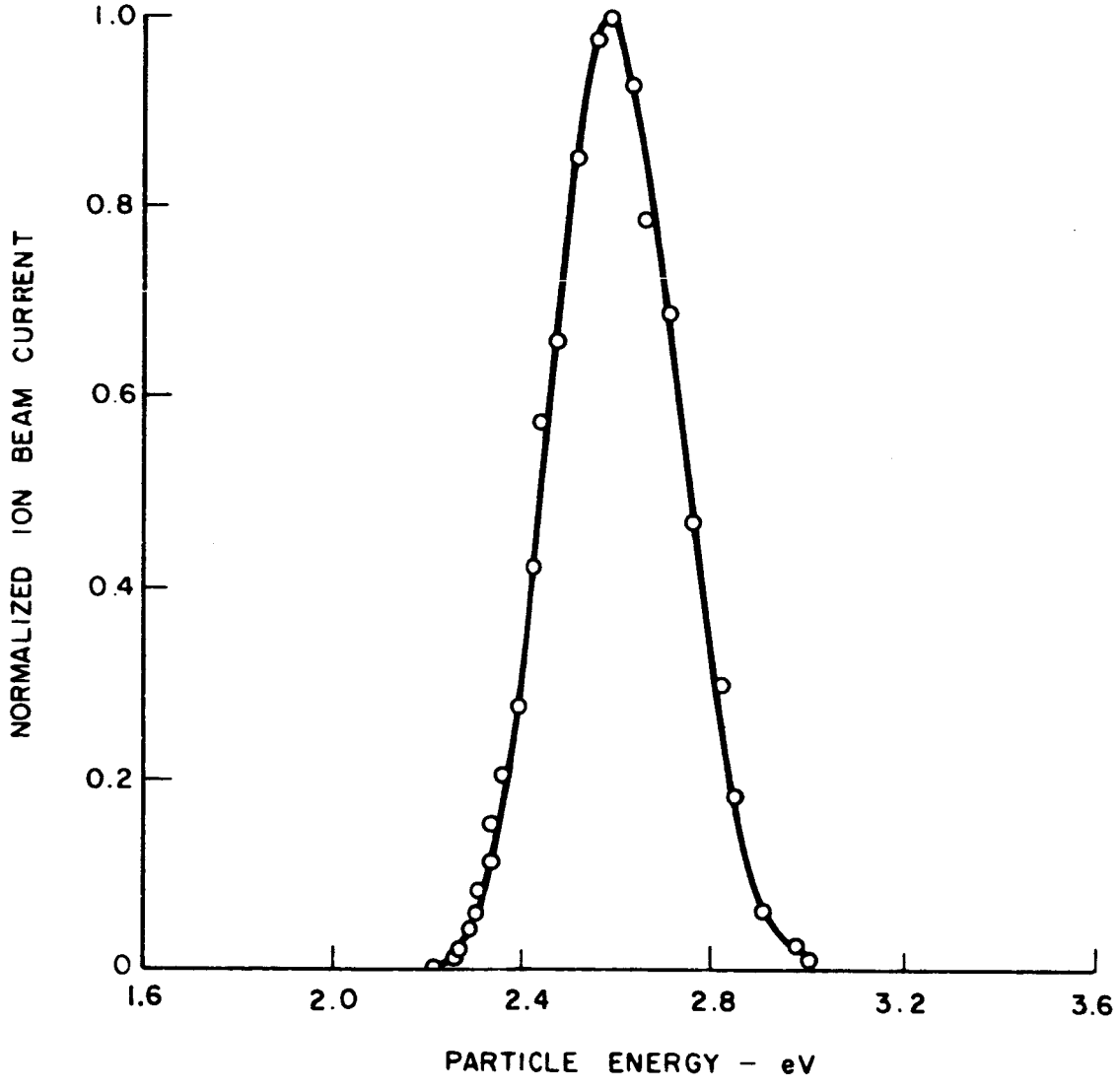

FIG. 19

ION BEAM HALF - WIDTHS

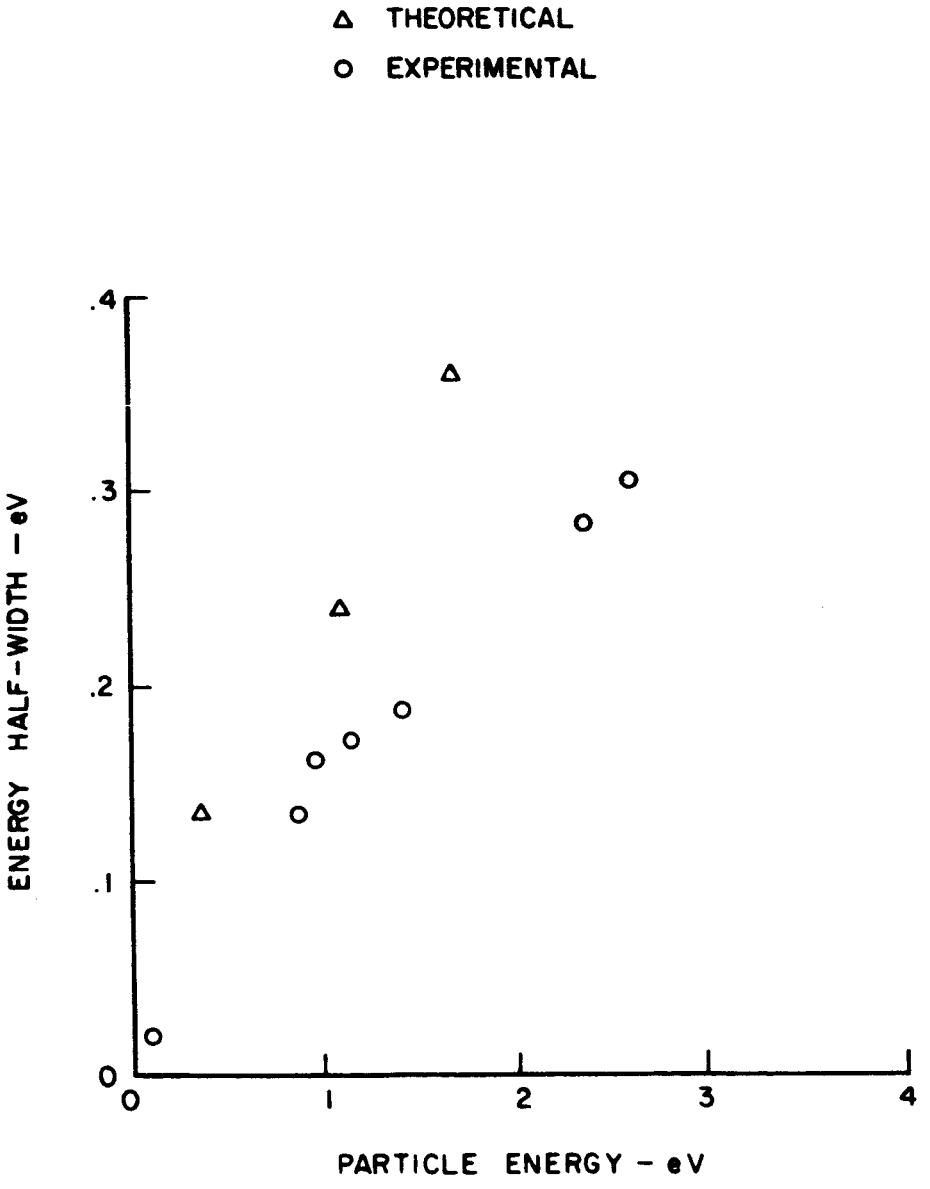

FIG. 20

X- RAY OF ELECTRO- FORMED COLLISION CHAMBER

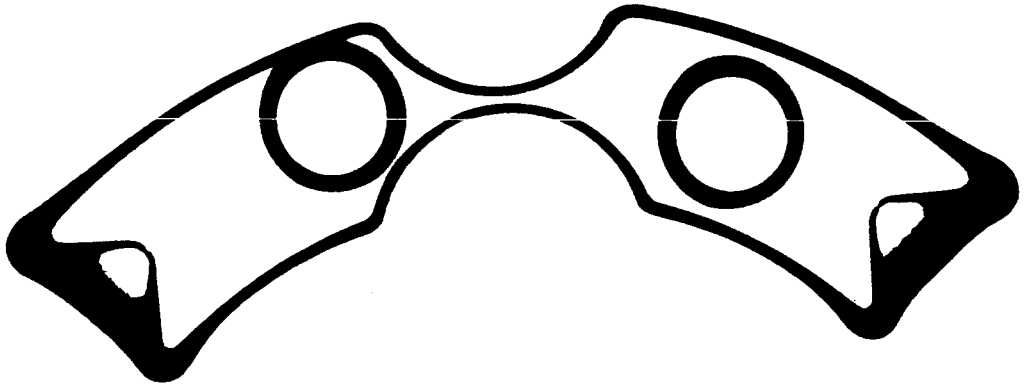

FIG. 21

VARIATION OF APPLIED CAP POTENTIAL WITH MEASURED ION ENERGY

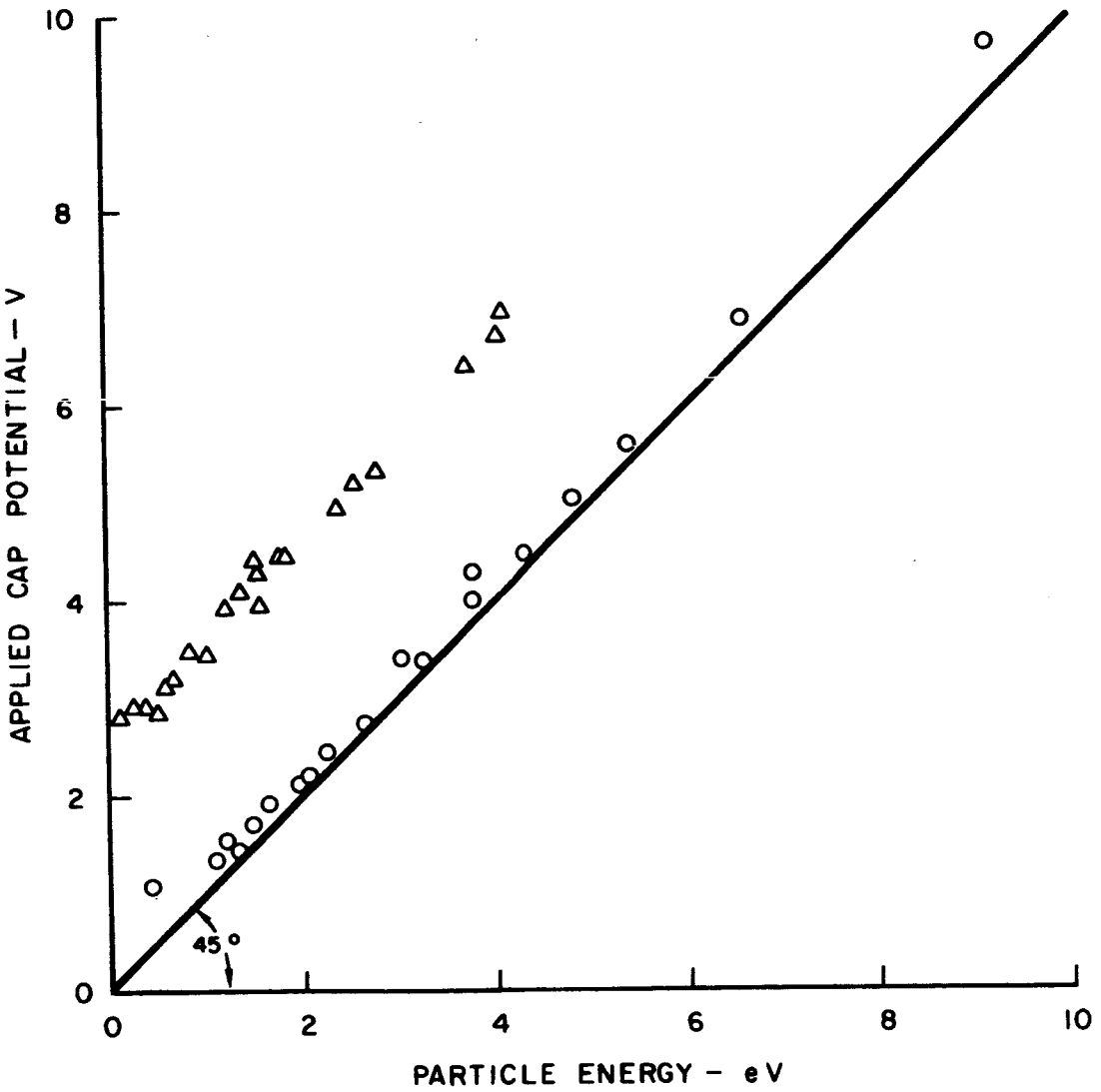

FIG. 22

ION COLLISION CHAMBER AND CESIUM RESERVOIR

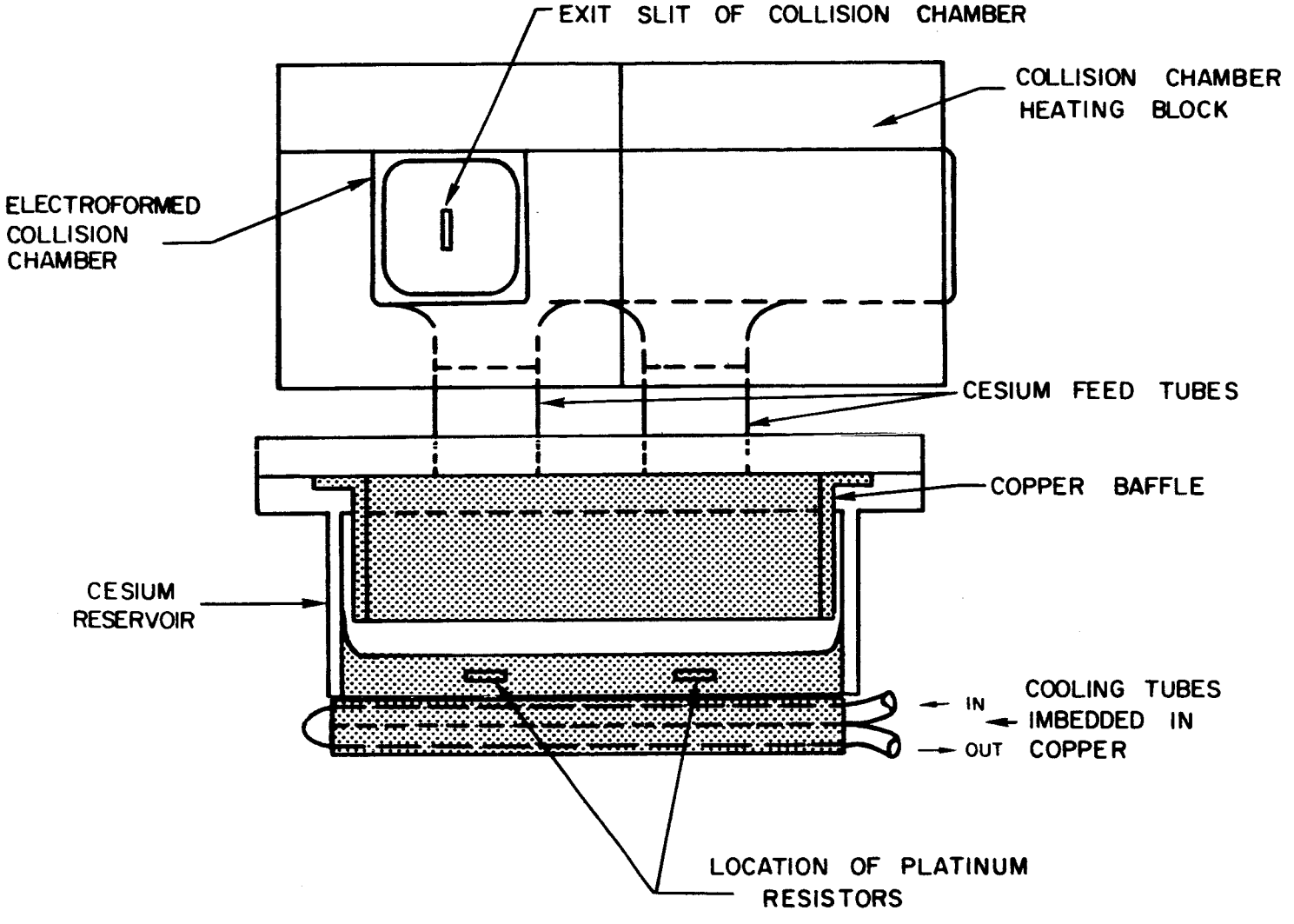

CESIUM RESERVOIR SHOWN IN SECTION

FIG. 23

SCHEMATIC OF NEUTRAL EFFLUX SOURCE

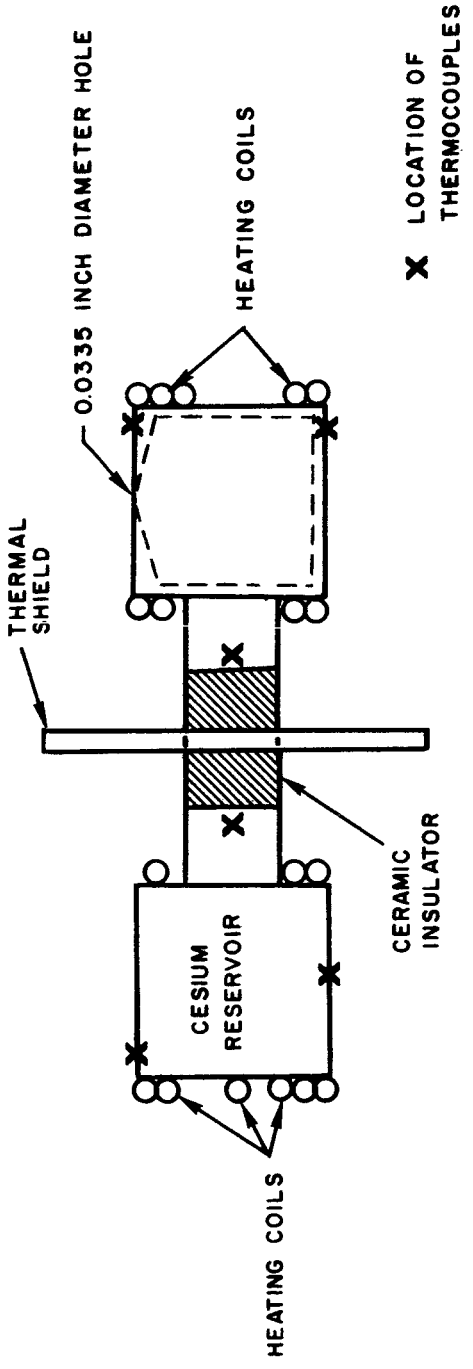

FIG. 24

TIME VARIATION OF CESIUM ION CURRENT

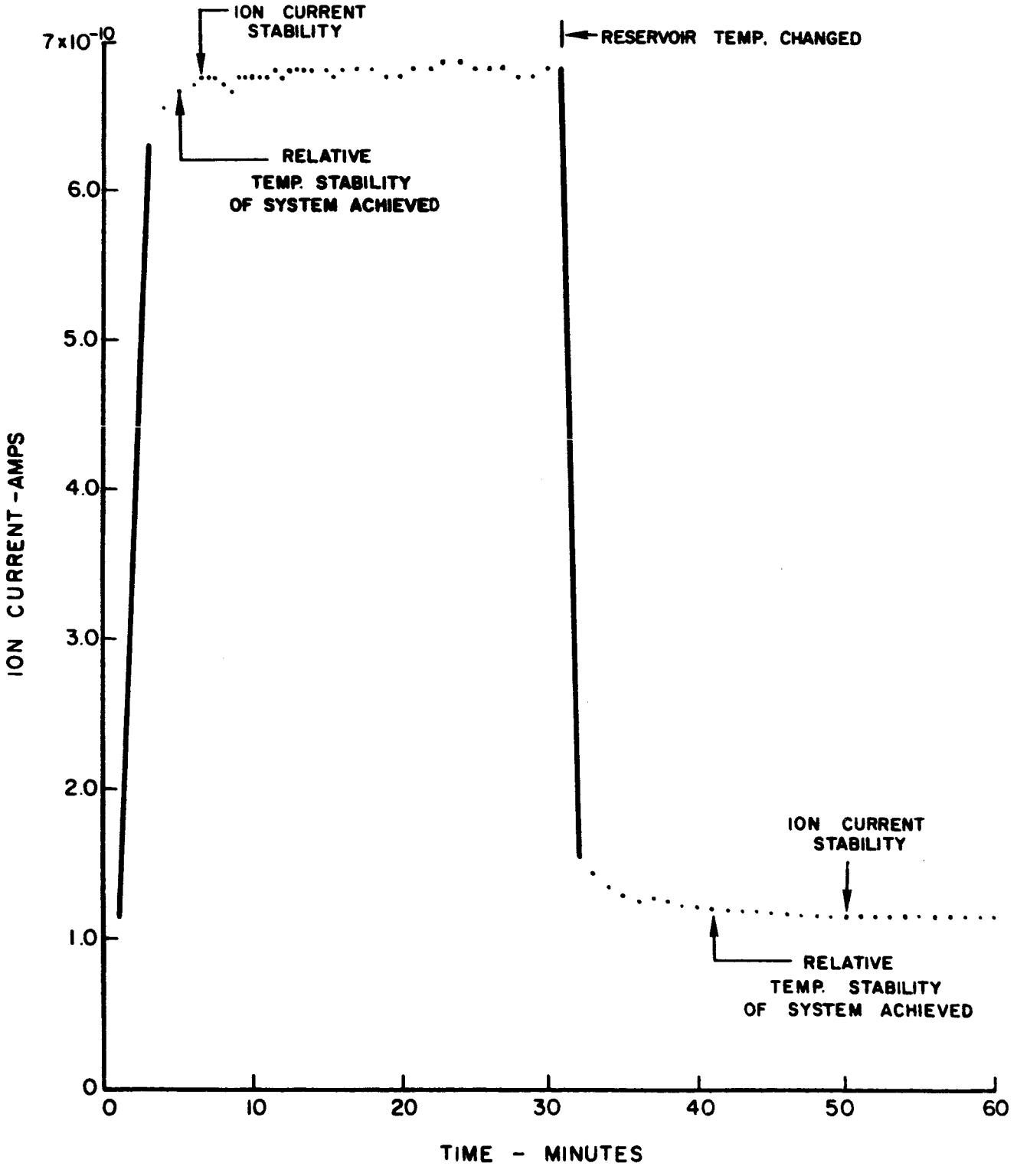

FIG. 25

MEASURED ION CURRENT VARIATION WITH RESERVOIR TEMPERATURE

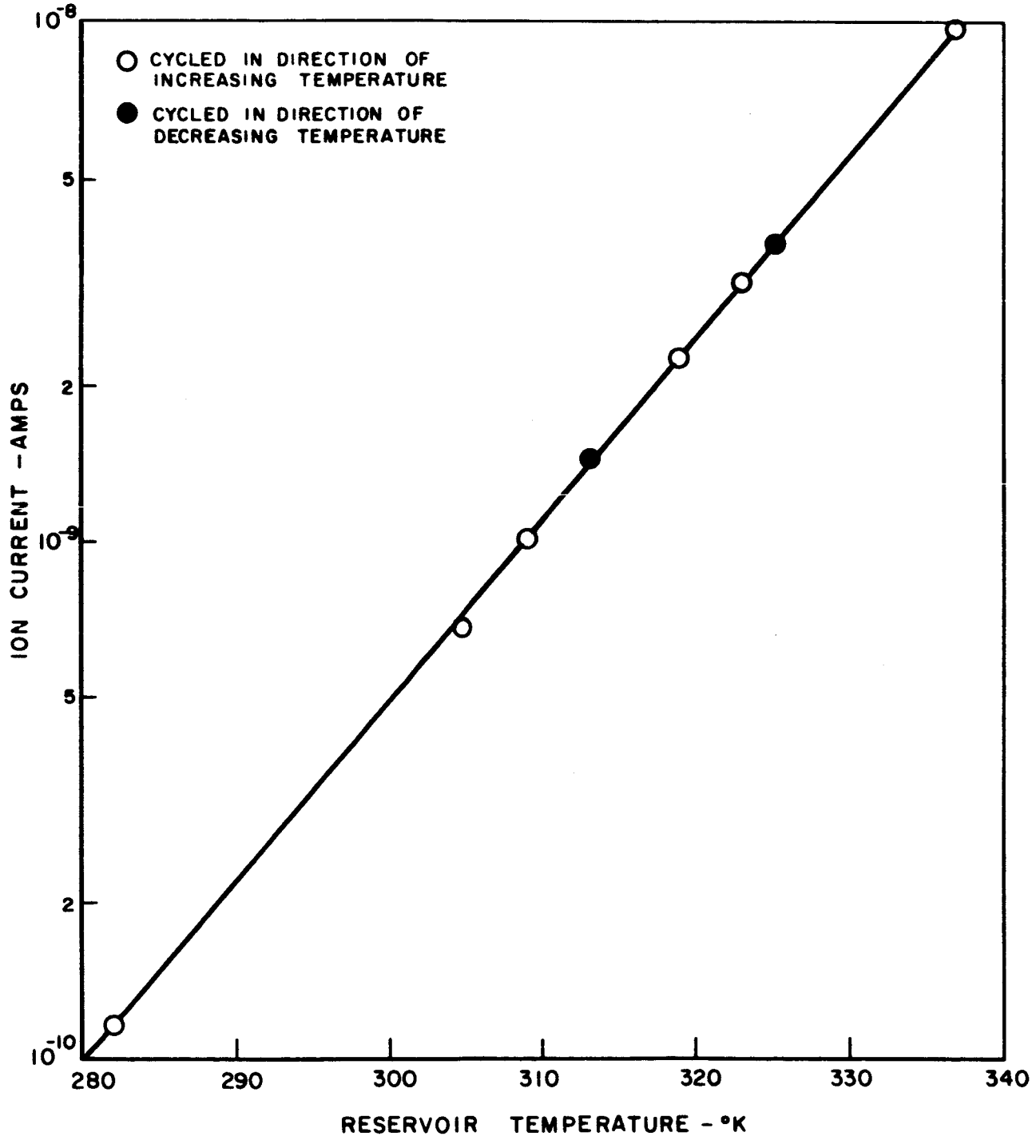

FIG. 26

PRESSURE DETERMINATION BY SURFACE IONIZATION GAUGE MEASUREMENTS

SYMBOL	TOP BLOCK TEMPERATURE
○	403°K
□	541°K
◇	565°K
△	653°K
—	CALC. CURRENT BASED ON DATA OF REF. 35

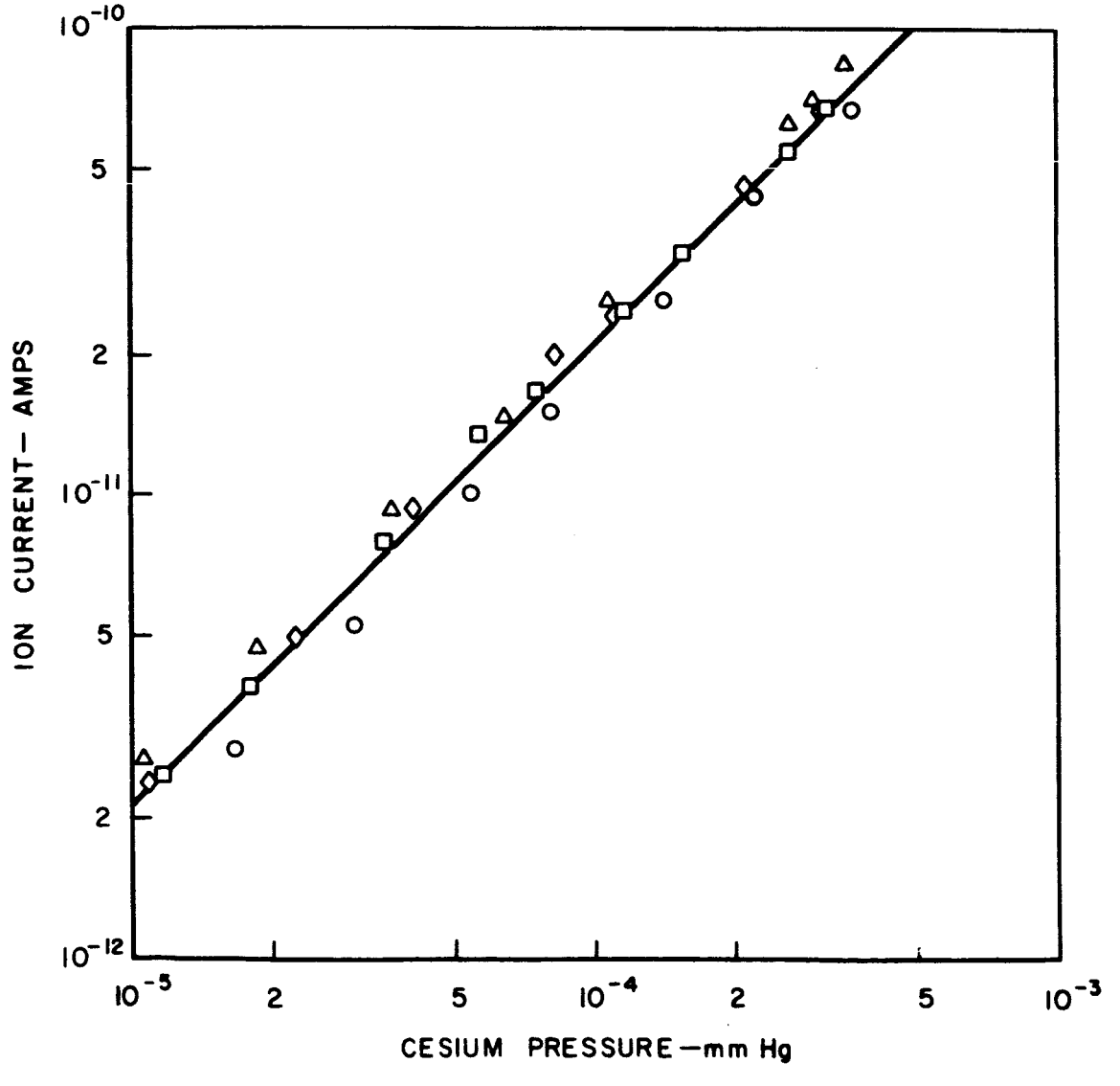

E-920243-27

FIG. 27

CESIUM PRESSURE ERROR AS A FUNCTION OF RESERVOIR TEMPERATURE ERROR

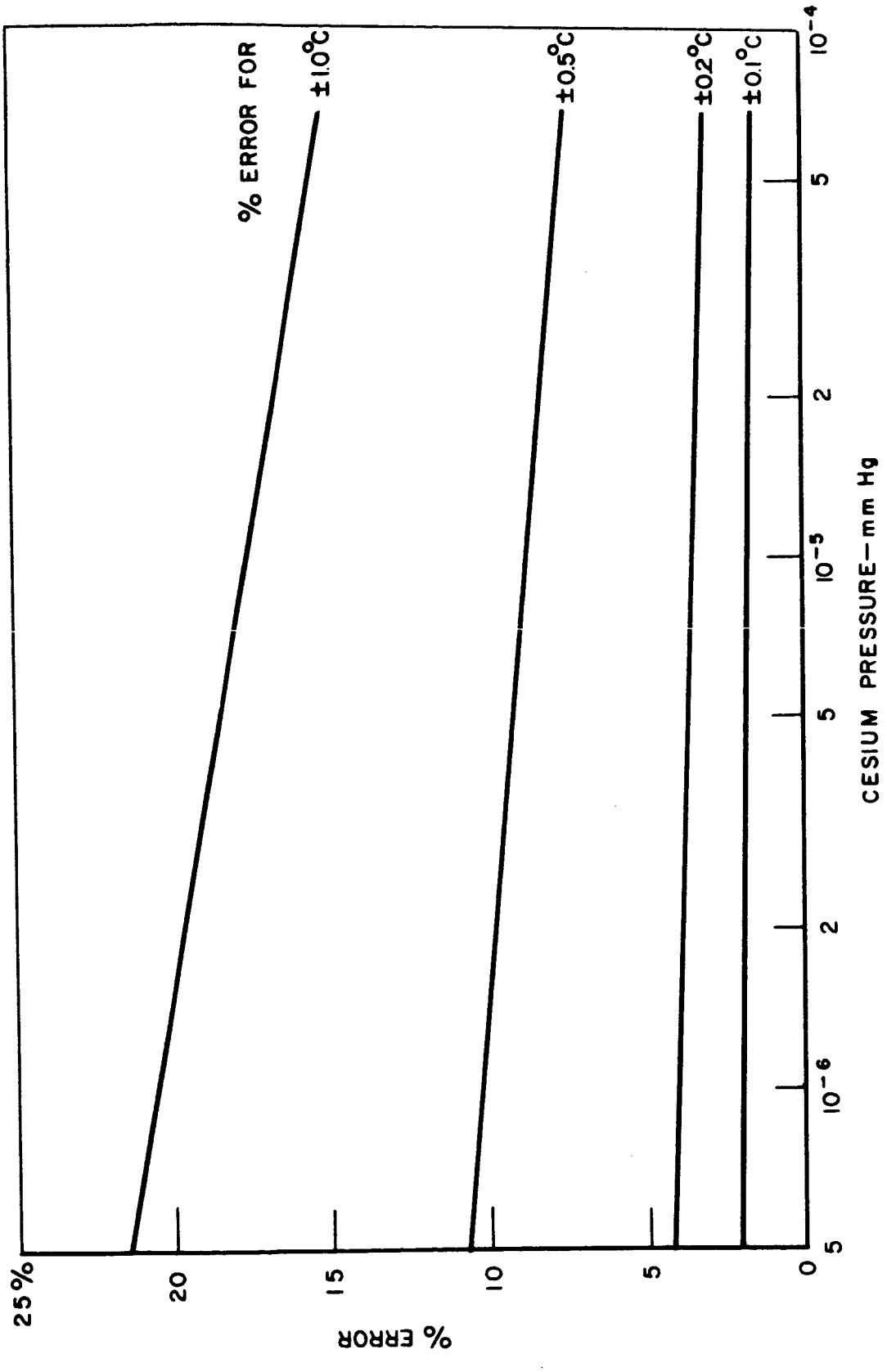

FIG. 28

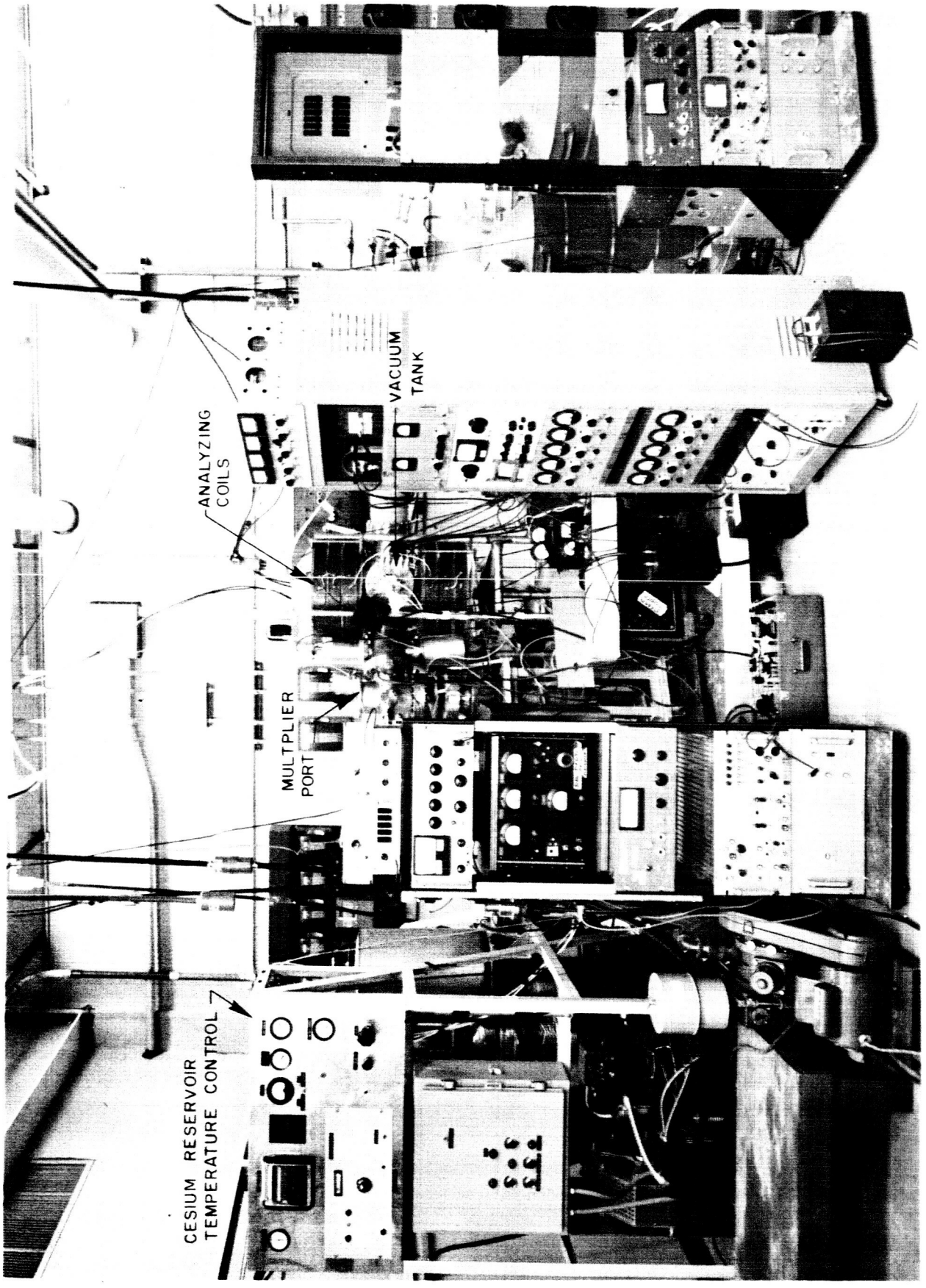
ION-ATOM COLLISION CROSS SECTION APPARATUS
CESIUM RESERVOIR TEMPERATURE CONTROL
MULTPLIER PORT
ANALYZING COILS
VACUUM TANK

TYPICAL NEUTRAL ATOM FLUX SPATIAL DISTRIBUTION

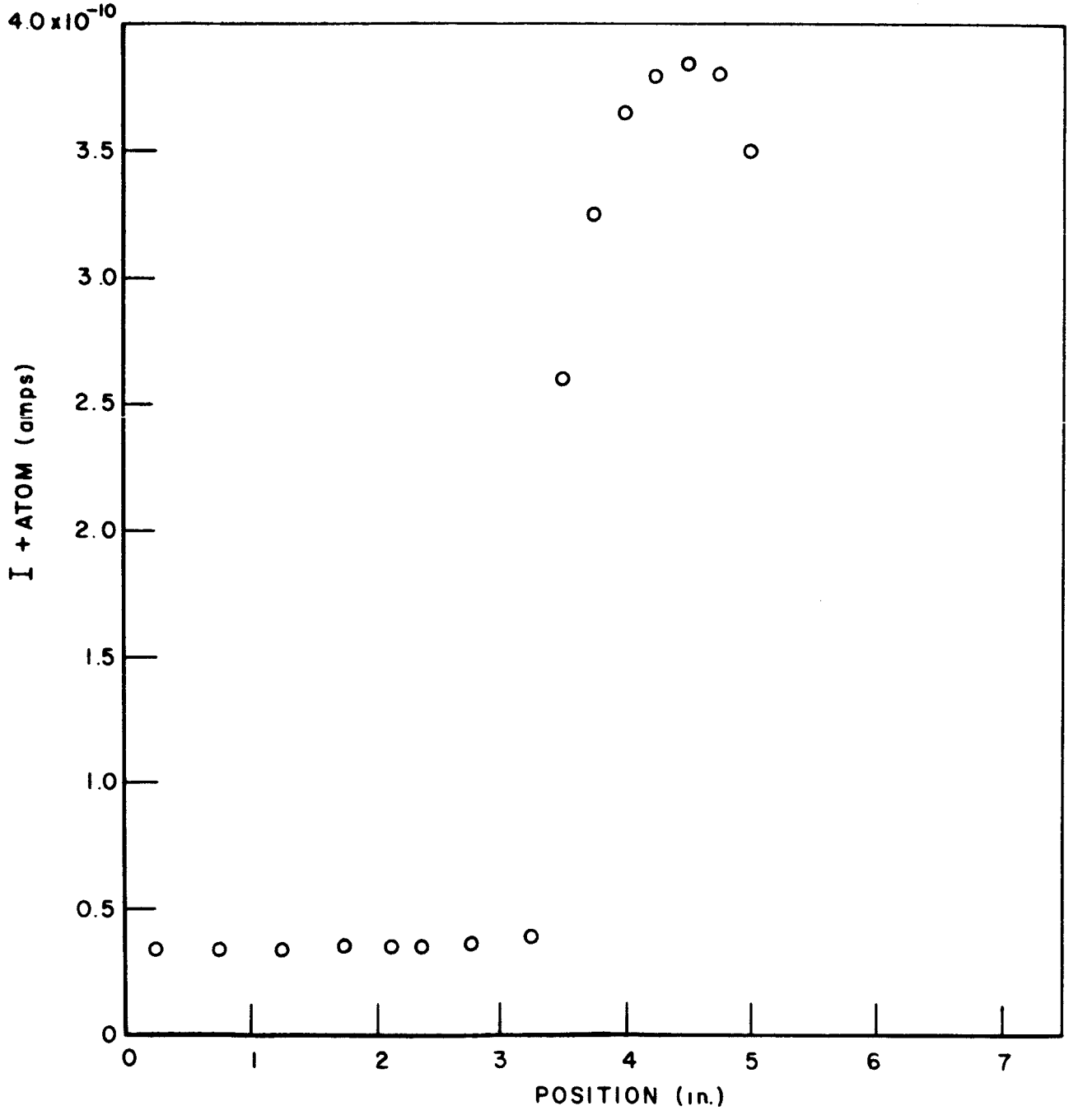

COLLISION CHAMBER EFFLUX MEASUREMENTS

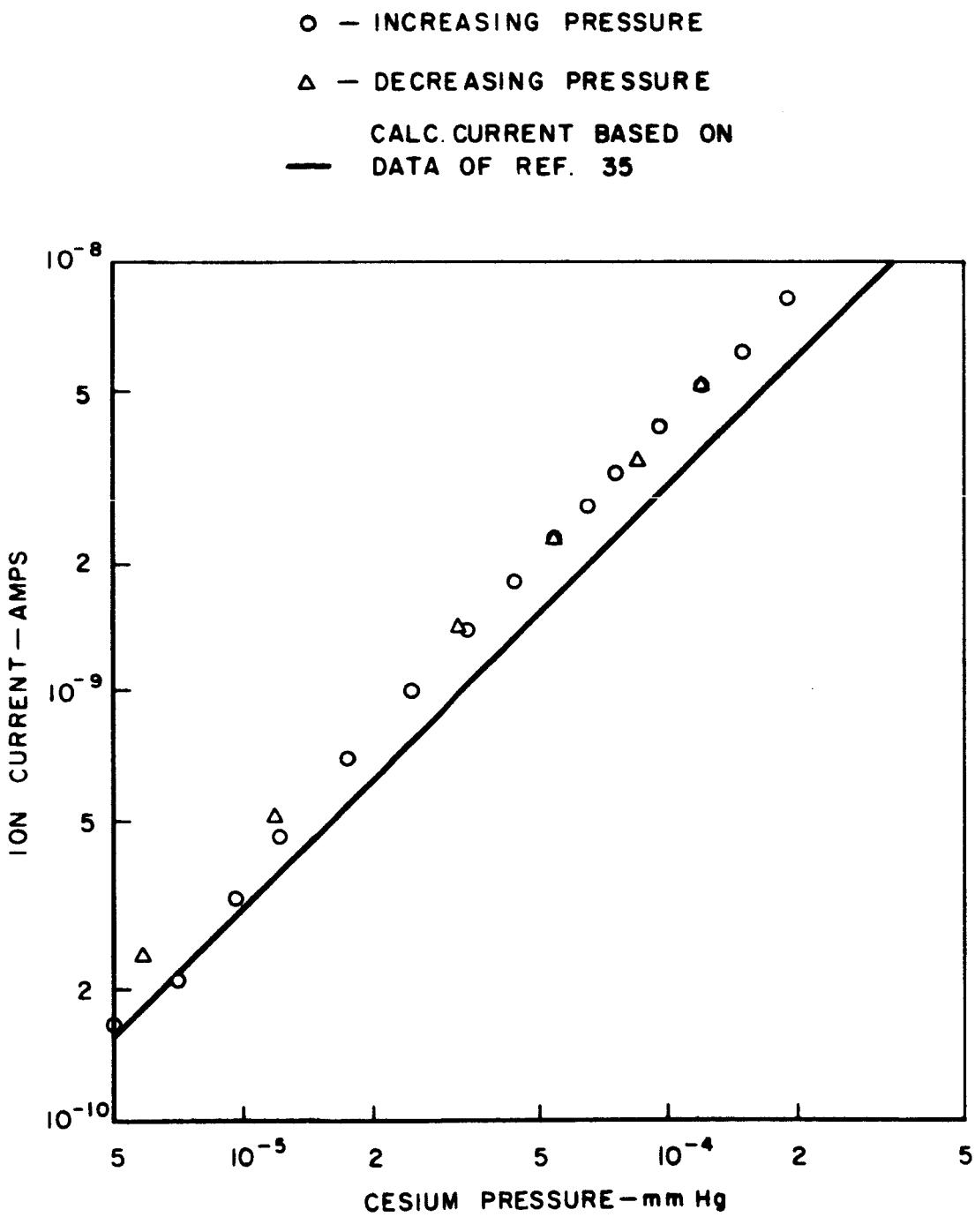

E-920243-27

FIG. 31

COLLISION CHAMBER PRESSURE RESPONSE

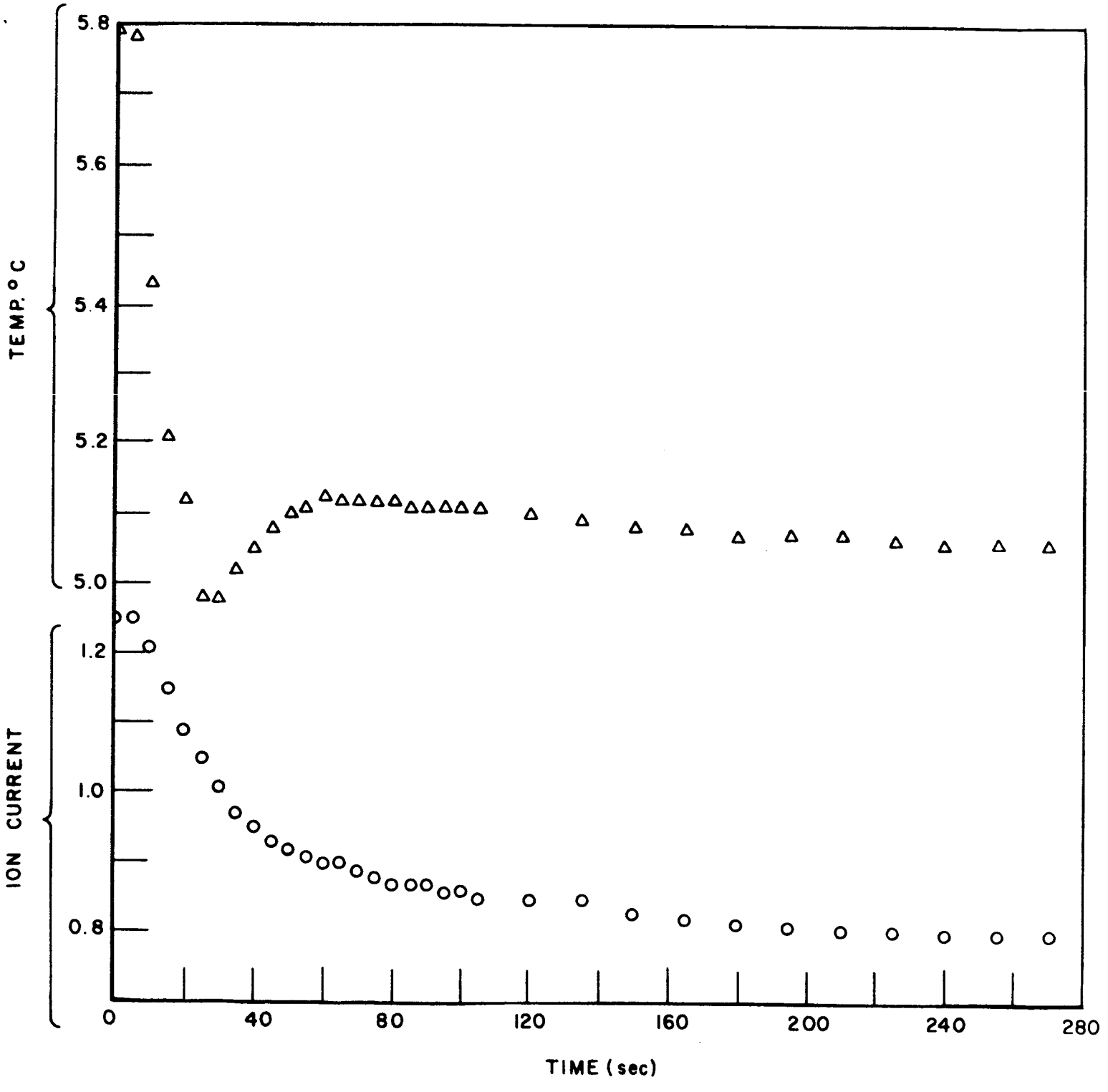

FIG 32

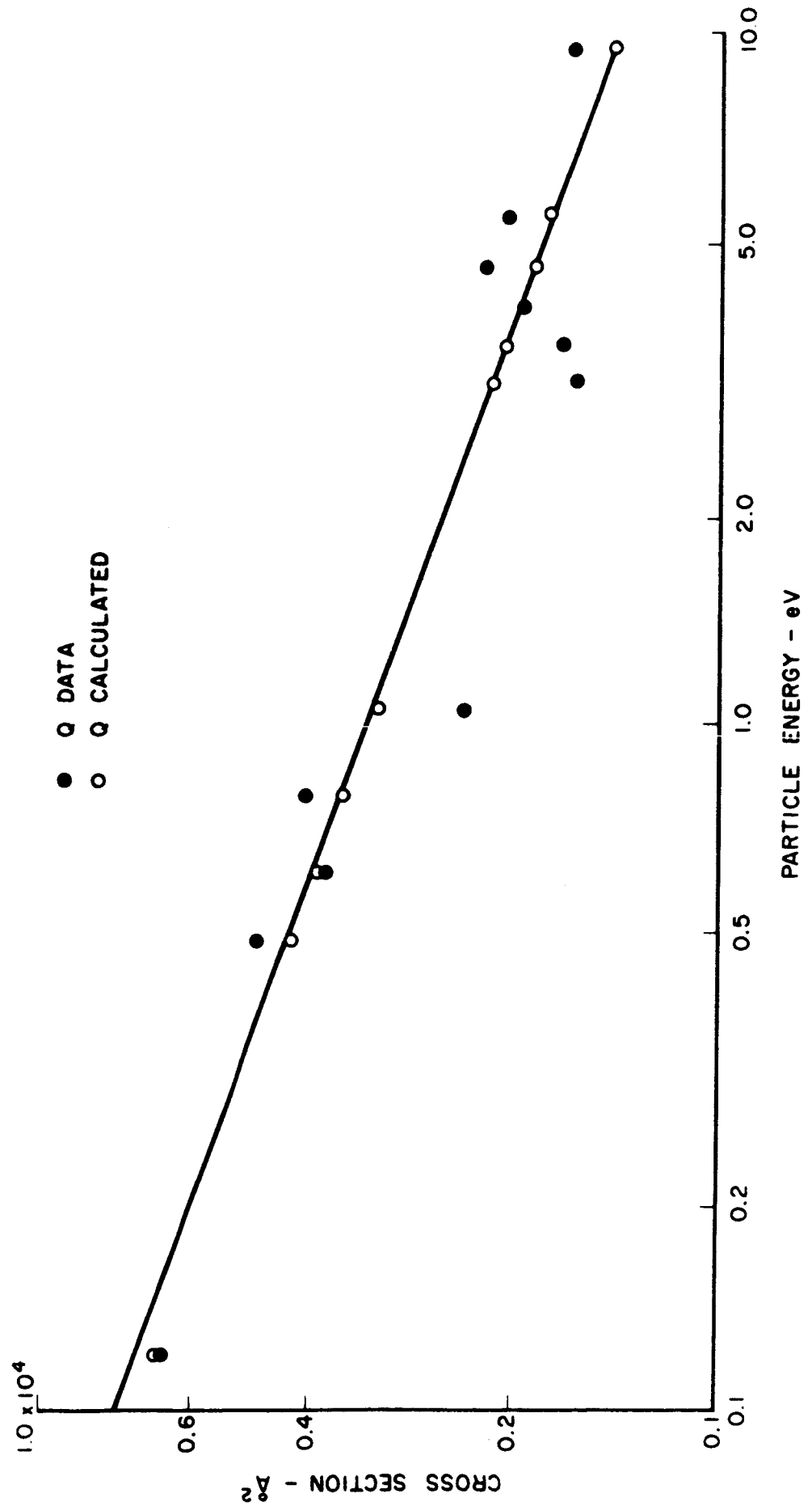
CORRECTED TOTAL COLLISION CROSS SECTION
Q DATA
Q CALCULATED
CROSS SECTION - A_o^2
1.0 x 10^4
0.6
0.4
0.2
0.1
0.1
0.2
0.5
1.0
2.0
5.0
10.0
PARTICLE ENERGY - eV

CALCULATED DIFFERENTIAL SCATTERING CROSS SECTION

3.38 eV

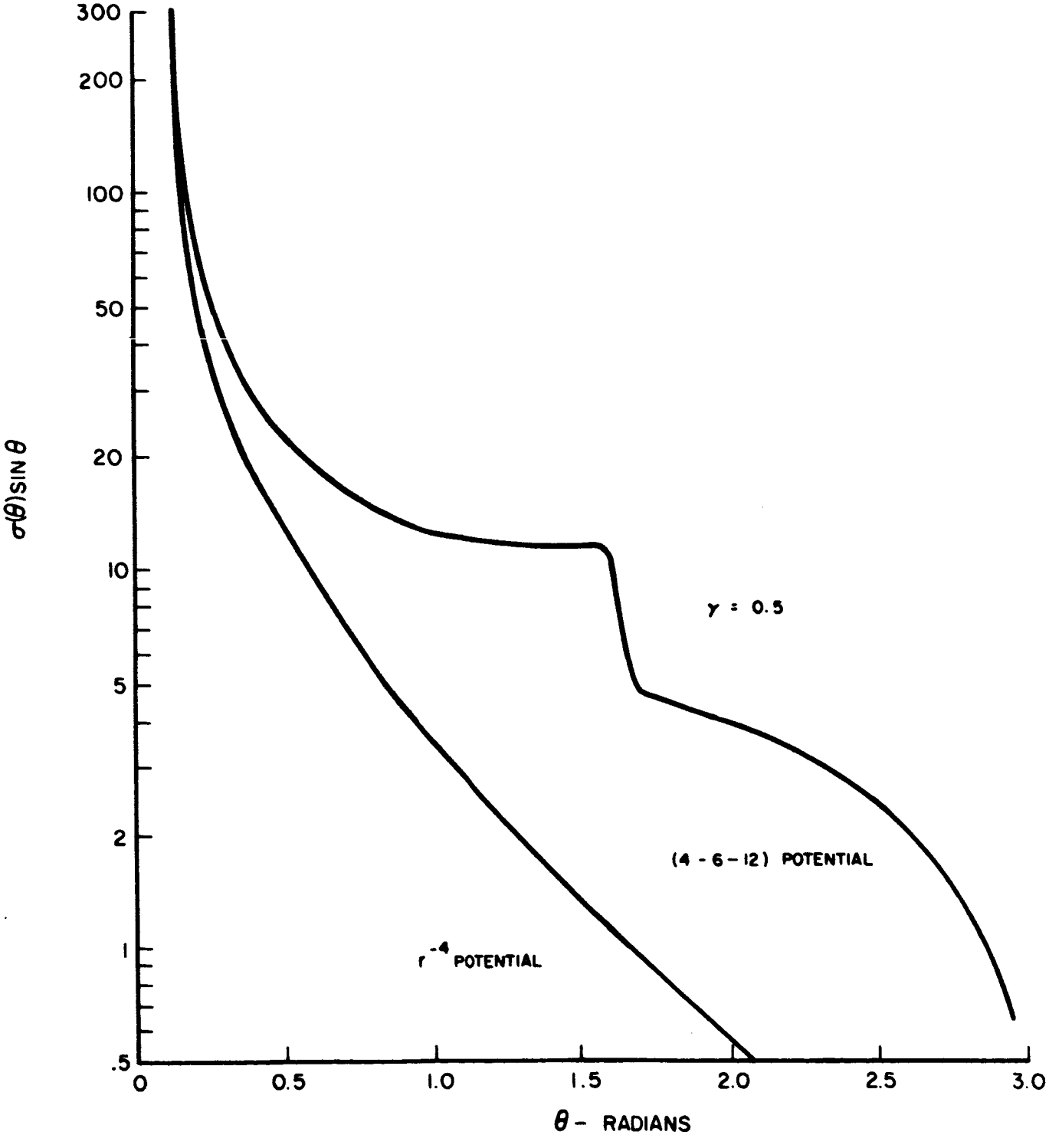

CALCULATED DIFFERENTIAL SCATTERING CROSS SECTION
0.543 eV

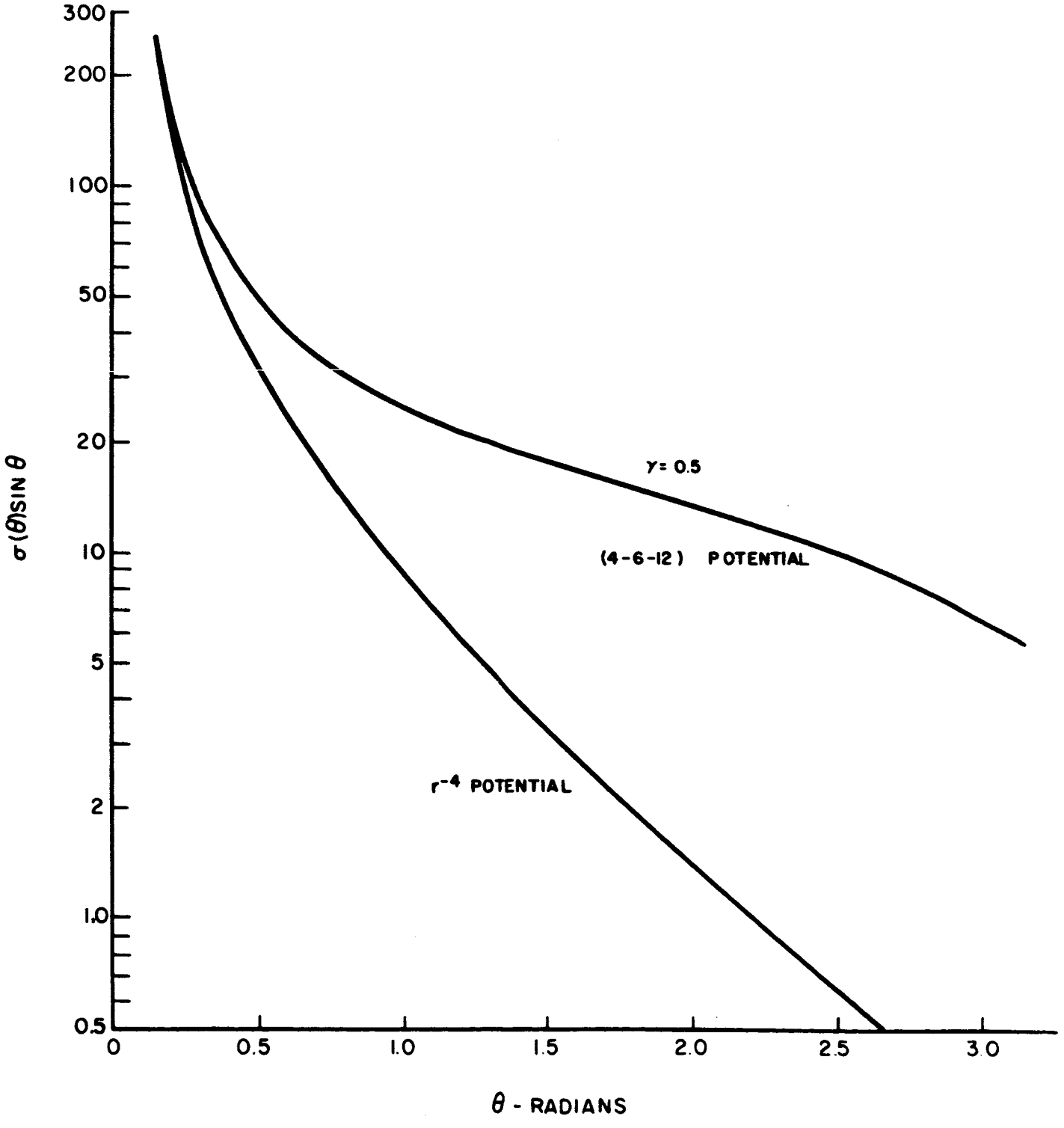

FIG. 35

COMPARISON OF CURRENT DATA AND PREVIOUSLY REPORTED DATA

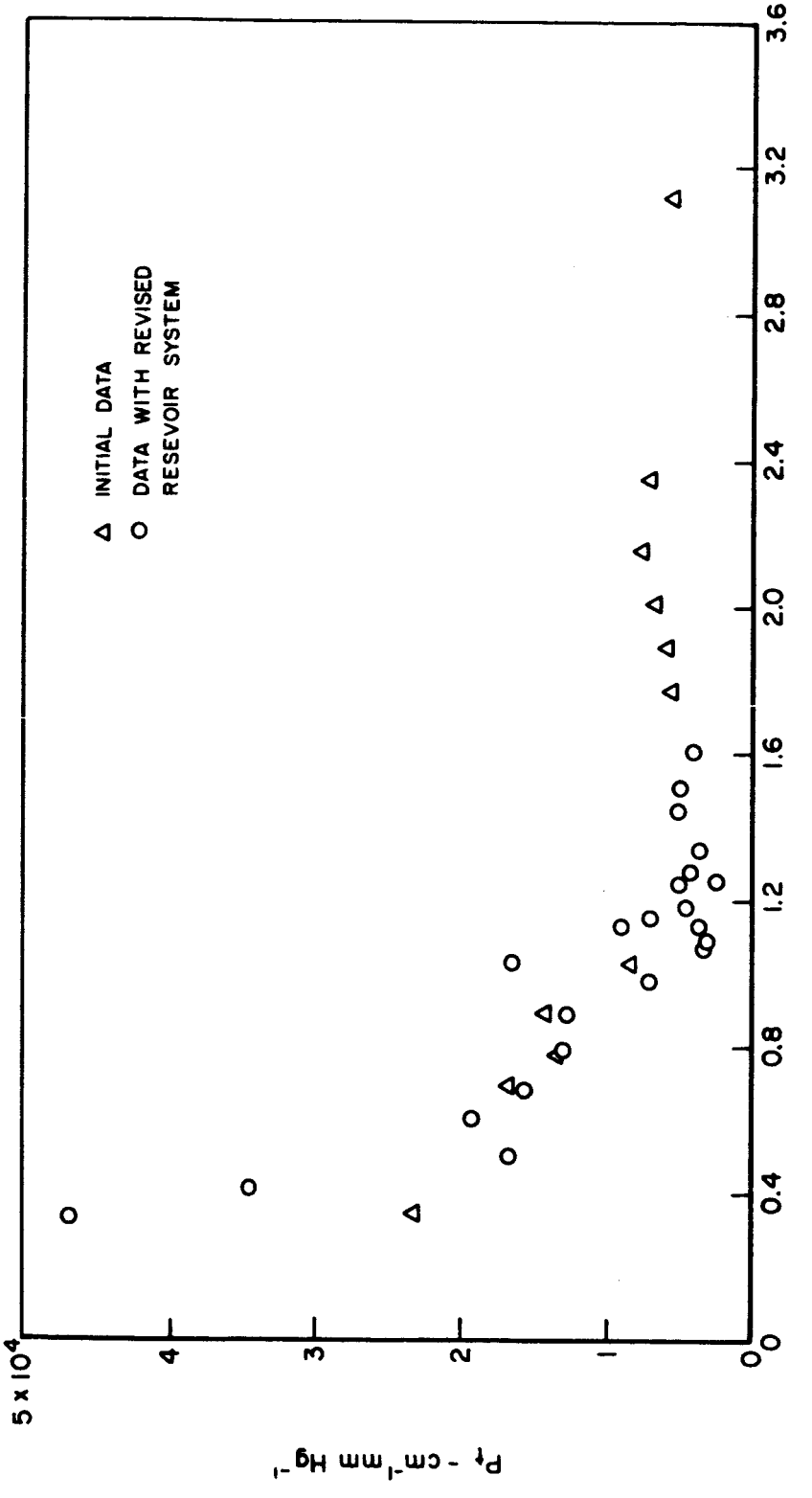

SCHEMATIC DIAGRAM OF ELECTRON COLLISION CROSS-SECTION APPARATUS

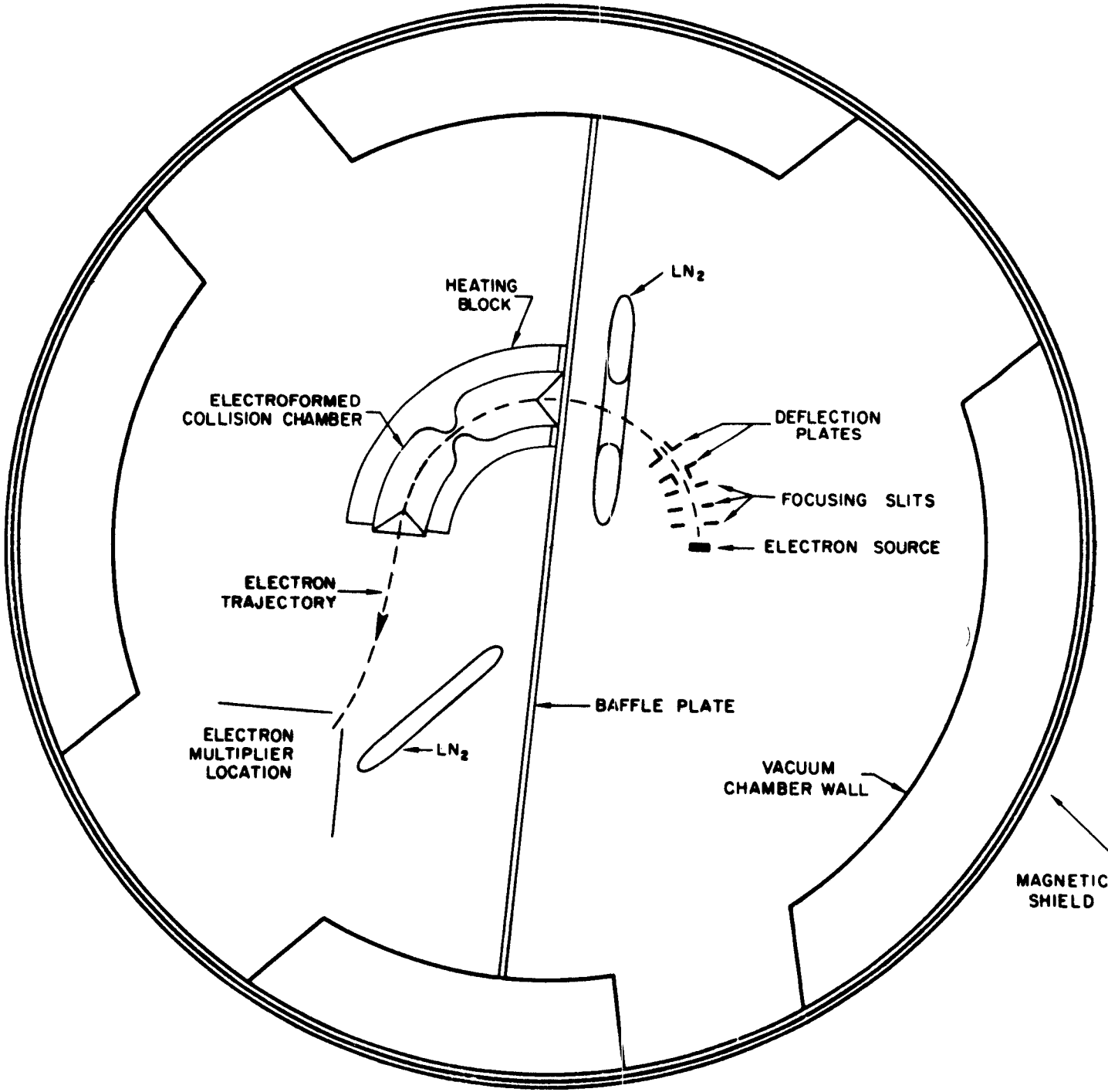

E-920243-27

FIG. 36

ELECTRON – ATOM COLLISION CROSS SECTION APPARATUS

VACUUM CHAMBER (INSIDE MAGNETIC SHIELD)

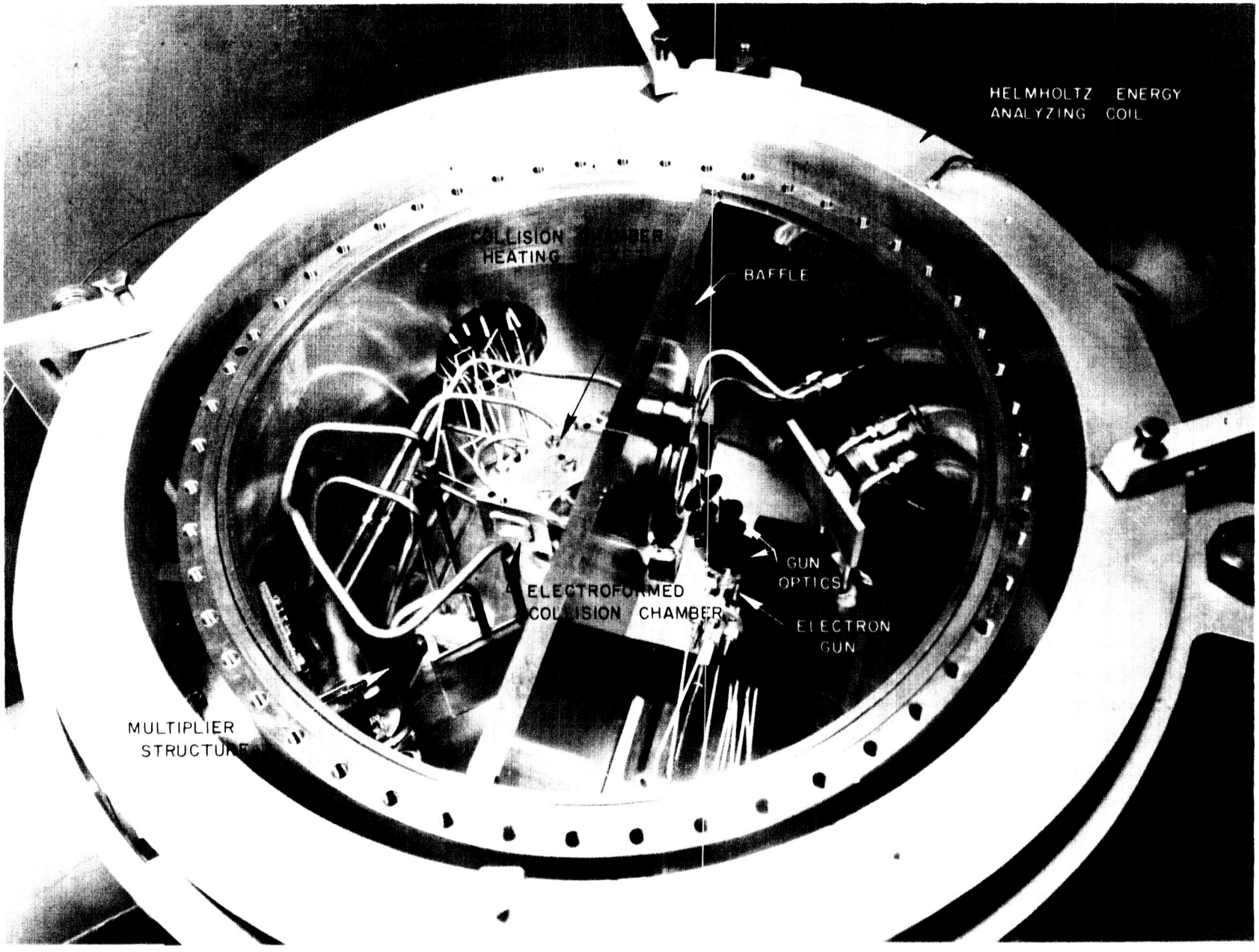

E-920243-27

FIG. 37

FIG. 38

ELECTRON-ATOM COLLISION CROSS SECTION APPARATUS

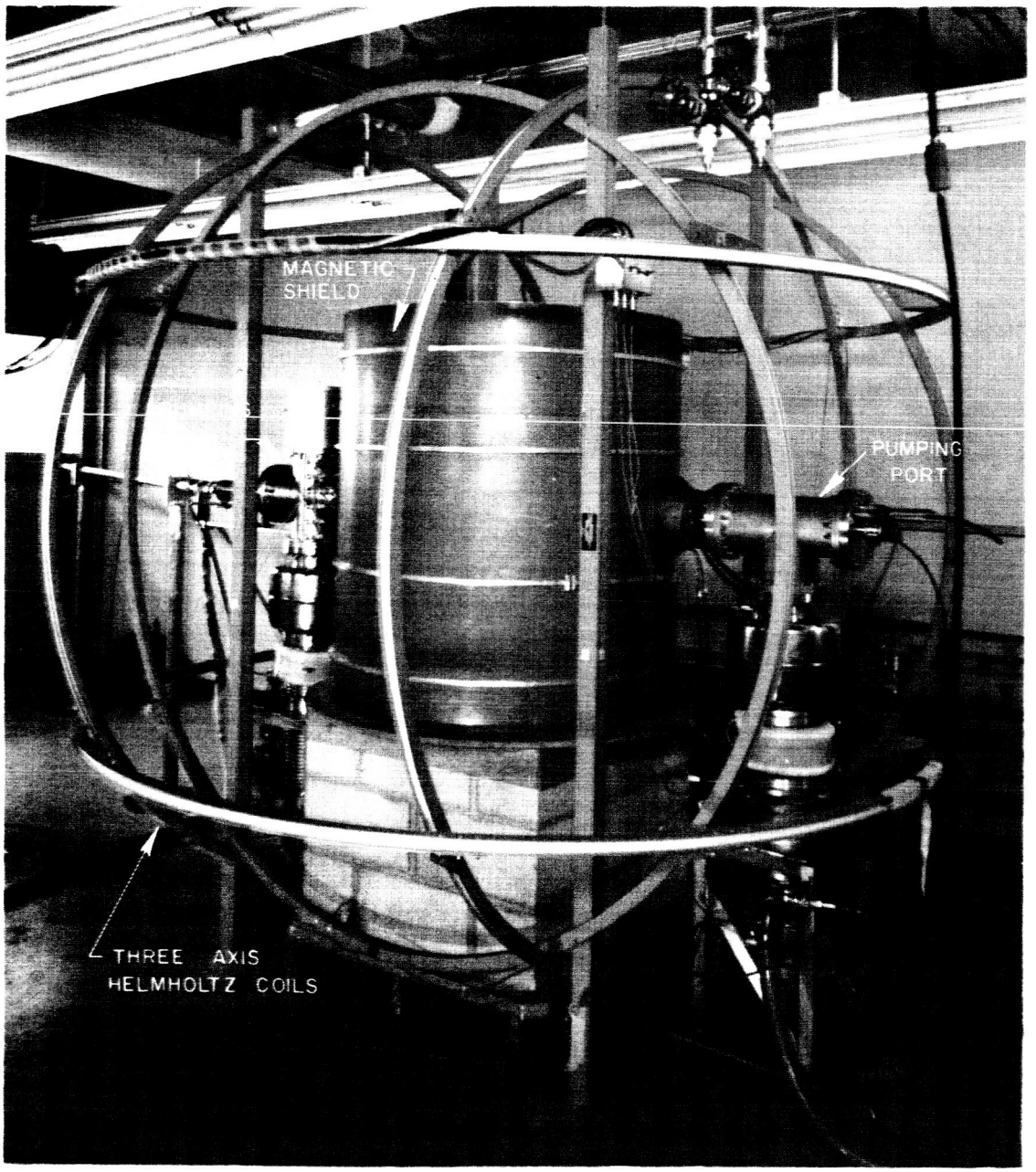

FIG. 39

ELECTRON COLLISION CHAMBER AND CESIUM RESERVOIR

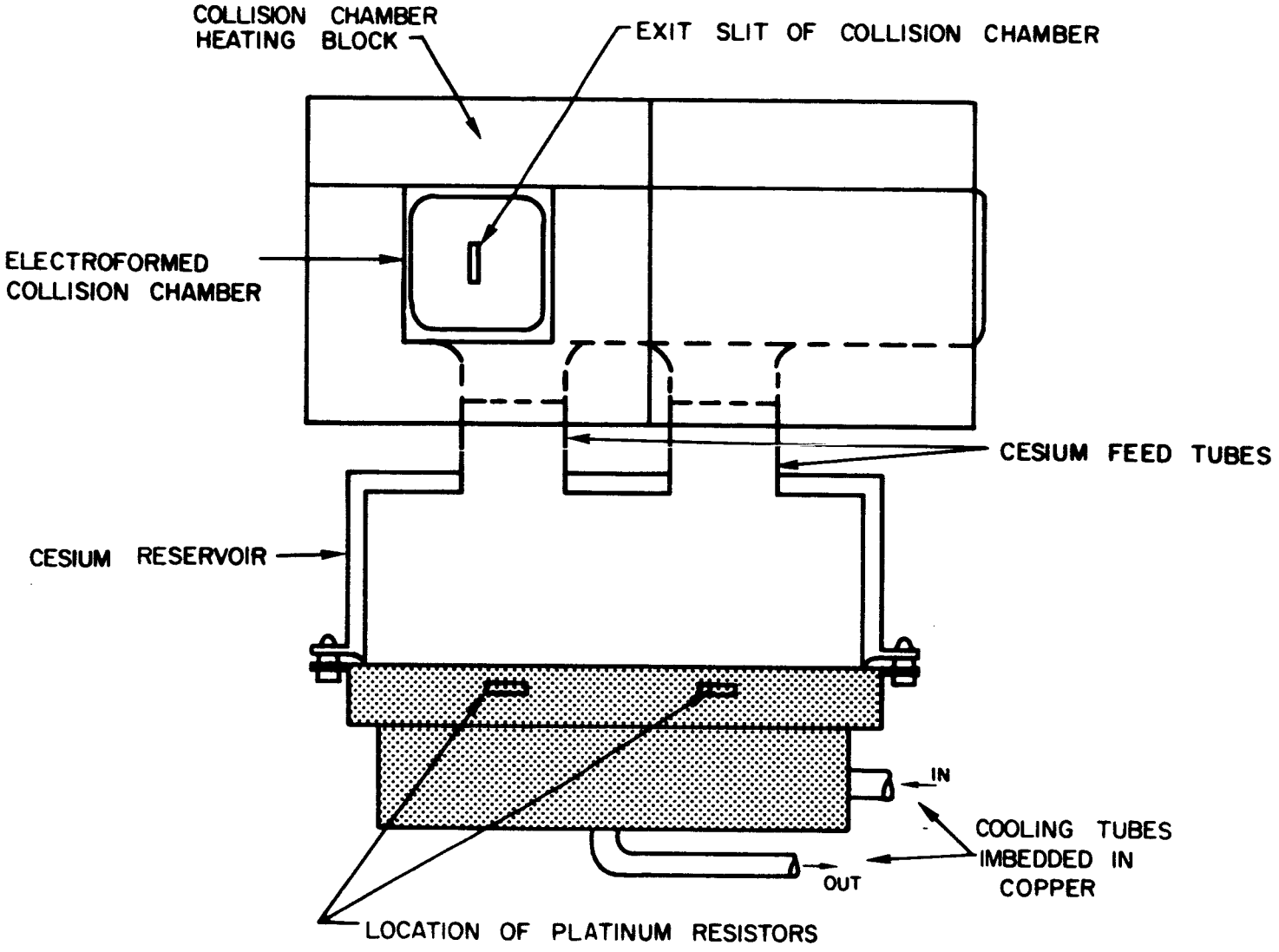

CESIUM RESERVOIR SHOWN IN SECTION

FIG. 40

NORMALIZED ELECTRON BEAM ENERGY DISTRIBUTION

PEAK ENERGY = 0.090 eV

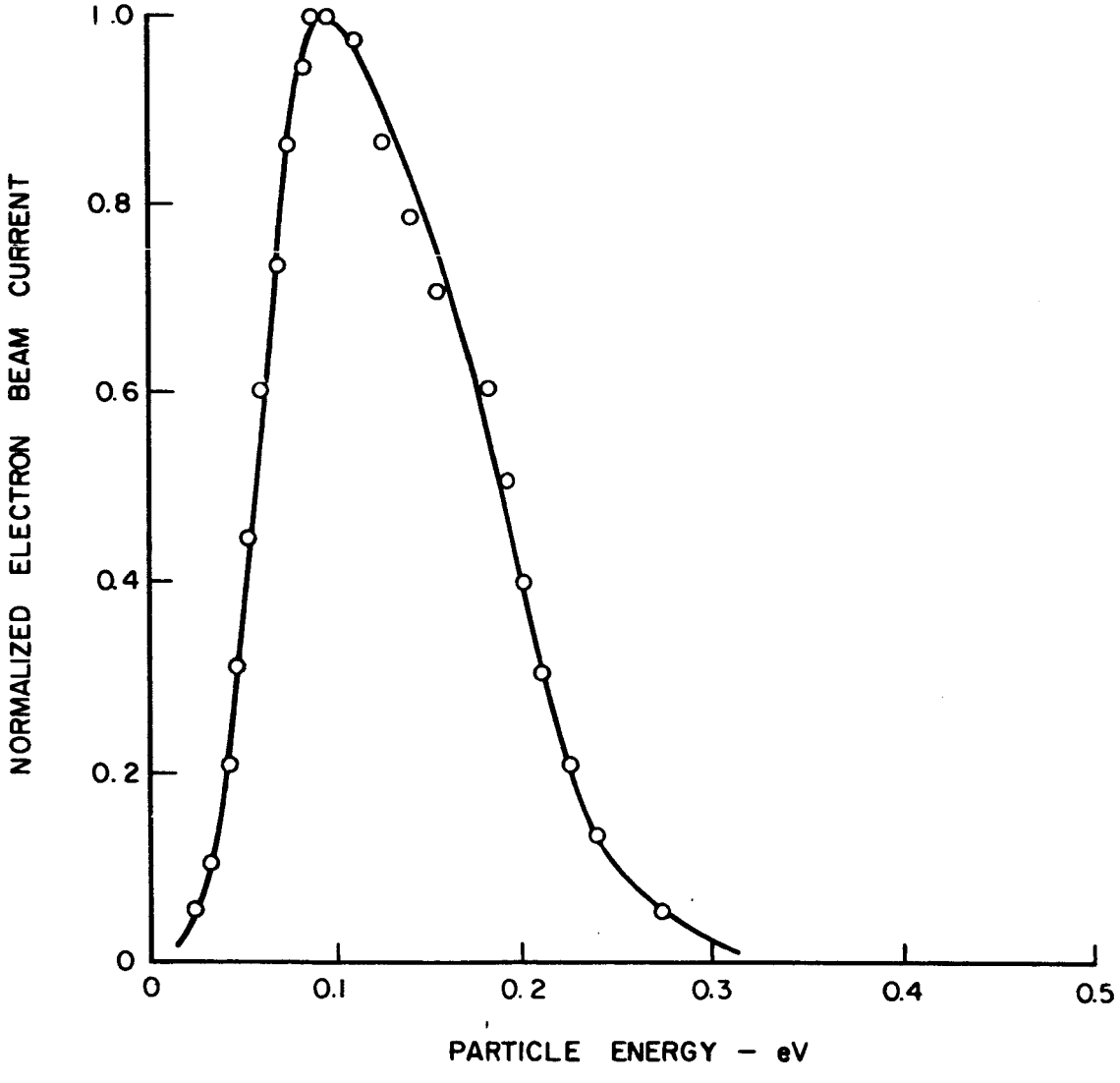

FIG. 41

NORMALIZED ELECTRON BEAM ENERGY DISTRIBUTION

PEAK ENERGY = 0.140 eV

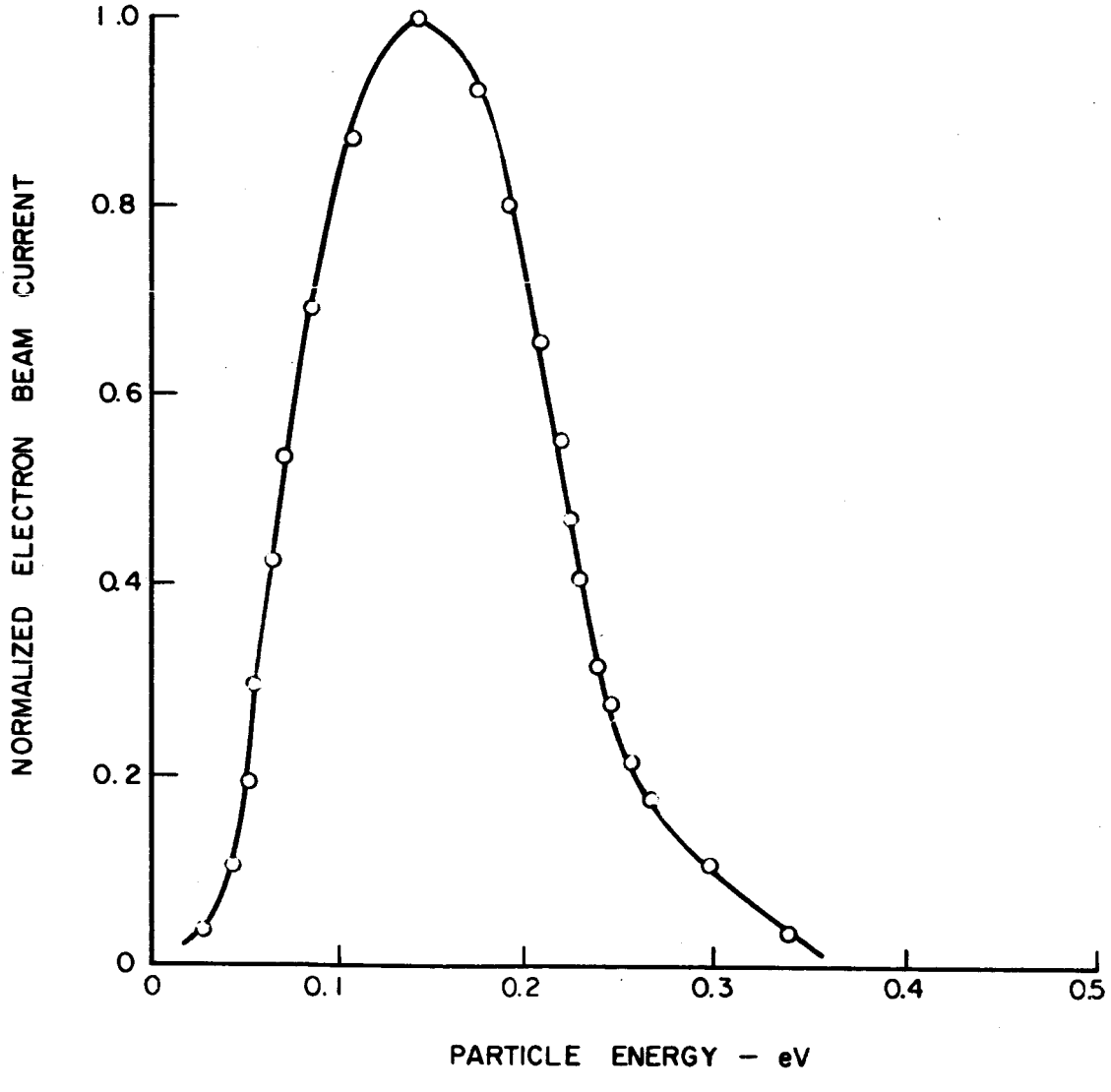

FIG. 42

NORMALIZED ELECTRON BEAM ENERGY DISTRIBUTION

PEAK ENERGY = 0.423 eV

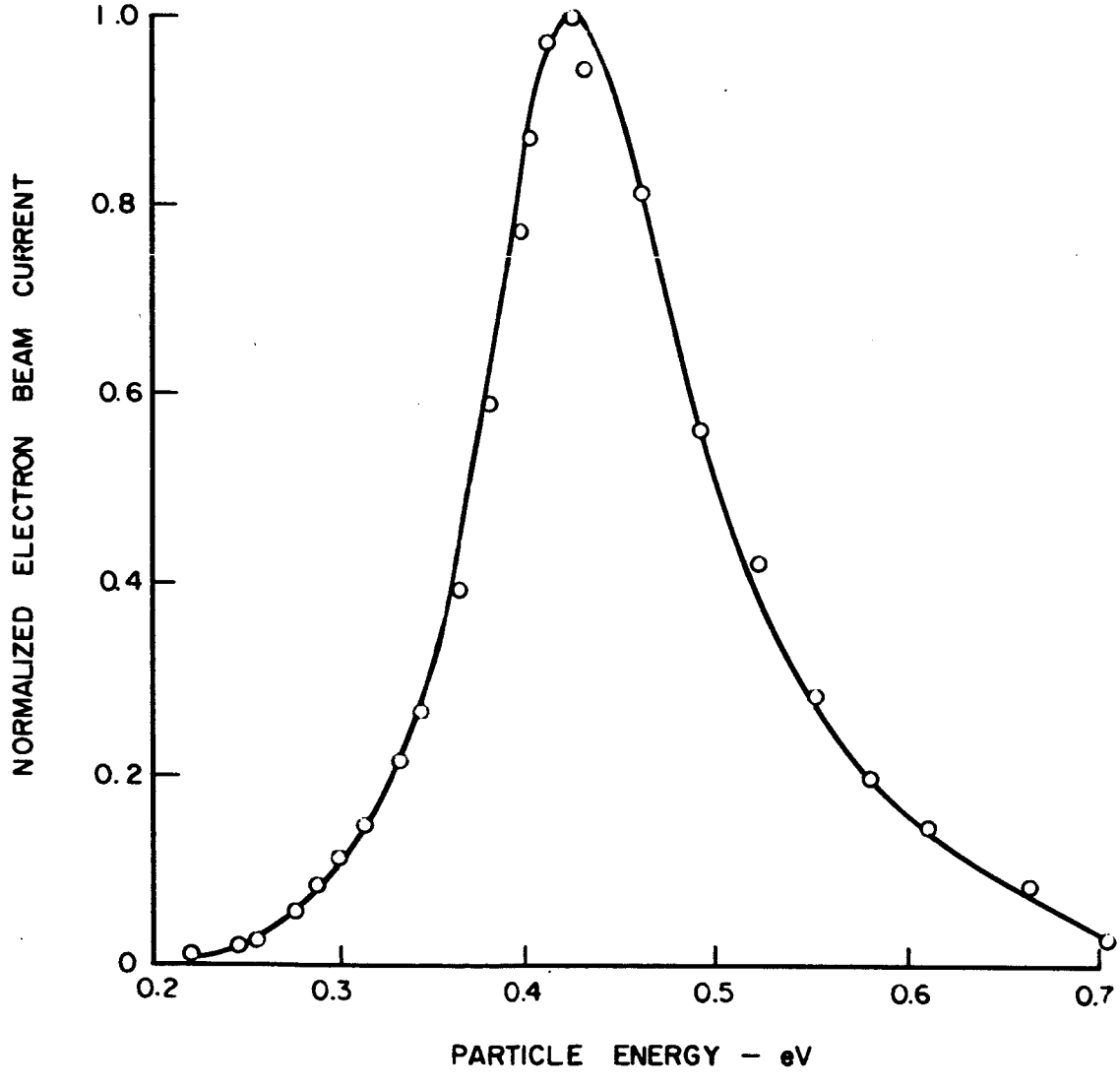

NORMALIZED ELECTRON BEAM ENERGY DISTRIBUTION

PEAK ENERGY = 0.520 eV

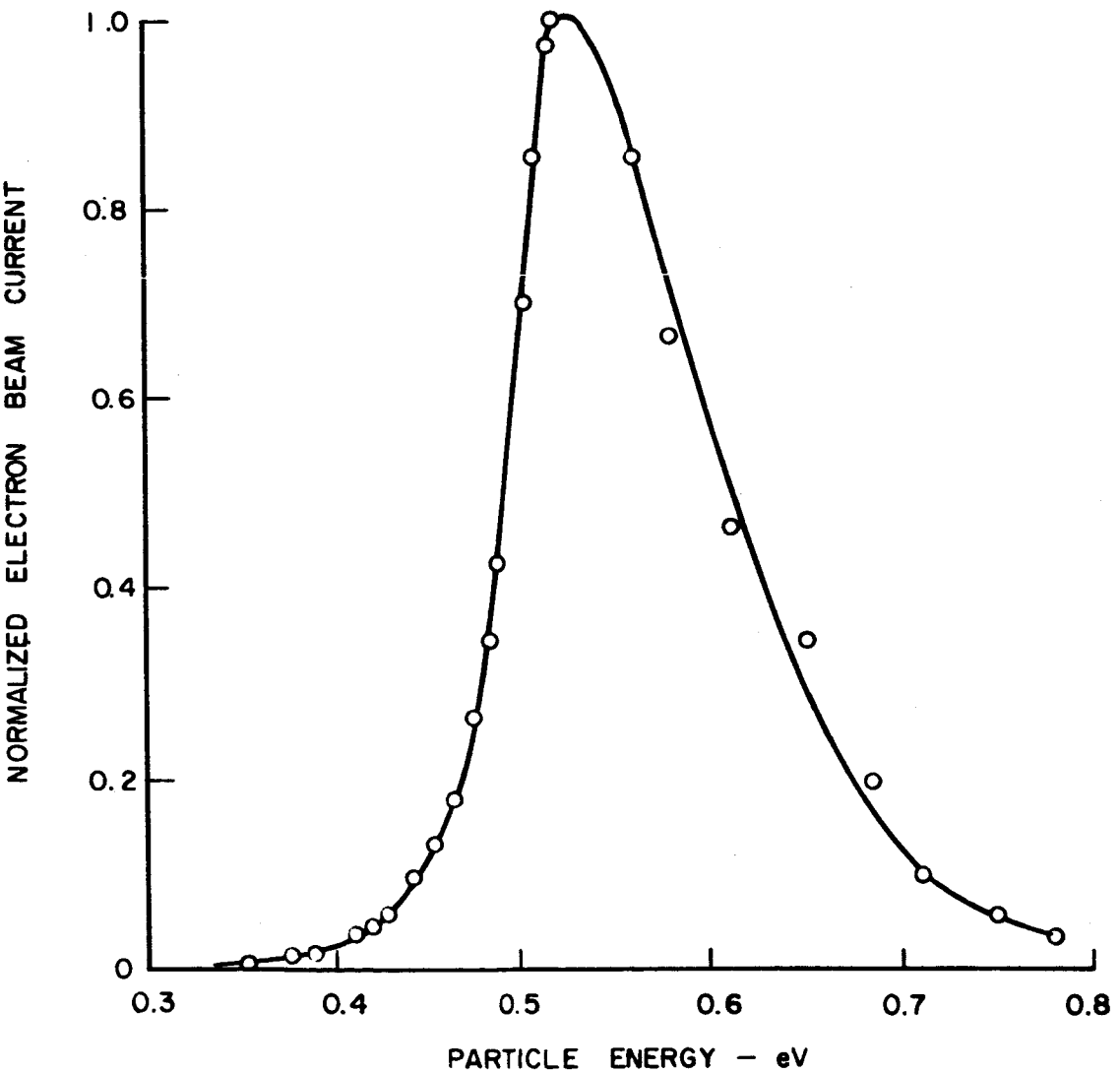

FIG. 44

NORMALIZED ELECTRON BEAM ENERGY DISTRIBUTION

PEAK ENERGY = 1.73 eV

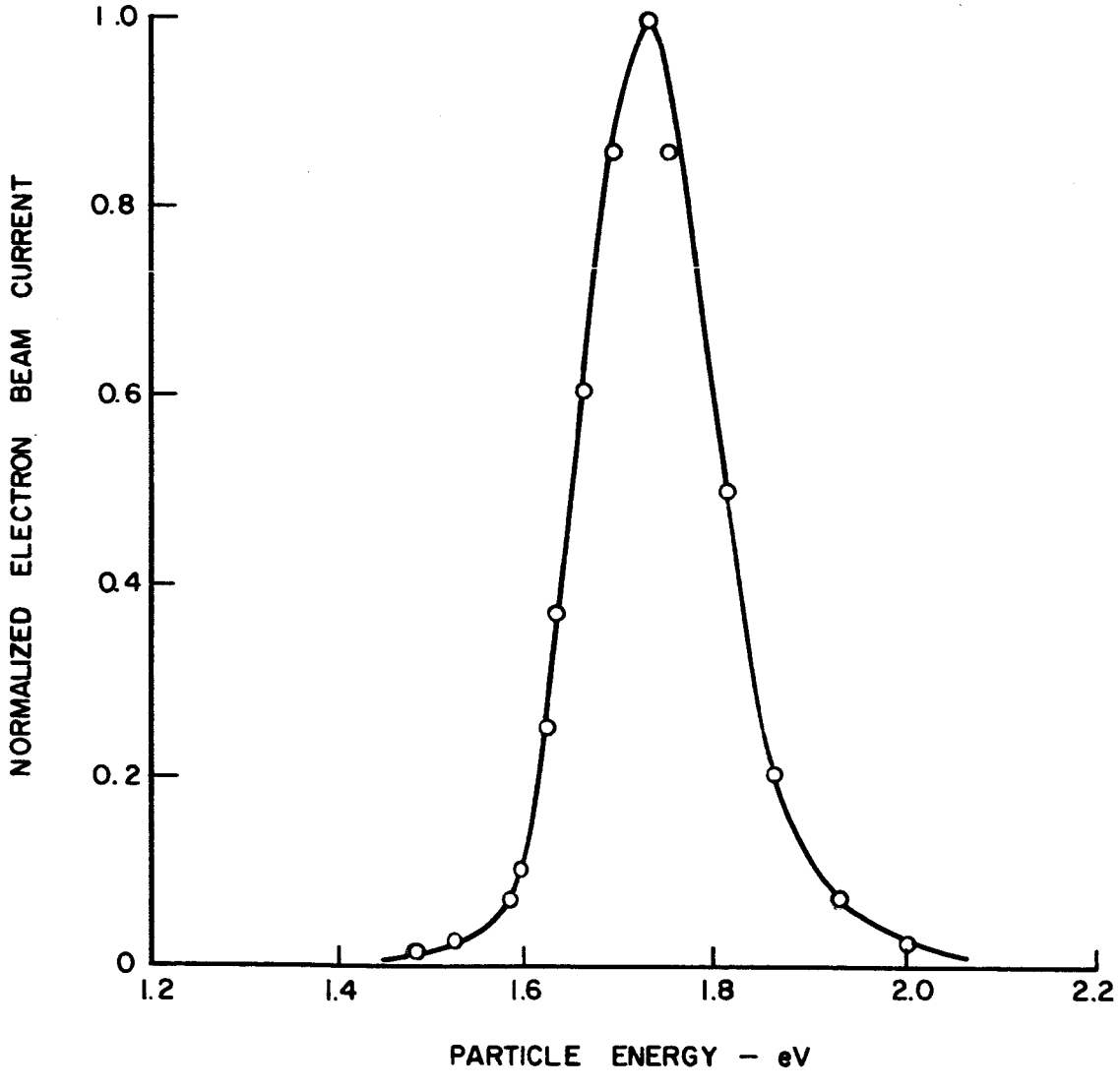

FIG. 45

NORMALIZED ELECTRON BEAM ENERGY DISTRIBUTION

PEAK ENERGY = 1.96 eV

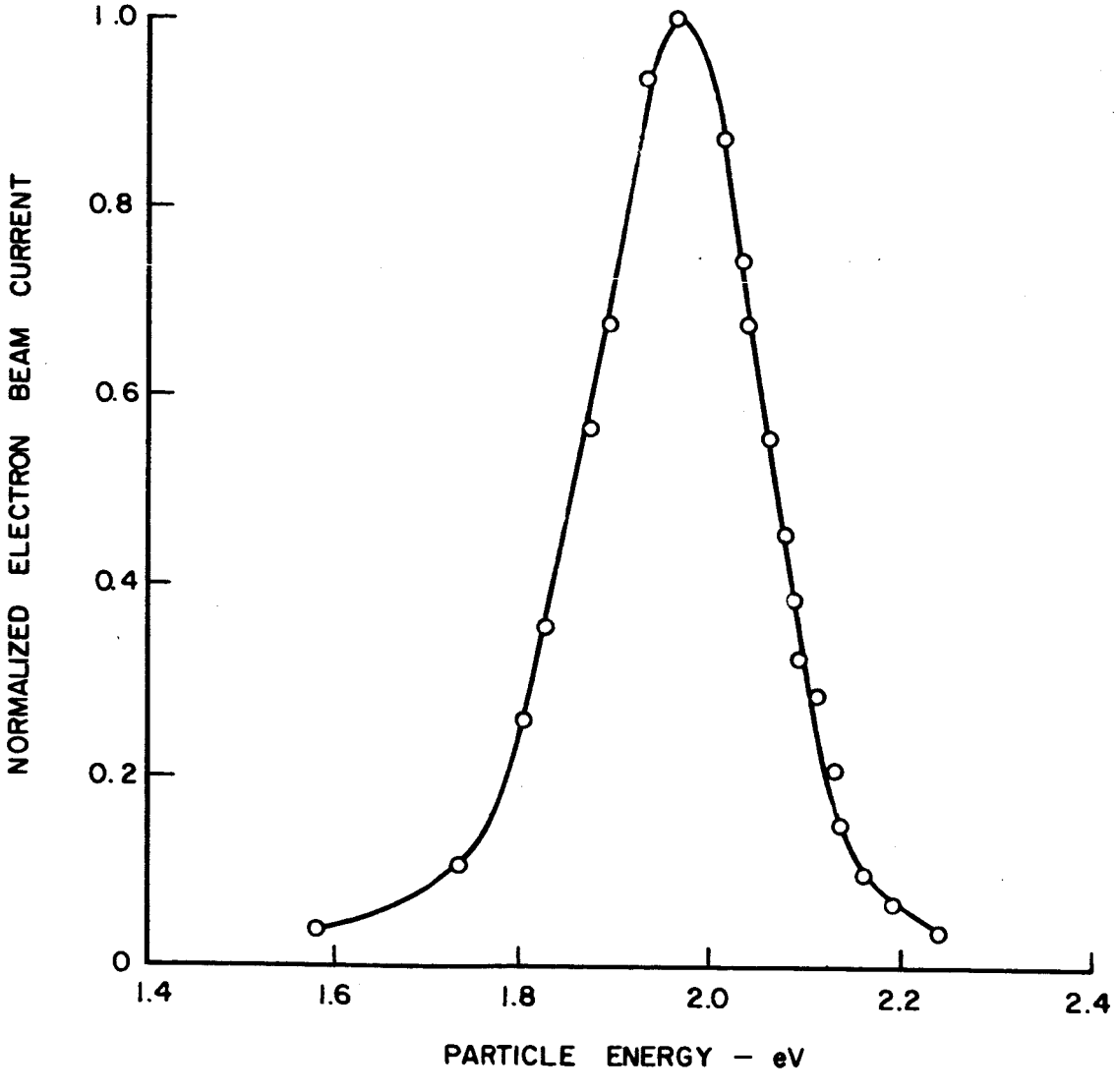

FIG. 46

NORMALIZED ELECTRON BEAM ENERGY DISTRIBUTION

PEAK ENERGY = 2.47 eV

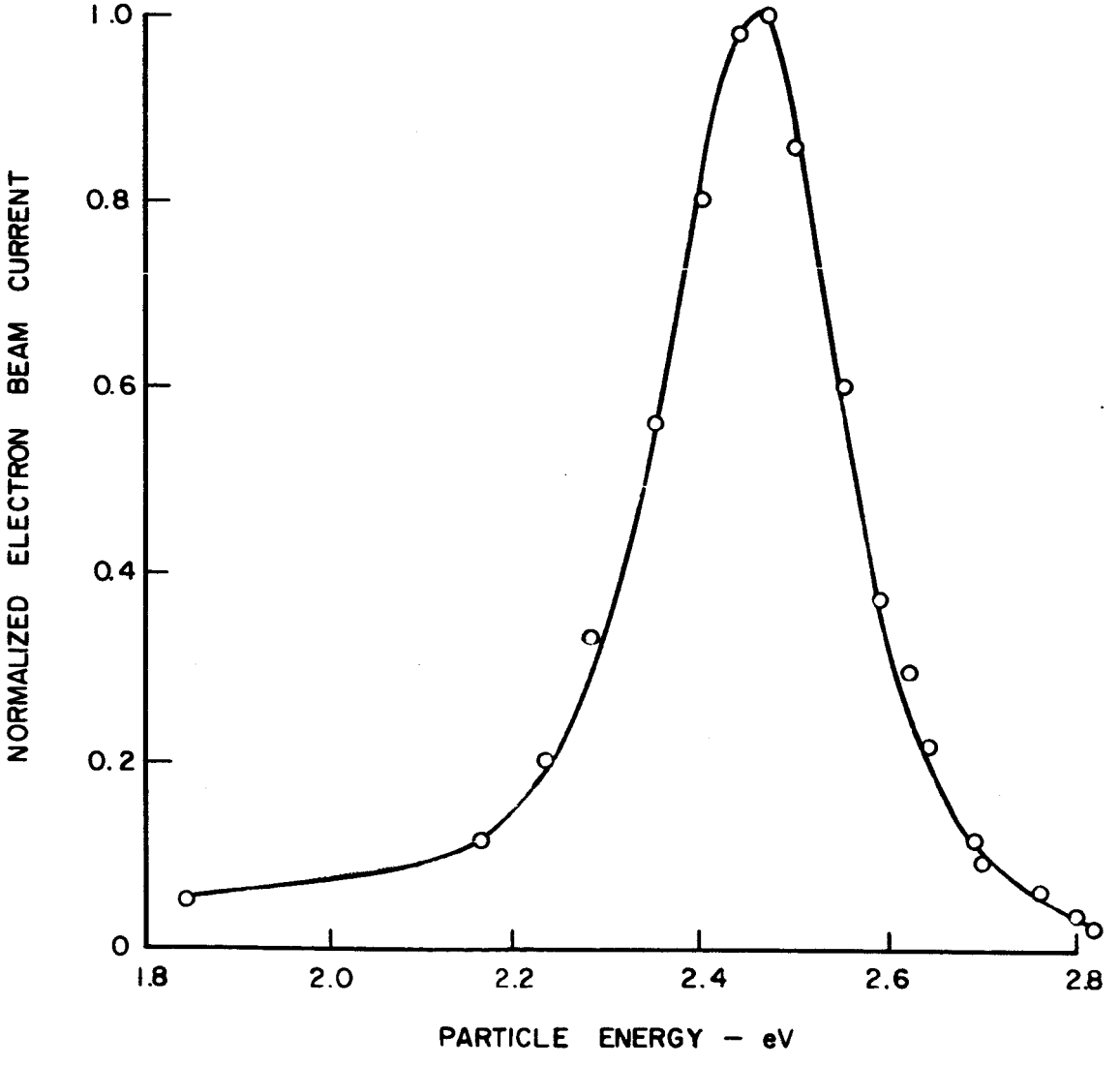

DISTRIBUTION LIST FOR UNITED AIRCRAFT CORPORATION
Contract No. NAS3-4171
Semiannual and Final Reports

	No. of Copies
Aerojet General Nucleonics San Ramon, California Attention: K. Johnson	1
Aerospace Corporation El Segundo, California Attention: Librarian	1
Air Force Cambridge Research Center (CRZAP) L. G. Hanscom Field Bedford, Massachusetts	1
Air Force Spacial Weapons Center Kirkland Air Force Base Albuquerque, New Mexico Attention: Chief, Nuclear Power Division	1
Air Force Systems Command Aeronautical Systems Division Flight Accessories Laboratory Wright-Patterson AFB, Ohio Attention: AFAPL (APIP-2, A. E. Wallis)	1
Allison Division General Motors Corporation Indianapolis 6, Indiana Attention: J. D. Dunlop II	1
Aracon Laboratories Virginia Road Concord, Massachusetts Attention: S. Ruby	1
Argonne National Laboratory 9700 South Cass Avenue Argonne, Illinois Attention: Aaron J. Ulrich	1

Illinois Institute of Technology
Research Institute
10 West 35th Street
Chicago 16, Illinois
Attention: D. W. Levinson 1

Atomics International
P. O. Box 309
Canoga Park, California
Attention: Robert C. Allen 1
Charles K. Smith 1

The Babcock & Wilcox Company
1201 Kemper Street
Lynchburg, Virginia
Attention: Russell M. Ball 1

Battelle Memorial Institute
505 King Avenue
Columbus 1, Ohio
Attention: David Dingee 1
Don Keller 1

The Bendix Corporation
Research Laboratories Division
Northwestern Highway
Detroit 35, Michigan
Attention: W. M. Spurgeon 1

Bureau of Ships
Department of the Navy
Washington 25, D. C.
Attention: B. B. Rosenbaum 1
John Huth 1

Consolidated Controls Corporation
Bethel, Connecticut
Attention: David Mends 1

Mr. John McNeil
Market Development Manager
Research Division
Allis-Chalmers Manufacturing Company
Post Office Box 512
Milwaukee, Wisconsin 1

Douglas Aircraft Company
Missile & Space Engineering
Nuclear Research (AZ-260)
3000 Ocean Park
Santa Monica, California
Attention: A. Del Grosso 1

Electro-Optical Systems, Incorporated
300 North Halstead Avenue
Pasadena, California
Attention: A. Jensen 1

Ford Instrument Company
32-36 47th Avenue
Long Island City, New York
Attention: A. Medica 1

General Atomic
P. O. Box 608
San Diego 12, California
Attention: R. W. Pidd 1
L. Yang 1
A. Weinberg 1

General Electric Company
Missile & Space Vehicle Department
3198 Chestnut Street
Philadelphia 4, Pennsylvania
Attention: Library 1

General Electric Company
Knolls Atomic Power Laboratory
Schenectady, New York
Attention: R. Ehrlich 1

General Electric Company
Microwave Tube Business Section
Building 269
One River Road
Schenectady, New York 12305 1
Attention: D. A. Wilbur

General Electric Company
Nuclear Materials & Propulsion Operation
P. O. Box 15132
Cincinnati 15, Ohio 1
Attention: J. A. McGurty

General Electric Company
Research Laboratory
Schenectady, New York
Attention: Volney C. Wilson 1
John Houston 1

General Electric Company
Special Purpose Nuclear System Operations
Vallecitos Atomic Laboratory
P. O. Box 846
Pleasanton, California
Attention: E. Blue 1
B. Voorhees 1

General Motors Corporation
Research Laboratories
Warren, Michigan
Attention: F. E. Jamerson 1

Hughes Research Laboratories
3011 Malibu Canyon Road
Malibu, California
Attention: R. C. Knechtli 1

Institute for Defense Analyses
400 Army-Navy Drive
Arlington, Virginia 22202
Attention: R. C. Hamilton 1

Jet Propulsion Laboratory
California Institute of Technology
4800 Oak Grove Drive
Pasadena, California
Attention: Peter Rouklove 1
Library 1

Los Alamos Scientific Laboratory
P. O. Box 1663
Los Alamos, New Mexico
Attention: G. M. Grover 1
Walter Reichelt 1

Marquardt Corporation
Astro Division
16555 Saticoy Street
Van Nuys, California
Attention: A. N. Thomas 1

Martin - Nuclear
Division of Martin-Marietta Corporation
P. O. Box 5042
Middle River 3, Maryland
Attention: J. Levedahl 1

Massachusetts Institute of Technology
Cambridge, Massachusetts
Attention: Robert E. Stickney 1
Elias P. Gyftopolous 1

National Aeronautics & Space Administration
Manned Spacecraft Center
Houston, Texas
Attention: J. D. Murrell 1

National Aeronautics & Space Administration
600 Independence Avenue, N. W.
Washington 25, D. C.
Attention: Fred Schulman 1
James J. Lynch 1
H. Harrison 1
Arvin Smith 1

National Aeronautics & Space Administration
Lewis Research Center
21000 Brookpark Road
Cleveland, Ohio 44135
Attention: Roland Breitwieser (C&EC) 1
Robert Migra (NRD) 1
Bernard Lubarsky (SPSD) 1
James J. Ward (SPSD) 1
Herman Schwartz (SPSD) 1
C. Walker (SPSPS) 1
R. Mather (SPSD) 1
H. E. Nastelin (SPSD) 3
John J. Weber (TUO) 1

National Aeronautics & Space Administration
Marshall Space Flight Center
Huntsville, Alabama
Attention: Library 1

National Aeronautics & Space Administration Scientific & Technical Information Facility P. O. Box 5700 Bethesda 14, Maryland Attention: NASA Representative	2 Copies & 1 Reproduction
National Aeronautics & Space Administration Goddard Space Flight Center Greenbelt, Maryland Attention: Joseph Epstein	1
National Bureau of Standards Washington, D. C. Attention: Library	1
Oak Ridge National Laboratory Oak Ridge, Tennessee Attention: Library	1
Office of Naval Research Power Branch Department of the Navy Washington 25, D. C. Attention: Cdr. J. J. Connelly, Jr.	1
Power Information Center University of Pennsylvania Moore School Building 200 South 33rd Street Philadelphia 4, Pennsylvania	1
Pratt & Whitney Aircraft Corporation East Hartford 8, Connecticut Attention: William Lueckel Franz Harter	1 1
Radio Corporation of America Electron Tube Division Lancaster, Pennsylvania Attention: Fred Block	1
Radio Corporation of America David Sarnoff Research Center Princeton, New Jersey Attention: Karl G. Hernqvist Paul Rappaport	1 1

The Rand Corporation
1700 Main Street
Santa Monica, California
Attention: Librarian 1

Republic Aviation Corporation
Farmingdale, Long Island, New York
Attention: Alfred Schock 1

Space Technology Laboratories
Los Angeles 45, California
Attention: Kenneth K. Tang 1

Texas Instruments, Incorporated
P. O. Box 5474
Dallas, Texas
Attention: R. A. Chapman 1

Thermo Electron Engineering Corporation
85 First Avenue
Waltham 54, Massachusetts
Attention: George Hatsopoulos 1
S. Kitrilakis 1

Thompson Ramo Wooldridge, Incorporated
7209 Platt Avenue
Cleveland, Ohio
Attention: W. J. Leovic 1

United Nuclear Corporation
Five New Street
White Plains, New York
Attention: Al Strasser 1

U. S. Army Signal R & D Laboratory
Fort Monmouth, New Jersey
Attention: Emil Kittil 1

U. S. Atomic Energy Commission
Division of Reactor Development
Washington 25, D. C.
Attention: Direct Conversion Branch 1

U. S. Atomic Energy Commission
Technical Reports Library
Washington 25, D. C.
Attention: J. M. O'Leary 3

U. S. Atomic Energy Commission
Department of Technical Information Extension
P. O. Box 62
Oak Ridge, Tennessee 3

U. S. Atomic Energy Commission
San Francisco Operations Office
2111 Bancroft Way
Berkeley 4, California
Attention: Reactor Division 1

U. S. Naval Research Laboratory
Washington 25, D. C.
Attention: George Haas 1
Library 1

Defense Research Corporation
P. O. Box 3587
Santa Barbara, California
Attention: Harold W. Lewis 1

Westinghouse Electric Corporation
Research Laboratories
Pittsburgh, Pennsylvania
Attention: R. J. Zollweg 1

The Boeing Company
Seattle, Washington
Attention: Howard L. Steele 1

Varian Associates
611 Hansen Way
Palo Alto, California
Attention: Ira Weissman 1